

**HEXATRIENE CYCLIZATION IN ACID ZEOLITES INVESTIGATED  
USING DENSITY FUNCTIONAL THEORY METHODS**

by

Jason Lee

A thesis submitted to the Faculty of the University of Delaware in partial fulfillment of the requirements for the degree of Master of Chemical Engineering

Fall 2019

© 2019 Jason Lee  
All Rights Reserved

**HEXATRIENE CYCLIZATION IN ACID ZEOLITES INVESTIGATED  
USING DENSITY FUNCTIONAL THEORY METHODS**

by

Jason Lee

Approved: \_\_\_\_\_  
Raul F. Lobo, Ph.D.  
Professor in charge of thesis on behalf of the Advisory Committee

Approved: \_\_\_\_\_  
Eric M. Furst, Ph.D.  
Chair of the Department of Chemical and Biomolecular Engineering

Approved: \_\_\_\_\_  
Levi T. Thompson, Ph.D.  
Dean of the College of Engineering

Approved: \_\_\_\_\_  
Douglas J. Doren, Ph.D.  
Interim Vice Provost for Graduate and Professional Education and  
Dean of the Graduate College

## ACKNOWLEDGMENTS

First, I would like to thank my advisor, Professor Raul F. Lobo. He has a unique talent for cultivating critical thinking and his optimism is contagious. Words can not express how truly grateful I am for his time and patience in helping me rediscover the independent researcher inside of me that I forgot I had believe in first. I look forward to continuing to grow and learn as a researcher, engineer, and communicator during my Ph.D. work under his tutelage.

I must also thank Dr. Stavros Caratzoulas, especially for his willingness to advise a student with no previous experience in computational research. He has a way of making computational work approachable for experimentalists. His perspectives complemented those of Professor Lobo, and were also essential to expanding my views of chemistry and catalysis.

To my thesis committee, Professor Douglas Buttrey, Professor Feng Jiao, and Professor Marat Orazov, I would like to express my gratitude. My discussions with them on various occasions brought new perspectives to my work and a greater appreciation for the big picture.

To Professor Mary Watson, I must thank for teaching a very informative graduate level course on physical organic chemistry. Not only did I come out with a greater understanding of the fundamentals of organic chemistry, but I also came out with a stronger appreciation for the “chemical” half of chemical engineering.

I would like to thank the administrative staff of the department, including Kathie Young, Cheryl Davis-Robinson, Chil Alba, and Cinda Young. I must also

thank Mary Walsh for fitting me into Professor Lobo's busy meeting schedule and for always having some candy to jumpstart the mind.

There are too many classmates—current and past—to name who have helped me get where I am now. I have to single out Mark LaFollete and Eric Steinman for nourishing discussions over lunch. Dr. Sha Li and Jon Lym in the Vlachos group for help troubleshooting calculations.

Finally, I have to thank my family. Despite all the difficulties up until this point, they always believed that I have what it takes to be a successful academic researcher. To my wife, Mary, my world. To my brother and my parents, thank you!

May all of you continue to walk alongside me as I continue this grand adventure!

## TABLE OF CONTENTS

LIST OF TABLES .....	viii
LIST OF FIGURES .....	xi
ABSTRACT .....	xiv

### Chapter

1	INTRODUCTION .....	1
1.1	Industrial Significance of BTEX .....	1
1.2	Challenges of Current BTEX Production .....	1
1.3	Opportunities for Growing Alternative Synthetic Processes .....	2
1.4	Converting Hydrocarbons to Aromatics over Acid Zeolites .....	2
1.5	Gaps in Current Understanding of the Aromatization Mechanism in Zn/Ga-ZSM-5 and Other Acid Zeolites .....	4
1.6	Proposed Investigation of Alternative Mechanism for C6 Olefins using Hexatriene as Model Reactant .....	7
2	COMPUTATIONAL METHODS .....	9
2.1	Quantum Chemical Calculations .....	9
2.1.1	Background on Density Functional Theory .....	9
2.1.2	Theory Level and General Procedures for Calculating Energetics .....	11
2.2	Modelling approaches .....	13
2.3	Models Considered .....	14
3	HEXATRIENE-HEXATRIENE DIELS ALDER REACTIONS IN THE GAS PHASE .....	16
3.1	Introduction .....	16
3.2	Methods .....	18
3.2.1	Reactions Considered .....	18
3.2.2	Computational Details .....	19

3.3	Results .....	20
4	PERICYCLIC ELECTROCYCLIZATION OF HEXATRIENE IN THE PRESENCE OF A CATION-EXCHANGED ZEOLITE CATALYST .....	22
4.1	Introduction .....	22
4.2	Methods .....	25
4.2.1	Cations and Cation-Exchanged Zeolite Models .....	25
4.2.2	Computational Details .....	29
4.3	Results .....	30
4.3.1	Calculated $\Delta G^{\ddagger}$ for Gas-Phase Electrocyclization is the Same Regardless of Basis Sets .....	30
4.3.2	Cation Size Plays Some Role in Catalysis .....	31
4.3.3	Zeolite Clusters Lower Activation Energy without Influencing Interaction Distances .....	37
5	CARBOCATION MEDIATED CYCLIZATION OF HEXATRIENE .....	38
5.1	Introduction .....	38
5.2	Methods .....	42
5.2.1	Reactions Considered .....	42
5.2.2	Calculation Details .....	43
5.3	Results .....	45
5.3.1	Two Independent Gas-Phase Carbocation Mediated Cyclization Mechanisms .....	45
5.3.2	Alternative Mechanism has Smaller RDS in Both Gas Phase and Cluster Calculations .....	49
6	COMPARISON OF MECHANISMS AND IMPACTS ON FUTURE WORK .....	55
6.1	Low Alkoxide Strength and Heats of Adsorption for Hexatriene and Cyclohexadiene .....	55
6.2	Electrocyclization and Carbocation Mediated Cyclization are Predicted to be the Dominant Cyclization Pathways for Hexatriene in Cation-Exchanged Faujasite .....	56
6.3	Future Directions with Microkinetic Modelling and <i>Ab Initio</i> Molecular Dynamics .....	58

REFERENCES .....	61
------------------	----

Appendix

A	SUPPORTING DATA FOR DIELS-ALDER STUDIES .....	69
B	SUPPORTING DATA FOR ELECTROCYCLIZATION STUDIES .....	75
C	SUPPORTING INFORMATION FOR CARBOCATION STUDIES .....	90
D	STRUCTURE INFORMATION FOR OPTIMIZED ZEOLITE CLUSTERS	94

## LIST OF TABLES

Table 4.1:	Comparison of $\Delta G^{\ddagger}$ for gas phase cation-mediated electrocyclization of cis-hexatriene for 4 different basis sets.....	31
Table A.1:	DFT-calculated $\Delta E^{\ddagger}$ (Single Point Electronic energy), $\Delta H^{\ddagger}$ , $\Delta G^{\ddagger}$ of the 12 Diels-Alder Cycloadditions using an energy span approach at the M06-2X/6-31g(d,p) level of theory.....	69
Table A.2:	DFT-calculated $\Delta E^{\ddagger}$ (Single Point Electronic energy), $\Delta H^{\ddagger}$ , $\Delta G^{\ddagger}$ of the 12 Diels-Alder Cycloadditions using a preceding intermediate approach at the M06-2X/6-31g(d,p) level of theory.....	70
Table A.3:	DFT-calculated $\Delta E^{\circ}$ (Single Point Electronic energy), $\Delta H^{\circ}$ , $\Delta G^{\circ}$ of reaction for the 12 Diels-Alder Cycloadditions the M06-2X/6-31g(d,p) level of theory.....	71
Table A.4A:	Summary (Part A) of log files for specific DFT calculations (Diels Alder).....	71
Table A.4B:	Summary (Part B) of log files for specific DFT calculations (Diels Alder).....	73
Table B.1:	DFT-calculated $\Delta E^{\ddagger}$ (Single Point Electronic energy), $\Delta H^{\ddagger}$ , $\Delta G^{\ddagger}$ for monovalent cation-mediate electrocyclization in the gas phase using various basis sets at the M06-2X level of theory.....	75
Table B.2A:	Summary (Part A) of log files for monovalent cation-mediated electrocyclization at the M06-2X/6-31g(d,p) level of theory.....	76
Table B.2B:	Summary (Part B) of log files for monovalent cation-mediated electrocyclization at the M06-2X/6-31g(d,p) level of theory.....	77
Table B.3A:	Summary (Part A) of log files for monovalent cation-mediated electrocyclization at the M06-2X/6-311g(3df,2pd) level of theory.....	78
Table B.3B:	Summary (Part B) of log files for monovalent cation-mediated electrocyclization at the M06-2X/6-311g(3df,2pd) level of theory.....	79

Table B.4A: Summary (Part A) of log files for monovalent cation-mediated electrocyclization at the M06-2X/def2svp level of theory .....	80
Table B.4B: Summary (Part B) of log files for monovalent cation-mediated electrocyclization at the M06-2X/def2svp level of theory .....	81
Table B.5A: Summary (Part A) of log files for monovalent cation-mediated electrocyclization at the M06-2X/def2tzvpp level of theory.....	82
Table B.5B: Summary (Part B) of log files for monovalent cation-mediated electrocyclization at the M06-2X/def2tzvpp level of theory.....	83
Table B.6: Crystal ionic radii of relevant cations.....	84
Table B.7: DFT-calculated $\Delta E^{\circ\dagger}$ (Single Point Electronic energy), $\Delta H^{\circ\dagger}$ , $\Delta G^{\circ\dagger}$ for divalent cation-mediate electrocyclization in the gas phase at the M06-2X/6-31g(d,p) level of theory.....	84
Table B.8: Summary of log files for divalent cation-mediated electrocyclization at the M06-2X/6-31g(d,p) level of theory .....	85
Table B.9: DFT-calculated $\Delta E^{\circ\dagger}$ (Single Point Electronic energy), $\Delta H^{\circ\dagger}$ , $\Delta G^{\circ\dagger}$ for cation-mediate electrocyclization in the FAU cluster (Site II) at the M06-2X/6-31g(d,p) or M06-2X/def2svp (*) level of theory .....	86
Table B.10: Summary of log files for electrocyclization at FAU Site II at the M06-2X/6-31g(d,p) or M06-2X/def2svp (Rb, Cs) level of theory .....	86
Table B.11: Interaction distances between cation and hexatriene in the various transition states .....	88
Table B.12: DFT-calculated $\Delta E^{\circ\dagger}$ (Single Point Electronic energy), $\Delta H^{\circ\dagger}$ , $\Delta G^{\circ\dagger}$ for cation-mediate electrocyclization in the FAU cluster (Site III) at the M06-2X/6-31g(d,p) level of theory.....	88
Table B.13: Summary of log files for electrocyclization at FAU Site III at the M06-2X/6-31g(d,p) level of theory.....	89
Table C.1A: Gas phase calculation results for the Poutsma mechanism (electronic and zero point corrected energies).....	90
Table C.1B: Gas phase calculation results for the Poutsma mechanism (thermal corrections for internal energy, enthalpy, and free energy) .....	90

Table C.2A: Gas phase calculation results for the Alternative mechanism (electronic and zero point corrected energies) .....	91
Table C.2.B: Gas phase calculation results for the Alternative mechanism (thermal corrections for internal energy, enthalpy, and free energy) .....	91
Table C.3A: FAU zeolite cluster calculation results for the Poutsma mechanism (electronic and zero point corrected energies) .....	92
Table C.3B: FAU zeolite cluster calculation results for the Poutsma mechanism (thermal corrections for internal energy, enthalpy, and free energy) .....	92
Table C.4A: FAU zeolite cluster calculation results for the Alternative mechanism (electronic and zero point corrected energies) .....	93
Table C.4B: FAU zeolite cluster calculation results for the Alternative mechanism ..	93
Table D.1: Structure information for bare FAUH Brønsted acid site cluster .....	94
Table D.2: Structure information for bare FAU cation exchange site II cluster .....	97
Table D.3 Structure information for bare FAU cation exchange site III cluster .....	99

## LIST OF FIGURES

Figure 1.1:	Summary of overall mechanistic steps proposed by Ono to convert light alkanes to aromatics using zeolite catalysts .....	5
Figure 1.2:	Example of a dual-cycle carbon pool mechanism with an aromatic cycle (orange) and an olefin cycle (green) .....	6
Figure 3.1:	Arrow pushing mechanism for Diels-Alder cycloaddition (Top). Diels-Alder transition state shown with interacting orbitals (Bottom) ...	16
Figure 3.2:	Substituted diene and dienophile and the resulting stereochemistry of the final cycloaddition product.....	17
Figure 3.3:	The 12 Diels-Alder cycloadducts of two 1,3,5-hexatriene molecules studied .....	18
Figure 3.4:	$\Delta G^{\ddagger}$ for the 12 Diels-Alder cycloadditions investigated in the gas phase at the M06-2X/6-31g(d,p) level of theory .....	20
Figure 4.1:	The electron arrow pushing mechanism for pericyclic electrocyclization of cis-1,3,5-hexatriene to form 1,3-cyclohexadiene (top) and corresponding diagram of interacting orbitals during the bond rearrangement (bottom).....	23
Figure 4.2:	Framework topology of Faujasite and location of cation exchange sites .....	25
Figure 4.3:	Optimized quantum cluster models for Site II (Left) and III (Right) cation exchange sites shown with Li <sup>+</sup> cation (Magenta), aluminum (Pink), silicon (gray), oxygen (Red), and hydrogen (white) .....	26
Figure 4.4:	Simplified diagrams of various structures for Lewis acid sites on the surface of zeolites for monovalent cations and Zn <sup>2+</sup> .....	27
Figure 4.5:	Next-nearest neighbor (2N) configuration (Left) and Next-next-nearest neighbor (3N) configuration for aluminum tetrahedral in the Site II cluster model. Zn <sup>2+</sup> cation (Purple), aluminum (Pink), silicon (gray), oxygen (Red), and hydrogen (white).....	28

Figure 4.6:	$\Delta G^{\ddagger}$ in kcal/mol calculated at the M06-2X/6-31g(d,p) level of theory for cation mediated electrocyclization in the gas phase and in Faujasite cation exchange sites plotted against the crystal ionic radius of the cation .....	33
Figure 4.7:	Comparison of cation-transition state orientations in the gas phase and zeolite cluster models for $\text{Li}^+$ . $\text{Li}^+$ cation (Magenta), aluminum (Pink), silicon (Gray), carbon (Dark Gray), oxygen (Red), and hydrogen (white) .....	34
Figure 4.8:	Minimum interaction distance between cation and transition state plotted against crystal ionic radius of the cation .....	36
Figure 5.1:	Reproduction of the cyclization mechanism for 1,4-hexadiene cyclization via carbocation intermediates established by Joshi et al.....	38
Figure 5.2:	A consensus of literature mechanisms that trace their roots to the work of Poutsma that describes the conversion of hexatriene to cyclohexadiene via carbocation intermediates .....	39
Figure 5.3:	Summary of Olah's observations on cyclic carbocation rearrangements .....	40
Figure 5.4:	Extension of Olah's findings on carbocation rearrangements based on calculations in this work (blue box) .....	41
Figure 5.5:	Quantum cluster built for the Brønsted acid site located as shown on the left in Faujasite .....	44
Figure 5.6:	Detailed version of the Poutsma mechanism developed in this thesis ....	45
Figure 5.7:	Rendering of the final cyclization transition states in the gas phase for the Poutsma (left) and Alternative (right) mechanisms.....	46
Figure 5.8:	Rendering of the ring expansion transition states in the gas phase for the Poutsma (left) and Alternative (right) mechanisms.....	47
Figure 5.9:	The Alternative mechanism in detail.....	48
Figure 5.10:	Reaction coordinate diagram comparing Poutsma (Red) and Alternative (Blue) reaction mechanism in the gas phase .....	50
Figure 5.11:	Reaction coordinate diagram comparing Poutsma (Red) and Alternative (Blue) reaction mechanism in the H-FAU cluster .....	52

Figure 5.12: Rendering of Poutsma (Left) and Alternative (Right) ring expansion transition states interacting with the Faujasite Brønsted acid site cluster .....	54
Figure 6.1: Reaction coordinate diagram comparing the Alternative carbocation mechanism in Faujasite to electrocyclization in the gas phase and on $Zn^{2+}$ in a 2N configuration of Site II in Faujasite.....	57

## ABSTRACT

Aromatic compounds are an important segment of the chemical industry that impacts many aspects of everyday life. Although the majority of aromatic compounds are made from petroleum, there is renewed interest in converting shale-gas derived light alkanes into aromatics over acid zeolite catalysts. It is known that these catalysts are good at converting light hydrocarbons into higher olefins, which can then form aromatic compounds. However, there is very little mechanistic understanding about the elementary steps and intermediates between linear olefins and cyclic precursors to aromatics.

Hexatriene was used as a model olefin to gain new insights into the cyclization mechanisms that happen in acid zeolites. With the aid of electronic structure calculations, mechanisms involving Diels-Alder cycloaddition, pericyclic electrocyclization, and carbocation mediated cyclization were investigated in the gas phase. In the process, new and more complete mechanisms were developed to connect hexatriene to cyclic products via carbocation intermediates. The effect of zeolite acid sites on these reaction pathways was then investigated. This work paves a new path towards understanding aromatization in acid zeolites by shedding light on the underlying fundamental chemistry.

## **Chapter 1**

### **INTRODUCTION**

#### **1.1 Industrial Significance of BTEX**

Benzene, toluene, ethylbenzene, and xylenes (BTEX) make up an important segment of the global chemical industry. The everyday impact of BTEX production is most visible in the plastics industry. Benzene and ethyl-benzene are precursors to the monomers used to make polystyrenes, polycarbonates, and nylons. Toluene is a precursor to the monomers for polyurethanes and xylenes are precursors to polyesters.[1,2] Moreover, many of the intermediates produced from BTEX are also precursors to many fine and special chemicals, as well as fuel additives.[3] Assessing benzene on its own, global demand was about 46 million metric tons in 2015. At one point in time, benzene was ranked the 15th most produced chemical in the United States.[1]

#### **1.2 Challenges of Current BTEX Production**

Although BTEX can be synthesized through various processes and chemical pathways, the majority is produced via catalytic reforming of naphtha and naphtha steam cracking, where BTEX is produced as a side product.[3,4] These processes are very energy intensive: at peak production, benzene production was ranked 4th in energy consumption among chemicals produced in the United States.[1]

About 60-80% of the cost of BTEX production comes from the price of naphtha, a petroleum-based feedstock.[4,5] Global production and supply of BTEX

compounds is therefore tied to the demand for naphtha derived products, namely fuels and petroleum products, not actual global demand for BTEX. Paradoxically, it is possible for BTEX production to decrease while demand increases, as was the case in the United States around 2013. Naphtha-free processes for producing BTEX could decouple the economics of BTEX production from the rest of the petrochemical industry.[3,5]

### **1.3 Opportunities for Growing Alternative Synthetic Processes**

Over the decades, more direct synthesis routes have been developed for alternative feedstocks. Methanol derived from renewable sources, such as lignocellulosic biomass[6] or photochemical production coupled with carbon capture technologies and/or electrolytic hydrogen production,[7] can be converted to aromatics over zeolite catalysts through a methanol-to-olefins (MTO) process.[8] Light alkanes are also becoming more available due to rapid growth since the mid-2010s in the production of shale gas, a source of not only natural gas, but also natural gas “liquids” such as ethane and propane.[1] Acid zeolite catalysts are also known to convert methanol and light alkanes to olefins, which then also form aromatics within certain zeolites.[9-11]

### **1.4 Converting Hydrocarbons to Aromatics over Acid Zeolites**

Zeolites are microporous, crystalline aluminosilicates that can be synthesized with numerous topologies as well as varying ratios of aluminum to silicon. The framework itself is comprised of tetrahedral aluminum and silicon atoms bonded to oxygen atoms that are shared between two neighboring “T atoms”.[12] In the zeolite, every aluminum tetrahedron has a  $-1$  formal charge that must be balanced by a

counter-cation, such as ammonium ( $\text{NH}_4^+$ ). Protons ( $\text{H}^+$ ) can also act as the counter-ion to create Brønsted acid sites (BAS).[13] The counter-ion at aluminum sites in zeolites can be exchanged for other metal cations, including lithium, sodium, and even divalent cations such as zinc cations that also have Lewis acid properties. In short, these aluminum centers act as Lewis acids. Typically, zeolites with lower silicon to aluminum ratios have more, but weaker acid sites.[12,14]

Acid zeolites have been ubiquitous in the petrochemical industry for decades. Many industrial applications of zeolites rely on these acid sites for heterogeneous catalysis.[11,15] Early on, acid zeolites were identified as potential catalysts for the direct conversion of low-carbon number alkanes to benzene and other aromatics. The framework ZSM-5 stood out among all others.[9,10]

ZSM-5, also known as the MFI framework type, has two sets of channels that run almost perpendicular to each other. Straight channels with an effective diameter of 5.4-5.6 Å intersect with sinusoidal channels with an effective diameter of 5.1-5.4 Å. At the intersection of these channels are 10-membered ring openings. Such a ring is comprised of 10 oxygen atoms and 10 silicon or aluminum atoms.[16]

H-ZSM-5, a ZSM-5 with only Brønsted acid sites, can be exchanged with  $\text{Zn}^{2+}$  or  $\text{Ga}^{3+}$  cations to form Zn-ZSM-5 or Ga-ZSM-5, respectively. Unlike monovalent cations that exchange one-to-one with protons at Brønsted acid sites to form Lewis acid sites, multivalent cations can exist in multiple forms inside a zeolite. Zinc can exist as divalent zinc cation associated with two “paired” aluminum sites; as zinc hydroxide ( $\text{ZnOH}^+$ ) associated with one acid site; or as zinc oxide ( $\text{ZnO}$ ) clusters. Furthermore, adjacent zinc cations might be bridged by an oxygen atom to form a dimer. It is difficult to characterize and differentiate the different species.[4] Both Zn-

ZSM-5 and Ga-ZSM-5 have been shown to selectively transform light hydrocarbons into aromatics and are used in the patented M2 forming process by ExxonMobil and Cyclar process by UOP.[17]

### **1.5 Gaps in Current Understanding of the Aromatization Mechanism in Zn/Ga-ZSM-5 and Other Acid Zeolites**

One of the oldest and most extensive studies of hydrocarbon aromatization in ZSM-5 was conducted by Ono et al. Linear C<sub>2</sub>-C<sub>6</sub> alkanes were individually reacted over H-ZSM-5, Zn-ZSM-5, and Ga-ZSM-5 at 773K. Based on the resulting product distributions, an acid-catalyzed reaction mechanism was put forth based on earlier work in the literature.[18] Light alkanes are cracked to form ethylene, which then oligomerizes into a linear hexadienyl cation near a Brønsted acid site. This then forms a methyl-cyclopentenyl cation that rearranges into a cyclohexenyl cation that eventually gets dehydrogenated to form benzene. They claimed their ratio of alkanes to aromatics in the product distribution for H-ZSM-5 was consistent with this mechanism. However, the product distribution was very different over Zn-ZSM-5 and Ga-ZSM-5, which was evidence that the exchanged metals affect selectivity through alternative mechanisms that were yet to be determined.[10]

As stated earlier, multivalent cations can form multiple types of sites within the zeolite. Given how difficult it is to characterize and differentiate different types of cation sites, elucidating the catalytic role of each type of cation site remains a challenge. Furthermore, hydrocarbon aromatization generates a lot of coke as well as cracking products inside of the zeolite pore, leading to catalyst deactivation. In fact, one of the motivations for better understanding the aromatization mechanism is to design better catalysts that produce less coke.[19,20]

Work led by Iglesia used a combination of kinetic isotope effects to identify rate-limiting steps, and in-situ x-ray absorption spectroscopy experiments to better characterize the zinc species inside of Zn-ZSM-5.[21,22] Combined with studies of methanol-to-olefins and methanol-to-hydrocarbons processes in acid zeolites, more complex pathways have been put forth that connect various olefins and aromatics in a “carbon pool”. In short, early NMR studies suggested that acid zeolites form large hydrocarbon species that are trapped within the pores. These species form an initial “carbon pool” from which desired and conventionally measured products could form, including aromatics, olefins, and alkanes. This idea also explains a phenomenon observed across many aromatization studies: the induction period. A certain amount of contact time between the reactant feed and catalyst is required before product conversion is observed.[23-26]

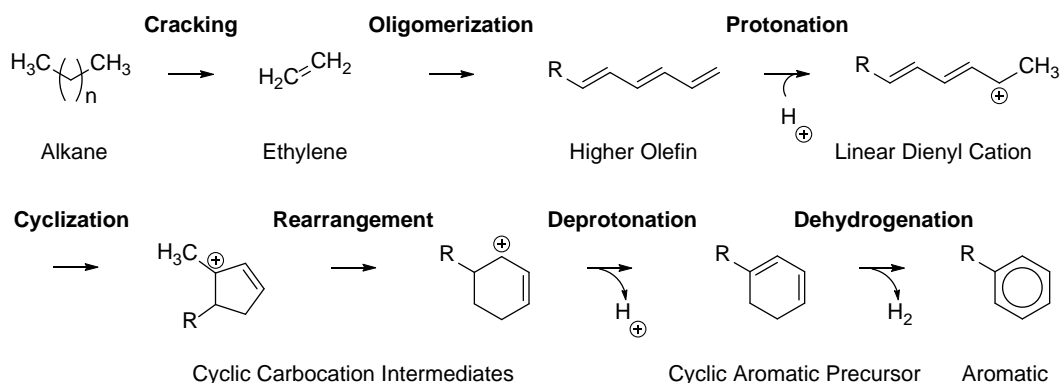


Figure 1.1: Summary of overall mechanistic steps proposed by Ono to convert light alkanes to aromatics using zeolite catalysts.[10,17,18,27]

The nature of these pools and the mechanistic cycles they contribute to has evolved over the years as other zeolites and light feedstocks have been

investigated.[25,27] Dehydrogenation and oligomerization are key processes towards aromatization.[4] But in spite of all of these advancements in the overall reaction network, there is still very little mechanistic detail or description of elementary steps that actually connect the proposed stable intermediates for zeolite hydrocarbon aromatization. One step in particular, cyclization, has been overlooked in terms of mechanistic detail. In short, there is very little understanding about how a linear molecule with at least six carbons can cyclize to form a cyclic intermediate that could later be dehydrogenated to form aromatics.

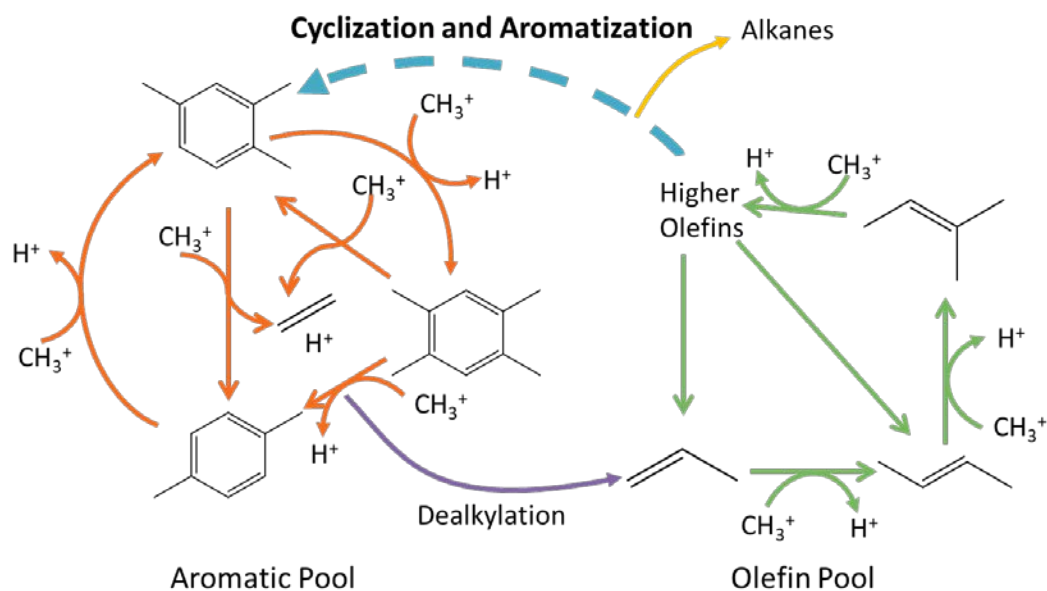


Figure 1.2: Example of a dual-cycle carbon pool mechanism with an aromatic cycle (orange) and an olefin cycle (green). Both cycles are connected by a mechanism for cyclization and aromatization (blue) that should be related to the earlier work of Ono and others. The details of such a mechanism are still not fully understood.[8,10,17,21-27]

## 1.6 Proposed Investigation of Alternative Mechanism for C6 Olefins using Hexatriene as Model Reactant

Decades of research on hydrocarbon aromatization in ZSM-5 has focused on the initial formation and oligomerization of olefins and the cycles that form the different aromatic species. However, less focus has been put on the cyclization steps that would be required to transform linear hydrocarbons into cyclic molecules that connect these reaction networks. At minimum, a C6 olefin is required to cyclize into a cyclic C6 molecule. There is little understanding of how this happens or what role the zeolite may play in these reactions. Understanding the mechanism of initial cyclization could provide insights into building better catalysts that directly produce aromatics from linear hydrocarbons while producing less coke and other unwanted products.

Given current understanding of olefin formation and growth in zeolites, 1,3,5-hexatriene is a reasonable starting point for studying cyclization. Recent experimental work from various groups have shown that adsorbing lower olefins, such as ethylene and 1-butene, will readily form polyenes inside Zn-ZSM-5 and other zeolites at temperatures as mild as 200°C. These polyenes were detected using *in situ* infrared (IR) and UV-vis spectroscopy. By combining the two techniques, Dwyer and his collaborators were able to show in several studies that the systems of 3 or more conjugated  $\pi$  bonds that were being detected did not belong to aromatic species.[29] Thus, experimental evidence shows that linear conjugated olefins with 3 or more double bonds can be formed from lower olefins in various acid zeolites.

Hexatriene is the simplest olefin with at least 3 conjugated double bonds, so it provides a good starting point for studying triene cyclization over zeolites. While there have been a handful of studies of cyclization of less conjugated C6 olefins, almost no work has been done for trienes. Due to extended conjugation, trienes can access

chemistry that olefins with less conjugation cannot. In particular, hexatriene could theoretically participate in pericyclic electrocyclization, a reaction that requires  $6\pi$  electrons. Hexatriene can also cyclize through Diels-Alder cycloaddition, a bimolecular pericyclic reaction. Both of these reactions do not involve acid catalysts or carbocations, but are known for fast rates that can be influenced by Lewis acids or cationic systems.[30] Of course, hexatriene could also participate in carbocation mediated cyclization mechanisms that may or may not be analogous to those developed for C<sub>6</sub> dienes. This means intermediates are carbocations that may or may not form alkoxide species when protonated by zeolite Brønsted acid sites.[10,17,18]

This thesis explores the possible mechanisms by which 1,3,5-hexatriene can cyclize to form a cyclic C<sub>6</sub> molecule. The three mechanisms explored are Diels-Alder cycloaddition, pericyclic electrocyclization, and carbocation mediated cyclization. Due to the availability of hexatriene and the difficulty to synthesize in high purity, experiments would be difficult and costly. Instead, computational calculations are used to study these reaction pathways and determine which are most likely to occur in both the gas phase and in the vicinity of zeolite acid sites. The results of these studies, which use Density Functional Theory (DFT), could potentially guide future experiments on triene cyclization in acid zeolites.

## Chapter 2

### COMPUTATIONAL METHODS

#### 2.1 Quantum Chemical Calculations

##### 2.1.1 Background on Density Functional Theory

In ideality, exact solutions to the time-independent Schrödinger equation would provide accurate electronic energies for molecular systems. These energies would form the basis for estimating macroscopic thermodynamic quantities such as internal energy, enthalpy, and Gibb's free energy. Mapping these quantities for reactants, intermediates, transition states, and products along a reaction coordinate diagram would provide *ab initio* insight into the kinetics and thermodynamics of a reaction network.

In practice, the Schrödinger equation can not be solved analytically for a many-electron system because of electron-electron repulsion. Applying the Born-Oppenheimer approximation, only electron wave equations are solved based on specified nuclear coordinates. This is because electrons have about three orders of magnitude less mass than nuclei, making the adiabatic assumption valid: nuclei essentially appear motionless to the electrons. Thus, interactions between nuclei and nuclei-electron pairs are simplified in the full wave equation.[31-33]

Hartree-Fock and Density functional theory (DFT) are some of the methods for obtaining a numerical solution to the electronic wave equation. Hartree-Fock methods approximate a many-electron wave equation with a single-electron and the field that

would be generated on average by the other electrons in the system. Linear combinations of atomic orbitals are used to build molecular orbitals. Linear combinations of these molecular orbitals are used as trial solutions to the wave function. The coefficients of this linear combination are varied until the energy of the system is minimized. Hartree-Fock methods always overestimate electronic energies, but can be corrected by calculating correlation energies using post-Hartree-Fock methods, such as Møller–Plesset perturbation theory with up to fourth order perturbation terms (MP, MP2, MP3, and MP4).[34] Computational work referenced in this thesis from the previous century often compared Møller–Plesset alongside DFT because it is much more computationally inexpensive compared to more accurate post-Hartree-Fock methods, such as Coupled Cluster (CC) methods and their successors. Even with modern computational resources, CC calculations are still limited to very small molecular systems.[35]

Density Functional Theory approximates a many-electron wave equation with a system described by a single distribution of electron density and a functional of electron density that describes the energy of the system. This functional captures the kinetic energy of non-interacting electrons, nuclei-electron interactions, and exchange-correlation.[36-38] The ground state electron density is obtained by minimizing the energy functional.[39] By applying Kohn-Sham theory, Coulombic electron-electron interactions can be modelled with an effective potential. Each functional attempts to correct for self-interaction and exchange-correlation differently.[40] The generalized gradient approximation (GGA) models exchange-correlation as a function of the electron density and the gradient of electron density at any point in space. Hybrid GGA functionals mix in Hartree-Fock exchange-correlation energy. Exchange

correlation is exact in Hartree-Fock and post-Hartree-Fock methods, but not in DFT. Hybrid-meta GGA functionals such as M06-2X also employ empirical data to calculate exchange-correlation.[41]

DFT is computationally inexpensive while yielding similar results to post-Hartree-Fock methods. Alongside advances in computational resources and user-friendly software packages, DFT has become commonplace in many fields, including that of zeolite catalysis.[42]

### **2.1.2 Theory Level and General Procedures for Calculating Energetics**

In general, all calculations were performed using Gaussian 09, Revision A.2 using the M06-2X DFT functional. M06-2X is a hybrid functional that incorporates 54% Hartree-Fock exchange that has been used extensively in the field of zeolite catalysis. It has been shown to accurately predict thermochemistry and kinetics in a number of studies that use zeolite cluster models. Because of computational costs, the majority of calculations were done with the 6-31g(d,p) basis set. This is a commonly used basis set for larger, non-embedded quantum cluster calculations. Some calculations for gas-phase reactions were also performed with the larger 6-311g(3df,2pd) basis set. In general, a larger basis set should yield more accurate results, but can only be compared to calculations performed at the same level of theory.[43]

Ground state structures for reactants, intermediates, products, and their complexes with zeolite clusters were obtained from energy optimization calculations. All atoms, with the exception of terminating hydrogens on clusters, were allowed to fully relax. After obtaining the electronic energy of a given system, a vibrational

frequency calculation was performed to calculate thermal corrections. These vibrational frequency calculations assume a harmonic oscillator model for all bonds.

For well-studied reaction mechanisms, guesses for transition state structures could be used as starting points for transition state optimization calculations. These calculations are analogous to energy optimizations, except Gaussian searches for a structure with only one imaginary vibrational frequency. Vibrational analysis is also used to obtain thermal corrections to electronic energies of optimized transition state structures.

For less understood mechanisms, possible reaction coordinates were “scanned.” A constraint is placed on geometry optimizations starting from a stationary point. This constraint, whether it is atomic distance, bond angle, or dihedral angle, is varied stepwise until it matches the next expected intermediate on the reaction pathway. The structure with the highest energy along this hypothetical reaction coordinate is chosen as a guess for a transition state optimization.

Once transition state structures are obtained, they are validated using intrinsic reaction coordinate (IRC) calculations. This calculation starts from the transition state and determines a minimum energy reaction pathway. The purpose of this type of calculation is to attempt to identify the stationary points that are connected by the transition state structure and verify that it is a relevant transition state to the mechanism of interest.

In general, heats of reaction and free energy change of reaction are defined as the difference between the respective thermally corrected electronic energies of the product minus the reactant. Activation energies are defined as the difference between the transition state and the reactant immediately prior. The reference state for most

reaction coordinate diagrams is the reactants (and catalyst) held infinitely apart. Effectively, this is simply the sum of (thermally corrected) electronic energies of each reactant and catalyst system calculated individually.

## **2.2 Modelling approaches**

Despite advances in computational power, computational time and resources are still finite. There will always be tradeoffs between accuracy of calculated energies and computational costs. Thus, after determining if quantum calculations are appropriate and necessary for a given research problem, it is also essential to model just enough of the physical system to capture the most relevant interactions while keeping computational costs down. DFT models of reactions in zeolites can be divided into two broad categories: periodic boundary condition calculations and cluster models.

Given that zeolites are three-dimensional crystalline materials, there are many researchers who regard periodic-DFT models as a “gold standard” for computational studies of zeolites. In such a model, the unit cell is effectively extended infinitely in all directions through the use of periodic boundary conditions. Periodic-DFT calculations are not feasible for the majority of zeolite frameworks and reactions of interest.[43] This is because the computational costs for most methods of quantum calculation scale with the number of electrons. The majority of industrially relevant frameworks have large unit cells with hundreds of atoms and consequently about ten times as many electrons.[44] Only a handful of small pore zeolites, such as Chabazite can be extensively studied with periodic-DFT calculations.[43]

Cluster models and embedded cluster models only consider atoms within the vicinity of the active site. In zeolite studies, the most expensive calculations are often

performed on the atoms within about 5-7 Å of the reactant and/or acid site. Embedded cluster models often model atoms further away with less expensive calculations, such as a lower level of theory or smaller basis set. With the advent of the ONIOM method, it has become more common place to use molecular mechanics or semi-empirical methods.[45] These methods are sufficient to capture the effects of long range dispersion without spending excessive computational time. Today, a cluster can encompass about 200 atoms and use less computational time than a periodic-DFT calculation while maintaining accuracy.[46-48] Cluster models were used in this study to model zeolite active sites. Then intention was to perform a preliminary study before performing more expensive calculations with an ONIOM cluster.

### 2.3 Models Considered

For all cluster calculations, Faujasite was chosen as a model zeolite for these studies because like ZSM-5, its pores are large enough to accommodate aromatic rings; however, all of its Lewis acid sites and the majority of its Brønsted acid sites are well characterized experimentally and computationally. With regards to Lewis acid sites and electrocyclization, Faujasite has three crystallographically distinct sites where cations can be exchanged. Only Site II and Site III face the supercage of the zeolite, which has a sufficient pore diameter to accommodate possible complexes between hexatriene and the cation site.[49,50] Cluster models of acid sites include framework atoms within 5.5Å of the cation. Terminating hydrogen atoms were fixed to all dangling bonds. All other atoms were allowed to relax.

Cation clusters were first optimized prior to incorporating hydrocarbons into subsequent calculations. The zeolite was assumed to have small effects on the geometries of intermediates and transition states. For this reason, the geometries of

reactants and products were placed in the vicinity of the cluster model as a starting point for geometry optimizations. Once the cluster-intermediate systems were optimized, the transition state structures from the gas phase could be substituted for the intermediate it most resembles at the same interaction distance with the zeolite. This produced a better initial guess for a cluster-transition state optimization, thus reducing computational time. This is important because transition state optimizations generally take longer than geometry optimizations of ground states.

A similar approach was taken for Brønsted acid sites. A cluster was built around one of the most accessible acid sites in Faujasite. This site was well studied computationally by other prominent research groups.[51] Faujasite was used again to be able to make better comparisons with cluster models for the non-BAS mechanisms.

## Chapter 3

### HEXATRIENE-HEXATRIENE DIELS ALDER REACTIONS IN THE GAS PHASE

#### 3.1 Introduction

The Diels-Alder cycloaddition is an example of a pericyclic reaction in organic chemistry. It can occur between a conjugated diene and a dienophile, typically an alkene, through a symmetry-allowed concerted mechanism involving a single transition state. This cyclic transition state is a suprafacial/suprafacial interaction between the  $4\pi$  electron system of the conjugated diene in an s-cis conformation and the  $2\pi$  electron system of the dienophile. Hence, the Diels-Alder reaction is also classified as a [4+2] cycloaddition that occurs under thermal conditions (as opposed to photochemical). The result is 2  $\pi$  bonds being converted into 2  $\sigma$  bonds to form a cyclic product.[30]

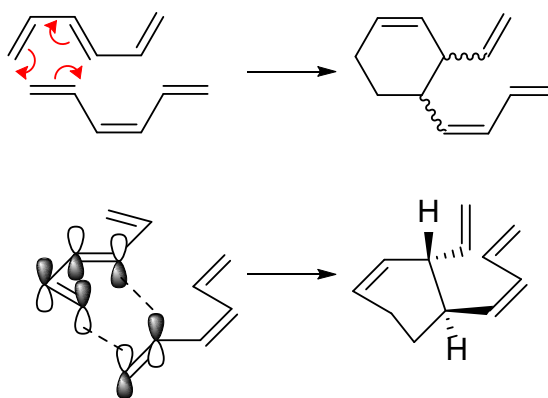


Figure 3.1: Arrow pushing mechanism for Diels-Alder cycloaddition (Top). Diels-Alder transition state shown with interacting orbitals (Bottom).

Like other pericyclic reactions, Diels-Alder cycloadditions obey Woodward-Hoffman rules for orbital symmetry. As a result, the regiochemistry and stereochemistry of products and their distribution depend on the interactions between diene and dienophile that favor certain spatial arrangements over others during the transition state. Some transition state arrangements are more favorable than others. Despite sterics, an endo product, such as an aldehyde substituent at position A of Figure 3.2, is usually favored over the exo product, which would place the substituent at position B. The effect is more pronounced with electron withdrawing or electron donating substituents on either the diene or dienophile, and this is reflected in product distributions. Secondary orbital interactions between the substituents have also been suggested as a reason for endo favored products.[30]

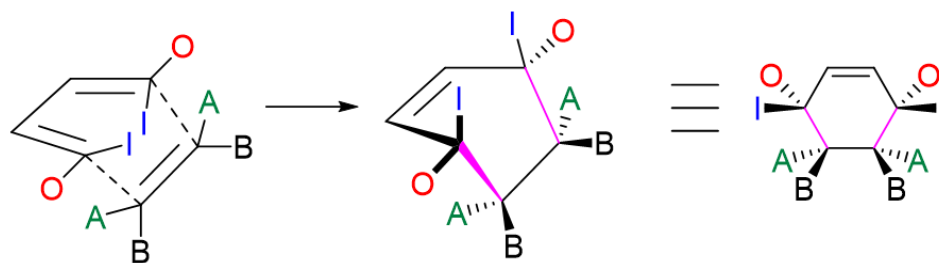


Figure 3.2: Substituted diene and dienophile and the resulting stereochemistry of the final cycloaddition product.

Although ethylene, butadiene and more conjugated alkenes could form inside of a zeolite, only Diels-Alder cycloadditions between two hexatriene molecules were considered. The goal of these calculations was to compare the calculated activation energy of Diels-Alder cycloaddition to other reaction pathways that start from pure hexatriene and end with a neutral product with a 6-membered ring.

## 3.2 Methods

### 3.2.1 Reactions Considered

Hexatriene is a conjugated system of 6  $\pi$  electrons. The triene molecule that acts as the s-cis diene can have a cis or trans double bond in the center. Only trans-hexatriene was considered in the role of diene because the cis-hexatriene with an s-cis configuration is almost identical to the transition state for pericyclic electrocyclization. As it will be shown in later chapters, the barrier to electrocyclization is lower than that of all Diels-Alder cycloadditions discussed here. Thus, it would be highly unlikely that a bimolecular reaction would occur faster than a unimolecular reaction with similar transition state geometry.

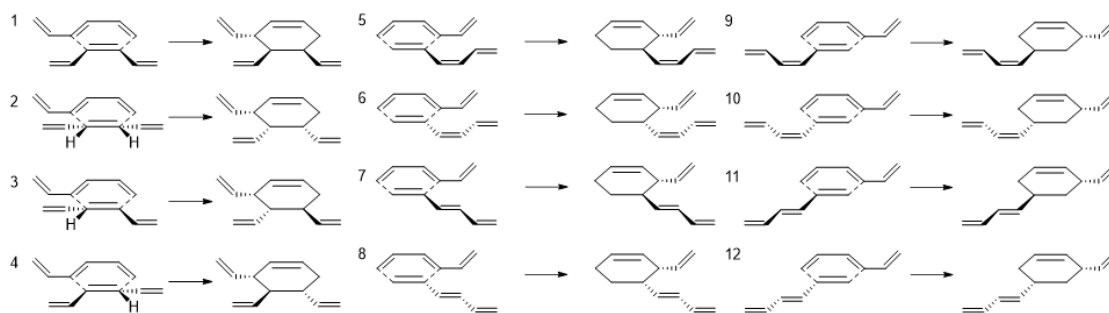


Figure 3.3: The 12 Diels-Alder cycloadducts of two 1,3,5-hexatriene molecules studied.

The second hexatriene molecule that acts as the dienophile has 3 double bonds that can be added to the dienophile as well as cis and trans isomers for the central double bond. As a result, there are 12 unique enantiomeric pairs of products that can form, depending on the orientation of the hexatriene molecules during the transition state. In theory, enantiomers should have the same energies. Likewise, if the transition

state geometries are enantiomers, then the activation energies should be the same. For this reason, calculations were performed for only a single enantiomer for each of the 12 pairs of Diels-Alder cycloadducts that can occur between a trans-hexatriene and either a cis- or trans-hexatriene, as shown in Figure 3.3. Reactions 3, 4, 7, 8, 11, and 12 occur between one cis- and one trans-hexatriene molecule while all other reactions occur between two trans-hexatriene molecules.

### 3.2.2 Computational Details

All calculations were performed using Gaussian 09, Revision A.2 at the M06-2X/6-31g(d,p) level of theory. Ground state structures for reactants and products were fully relaxed and vibrational frequencies were calculated. Transition states were obtained by some trial and error to find the appropriate separation between diene and dienophile. Overall, since the transition state geometry for Diels-Alder is well known, a good guess for the transition state could almost be constructed *ab initio*. The resulting transition state was confirmed by frequency analysis (there should only be one imaginary frequency) and by intrinsic reaction coordinate (IRC) calculations.

Thermal corrections were applied to electronic energies using the results of vibrational frequency calculations. The values reported in this chapter are either thermal corrections to enthalpy or thermal corrections to free energy calculated at 298 K. Thus, energy differences between structures may be equated to  $\Delta H^\circ$  or  $\Delta G^\circ$  respectively. As an example, the difference between the energy of a Diels-Alder transition state and two hexatriene molecules held infinitely apart is defined as the activation energy, which can be reported as a  $\Delta G^\circ^\ddagger$ .

Because gas-phase Diels-Alder had a significantly higher activation energy compared to other reactions studied in this thesis, models involving zeolite clusters

were not considered. The zeolite was not expected to lower the activation energy of the Diels-Alder cycloaddition so that it would be comparable to other competing reactions.

### 3.3 Results

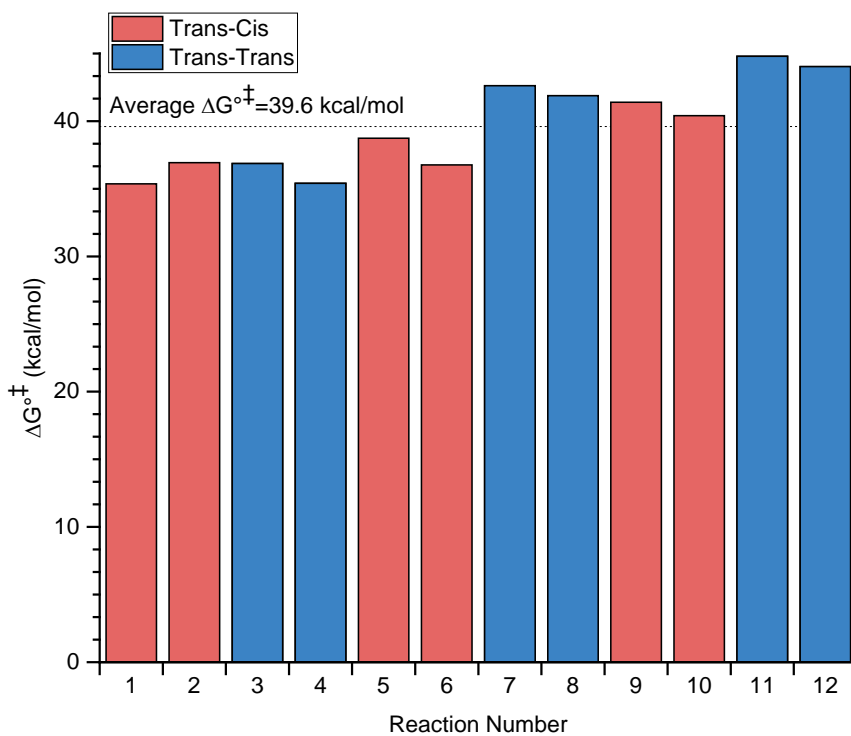


Figure 3.4:  $\Delta G^{\ddagger}$  for the 12 Diels-Alder cycloadditions investigated in the gas phase at the M06-2X/6-31g(d,p) level of theory.

Activation energies for Diels-Alder cycloaddition were calculated for all 12 reactions depicted in Figure 3.3. The average  $\Delta G^{\ddagger}$  is 39.6 kcal/mol and the lowest was for reaction 1, which occurs between two cis-hexatriene molecules with a

$\Delta G^{\ddagger}=35.4$  kcal/mol. Reactions 1-4 are cycloadditions to C3 and C4 of the dienophile and have the lowest calculated activation energies. One possible explanation is that addition to C3 and C4 of the dienophile is more entropically favored than addition to a terminal double bond of the dienophile. In the first addition, the dienophile has two free ends instead of only one in the second type of addition. In reactions 1-4, activation energies for exo transition states appear to be lower than their endo counterparts. Likely, steric hindrance wins over any secondary  $\pi$  interactions between the free ends of the diene and dienophile. After all, alkenyl substituents are neither electron withdrawing nor electron donating, which are best for accelerating Diels-Alder and favoring endo products. The expected endo product is favored in reactions 5-12, suggesting that the single free end in the dienophile can more favorably interact with the diene  $\pi$  system.

Overall, the activation energy for many of the Diels-Alder cycloadditions are higher than that of electrocyclization and carbenium ion mechanisms discussed in later chapters. This is true even for reactions that produce compact 3-substituent products that would more easily fit inside of a zeolite pore. Furthermore, the reaction is bimolecular so it should have a more significant concentration dependence compared to the unimolecular steps in electrocyclization and carbenium ion chemistry. Also, bimolecular reactions tend to have smaller  $A_0$  than unimolecular reactions because of the entropy loss from combining two molecules into one. Thus, in many cases, if the  $E_a$  is the same, the unimolecular reaction will have larger experimental rate constants and faster rates. Based on the calculated values for  $\Delta G^{\ddagger}$  these reactions, these generalizations appear to be true for hexatriene cycloaddition.[53]

## Chapter 4

### PERICYCLIC ELECTROCYCLIZATION OF HEXATRIENE IN THE PRESENCE OF A CATION-EXCHANGED ZEOLITE CATALYST

#### 4.1 Introduction

Like the Diels-Alder cycloaddition, electrocyclization is another class of pericyclic organic reactions that can occur in conjugated  $\pi$  systems. Electrocyclization occurs through a concerted mechanism involving a single transition state that must obey Woodward-Hoffman rules for orbital symmetry.[30] However, unlike Diels-Alder cycloaddition, one  $\pi$  bond is converted into one  $\sigma$  bond to form a cyclic product.

Additionally, electrocyclization can occur both thermally and photochemically, with each resulting in different stereoisomers due to differences in allowed orbital symmetry. Hexatriene has a  $4n+2$  electrons in the  $\pi$  system so the thermally-induced mechanism involves a disrotatory ring closing/opening while the photochemically-induced mechanism involves a conrotatory ring closing/opening. These disrotatory and conrotatory transition states, which are determined by orbital symmetry, dictate the product regiochemistry and stereochemistry for substituted reactants.[30] In the case of unsubstituted 1,3,5-hexatriene, no stereoisomers are produced, but it is important to correctly identify transition states with disrotatory imaginary vibrational frequencies to obtain appropriate estimates for activation energies under thermal conditions.

Jiao et al. performed DFT calculations at the B3LYP level of theory to study the effect of monovalent and divalent cations in the gas phase on the activation energy

electrocyclization of unsubstituted hexatriene. The activation energy was defined as the difference between the energies of the cation-bound reactant (hexatriene) and the cation-bound transition state. They justified their calculations by comparing their calculated activation energies for the uncatalyzed reaction, 30.6 kcal/mol, to the experimental values of  $E_a=29.9\pm 0.5$  kcal/mol and  $A_0=7.15\pm 5.2 \times 10^{11} \text{ s}^{-1}$  determined by Lewis and Steiner.[53]

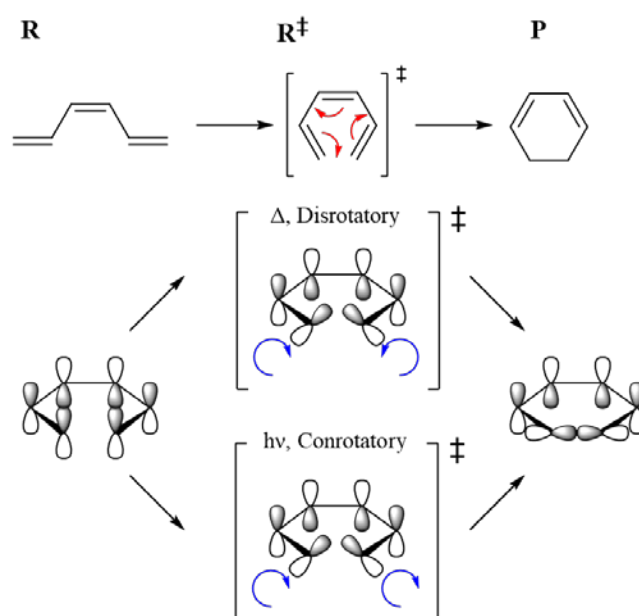


Figure 4.1: The electron arrow pushing mechanism for pericyclic electrocyclization of cis-1,3,5-hexatriene to form 1,3-cyclohexadiene (top) and corresponding diagram of interacting orbitals during the bond rearrangement (bottom). The thermally allowed disrotatory ring closing is shown in the center while the photochemically allowed conrotatory ring closing is shown on the bottom

They found that smaller cations with higher charge density had the largest catalytic effect on the electrocyclization reaction. For example, the predicted  $\Delta\Delta G^{\ddagger}$

for a lithium cation in the gas phase was  $-9.2$  kcal/mol. Although this prediction has never been verified experimentally, the predicted trends are consistent with reductions in activation energies measured for various Diels-Alder cycloadditions in the presence of perchlorate salts. The authors explain these phenomena by attributing an electrostatic effect exhibited by the cation that stabilizes the electrocyclization transition state. After all, conjugated  $\pi$  systems are highly polarizable.[53,54]

By extension, cation-exchanged zeolites could conceivably catalyze electrocyclization so long as the exchanged cation is accessible to hexatriene at the Lewis acid site. This chapter explores the possible catalytic activity of cations and cation-exchanged zeolites using modern DFT functionals and computational resources.

## 4.2 Methods

### 4.2.1 Cations and Cation-Exchanged Zeolite Models

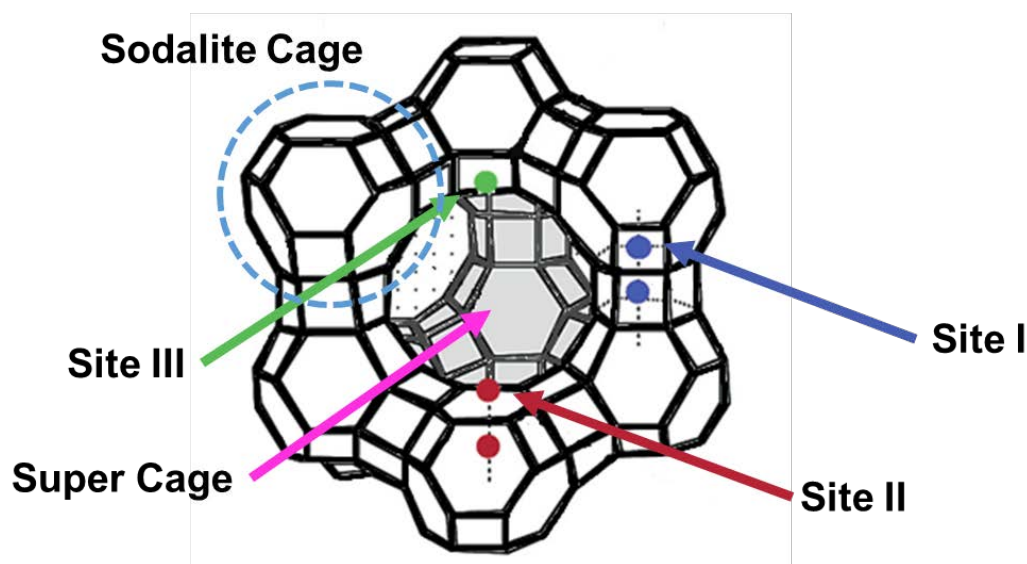


Figure 4.2: Framework topology of Faujasite and location of cation exchange sites. An example of the sodalite cage building unit is circled in blue. The super cage is the central cavity.

The catalytic effects on electrocyclization was first investigated in the gas phase for  $\text{Li}^+$ ,  $\text{Na}^+$ ,  $\text{K}^+$ ,  $\text{Rb}^+$ ,  $\text{Cs}^+$ ,  $\text{Mg}^{2+}$ ,  $\text{Zn}^{2+}$ , and  $\text{Ca}^{2+}$  cations. The reaction was also studied in quantum cluster models of cation-exchange sites in the Faujasite framework for monovalent cations and  $\text{Zn}^{2+}$ .

Faujasite was chosen as a model zeolite framework because its pores are large enough to accommodate hexatriene. There are only three crystallographically distinct sites, depicted in Figure 4.2 where cations can be exchanged and they have been

thoroughly characterized with a variety of experimental techniques, including solid state NMR and neutron diffraction. Of the three cation exchange sites, Site II and Site III face the super cage of the Faujasite unit cell and should be accessible to hexatriene and cyclohexadiene.[49,50] Quantum cluster models, depicted in Figure 4.3, were built for Site II and III by excising the region within 5.5 Å of a lithium cation placed at the center of the 6-membered and 4-membered rings of the respective acid sites. Capping hydrogens were attached to dangling bonds at the boundaries of the cluster. Site I was ignored because it does not face the super cage and should not be accessible to hexatriene through the interior of the sodalite cage. Overall, the high symmetry and structural simplicity of Faujasite could potentially mediate experiments that involve *in situ* characterization of interacting intermediates at cation-exchange sites.

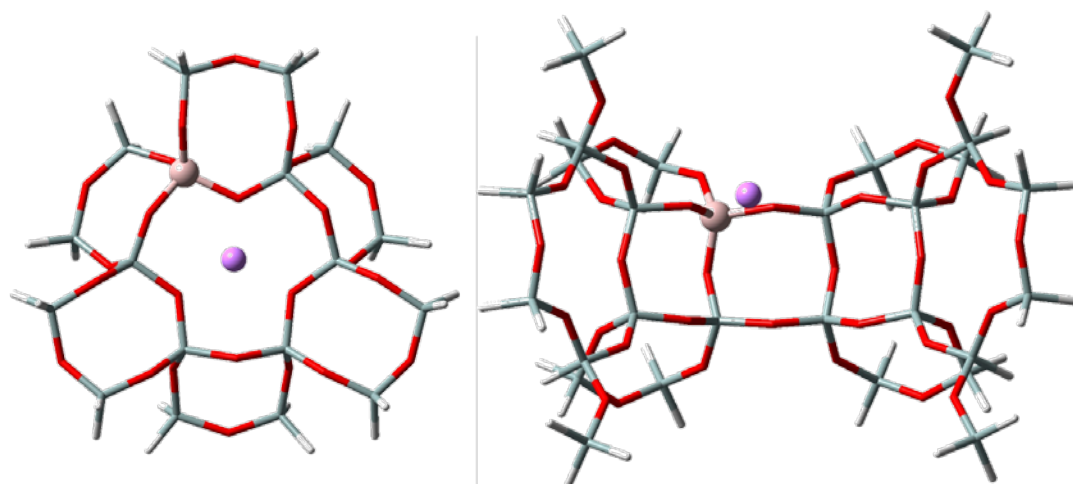


Figure 4.3: Optimized quantum cluster models for Site II (Left) and Site III (Right) cation exchange sites shown with  $\text{Li}^+$  cation (Magenta), aluminum (Pink), silicon (gray), oxygen (Red), and hydrogen (white). At Site III,  $\text{Na}^+$  and  $\text{Zn}^{2+}$  are both closer to the center of the central 4-membered ring.

Unlike monovalent cations, which exchange one-to-one with acidic protons to form Lewis acid sites, divalent zinc cation can form a variety of structures near zeolite aluminum sites that maintain proper charge balance. These include various oxide or hydroxide structures where the ratio of zinc to aluminum is 1:1 (Figure 4.4). In this study, only the structure referred to as a “paired” site will be considered. On paired sites, zinc is coordinated with two nearby aluminum tetrahedra. In all aluminosilicates, there must always be a silicon tetrahedron separating pairs of aluminum. Because Site III is on a 4-membered ring, only a next-nearest neighbor (2N) configuration was considered for  $Zn^{2+}$ . On the other hand, Site II is a 6-membered ring where a next-next-nearest neighbor (3N) configuration can also coordinate with  $Zn^{2+}$  at the center of the site. The 2N and 3N configurations are depicted in Figure 4.5.

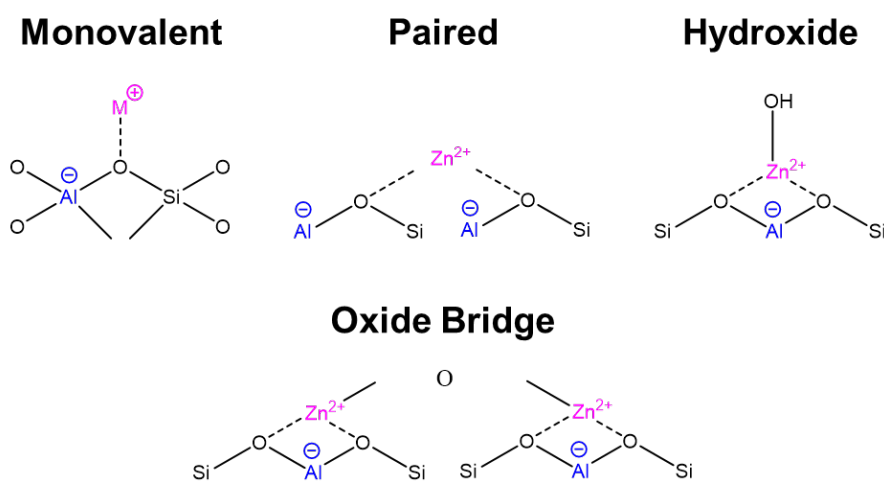


Figure 4.4: Simplified diagrams of various structures for Lewis acid sites on the surface of zeolites for monovalent cations and  $Zn^{2+}$ .

As constructed, the clusters have mirror symmetry, therefore the 2N and 3N configurations each have an enantiomeric configuration where the aluminum tetrahedra are shifted around the 6-membered ring by one position. Because they are enantiomers and should have the same energy, only one 2N and one 3N cluster needs to be considered. If these clusters were larger and encompassed more of the zeolite in an asymmetric manner, then there could potentially be multiple 2N and 3N configurations on the 6-membered ring that have different energies. This is because adjacent rings to the 6-membered ring of Site II will change the energetics associated with the shared aluminum tetrahedron. This has also been observed in periodic-DFT studies that model the entire zeolite unit cells.[55,56]

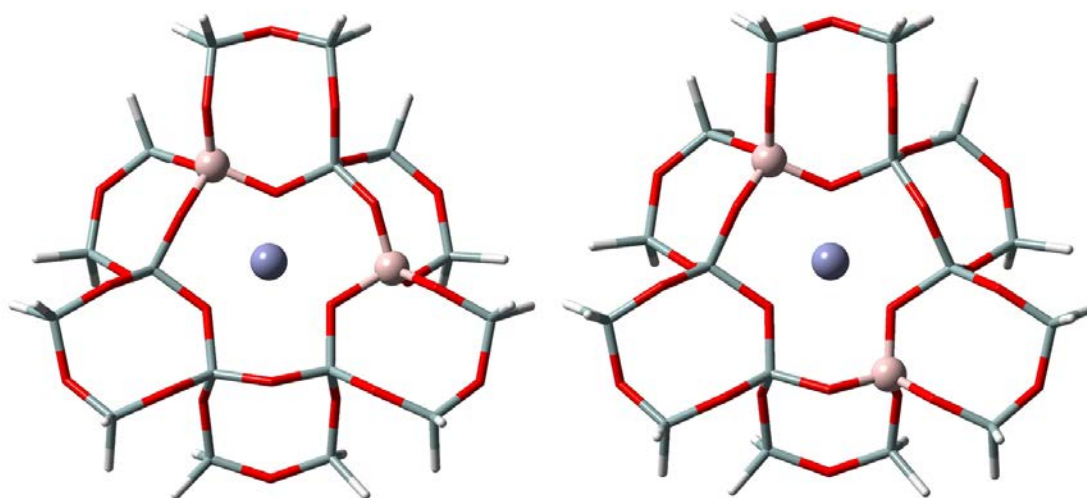


Figure 4.5: Next-nearest neighbor (2N) configuration (Left) and Next-next-nearest neighbor (3N) configuration for aluminum tetrahedral in the Site II cluster model.  $\text{Zn}^{2+}$  cation (Purple), aluminum (Pink), silicon (gray), oxygen (Red), and hydrogen (white). As constructed, a mirror image or rotation as shown by  $60^\circ$  will produce an enantiomeric cluster.

### 4.2.2 Computational Details

All calculations were performed using Gaussian 09, Revision A.2 at the M06-2X level of theory. Gas phase calculations involving  $\text{Rb}^+$  and  $\text{Cs}^+$  were conducted with the DEF2SVP and DEF2TZVPP basis sets. These basis sets include effective core potentials so that quantum calculations are tractable with elements with high atomic number. Otherwise, these two basis sets are effectively identical to 6-31g(d,p) and 6-311g(3df,2pd) respectively, which was used for the other monovalent cations and  $\text{Zn}^{2+}$ . [57-59]

Guesses for transition state structures were determined by placing the transition state for the uncatalyzed pericyclic electrocyclization in the vicinity of the cation to replicate the geometry from figures in Jiao et al. [53] Following a transition state optimization, the resulting transition state was confirmed by frequency analysis and by intrinsic reaction coordinate (IRC) calculations. In the case of electrocyclization under thermal conditions, there should be only one imaginary frequency that exhibits disrotatory motion.

Calculations were performed for cation-exchanged zeolite models using the 6-31g(d,p) basis set and the DEF2SVP basis set for  $\text{Rb}^+$  and  $\text{Cs}^+$ . The zeolite cluster model with the cation was first fully relaxed and optimized. This was successful except for  $\text{K}^+$ ,  $\text{Rb}^+$ , and  $\text{Cs}^+$  at Site III, where multiple attempts to optimize these Site III cation clusters failed to produce a structure where the cation was within a reasonable interaction distance of the framework. One possible explanation is that these cations are too big to fit near the 4-membered ring of Site III. To build initial guess structures, the reactant, transition state, and product were introduced to the optimized clusters so that the cation-triene complex reflected the same interaction distances as in the gas phase.

With the exception of capping hydrogens at the boundaries of cluster models, intermediate and transition state structures for reactants and products were allowed to fully relax. Unless otherwise noted, all calculations are reported with thermal corrections for free energy at 298 K based on vibrational frequency analysis, which uses the harmonic oscillator approximation. In short, differences between the thermally corrected reported energies of the disrotatory transition state and hexatriene-cation complex are effectively  $\Delta G^{\ddagger}$  for electrocyclization with that particular cation or cluster.

### 4.3 Results

#### 4.3.1 Calculated $\Delta G^{\ddagger}$ for Gas-Phase Electrocyclization is the Same Regardless of Basis Sets

The  $\Delta G^{\ddagger}$  for uncatalyzed, Li<sup>+</sup>-, Na<sup>+</sup>-, and K<sup>+</sup>-mediated electrocyclization of cis-1,3,5-hexatriene was calculated at the M06-2X level of theory with the following basis sets: 6-31g(d,p), 6-311g(3df,2pd), DEF2SVP, DEF2TZVPP. The average calculated value across all basis sets was 30.6, 24.0, 29.0, and 30.5 kcal/mol respectively for uncatalyzed and cation-mediated reactions. As expected, the similarly sized basis sets yielded similar values for  $\Delta G^{\ddagger}$ . For example,  $\Delta G^{\ddagger}$  was about 30 kcal/mol for 6-31g(d,p) and DEF2SVP, and about 31 kcal/mol for 6-311g(3df,2pd) and DEF2TZVPP. Over all, calculation results for the same reaction using different basis sets were within  $\pm 1.0$  kcal/mol of each other. In most cases, the difference was less than 0.25 kcal/mol. For comparison, the typical error of DFT calculations when compared to *ab initio* calculations or experimental data is  $\pm 1.0$  kcal/mol.[43]

Because  $\Delta G^{\ddagger}$  did not change much when going from smaller to larger basis sets, the smaller basis sets were deemed sufficient for estimating activation energies in

the other cations. The same conclusions cannot be immediately extended to the cluster models because there is a significant increase in the number of electrons. However, the results in the gas phase show a systematic increase in estimated activation energy when going from smaller to larger basis sets. Thus, any trends between different cations determined at a smaller basis set, such as 6-31g(d,p), should remain the same when comparing calculations performed with larger basis sets.

Table 4.1: Comparison of  $\Delta G^{\ddagger}$  for gas phase cation-mediated electrocyclization of cis-hexatriene for 4 different basis sets. All values are in kcal/mol.

Cation	Basis Set			
	6-31g	def2svp	6-311g	def2tzvpp
Uncatalyzed	30.17	30.21	30.90	31.12
Li <sup>+</sup>	24.10	23.81	24.01	24.11
Na <sup>+</sup>	27.27	28.09	29.09	29.01
K <sup>+</sup>	29.33	29.69	29.98	30.46

More importantly, because of the similar values obtained for DEF2SVP and 6-31g(d,p) for smaller cations, calculations for Rb<sup>+</sup> and Cs<sup>+</sup>, which can only be done with DEF2SVP, can be compared directly to calculations that used the 6-31g(d,p) basis set. It is unnecessary to repeat calculations with the effective core potential basis sets for the low atomic number cations. All values discussed in this chapter from here on will be thermally corrected calculations performed at the M06-2X/6-31g(d,p) or M06-2X/DEF2SVP level of theory.

### 4.3.2 Cation Size Plays Some Role in Catalysis

Figure 4.6 shows the calculated  $\Delta G^{\ddagger}$  for each calculation type plotted against the crystal ionic radius of the cation.[60] In the gas phase, the Na<sup>+</sup> or smaller cations

lower the activation energy more than large cations, with the exception of  $\text{Zn}^{2+}$ . Recall that in the case of electrocyclization,  $\Delta G^{\ddagger}$  is defined as the energy difference between the transition state and preceding hexatriene-cation complex. Of all the transition metals in the first row, zinc is known to form the most stable complexes with hydrocarbons. One possible explanation is that the  $\text{Zn}^{2+}$ -hexatriene complex is so stable compared to complexes with other cations that the activation energy is increased due to a decrease in energy of the preceding intermediate.[61]

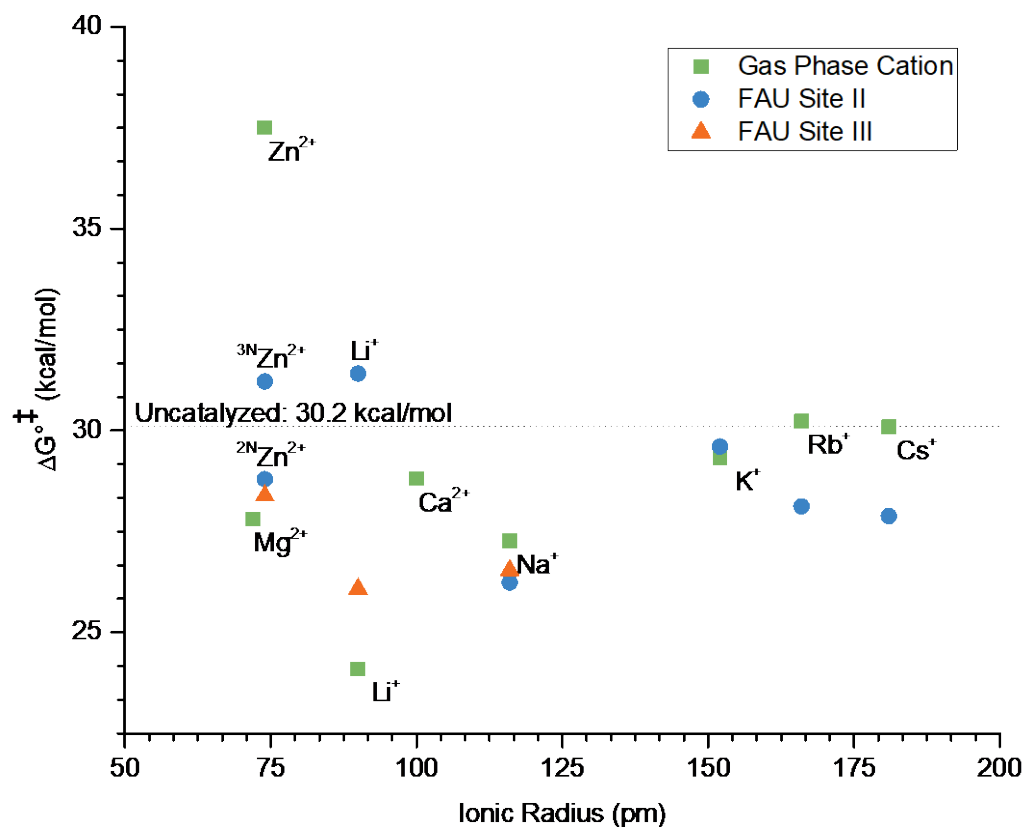


Figure 4.6:  $\Delta G^{\ddagger}$  in kcal/mol calculated at the M06-2X/6-31g(d,p) level of theory for cation mediated electrocyclization in the gas phase and in Faujasite cation exchange sites plotted against the crystal ionic radius of the cation. For most cations,  $\Delta G^{\ddagger}$  is lower in a zeolite than in the gas phase. The exception is  $\text{Li}^+$ . The calculated  $\Delta G^{\ddagger}$  for the uncatalyzed gas phase reaction is 30.2 kcal/mol. This value should be used for calculating  $\Delta\Delta G^{\ddagger}$  from these calculations.[60]

In the gas phase,  $\text{Li}^+$  is the most catalytically active with  $\Delta G^{\ddagger}=24.1$  kcal/mol. Of all monovalent cations,  $\text{Li}^+$  has the smallest ionic radius, but it is still larger than  $\text{Mg}^{2+}$  and  $\text{Zn}^{2+}$ , which have higher activation energies. Looking only at the gas phase data, it may seem at first that lithium simply has the optimal charge density and ionic radius. However, this is not the case in the Site II cluster model, where  $\text{Na}^+$  has the

lowest activation energy. For  $\text{Li}^+$  at Site II,  $\Delta G^{\ddagger}=31.4$  kcal/mol, which is higher than the calculated value for the uncatalyzed reaction. In contrast,  $\text{Li}^+$  in the gas phase and  $\text{Li}^+$  at Site III have activation energies of 24.1 and 26.1 kcal/mol respectively.

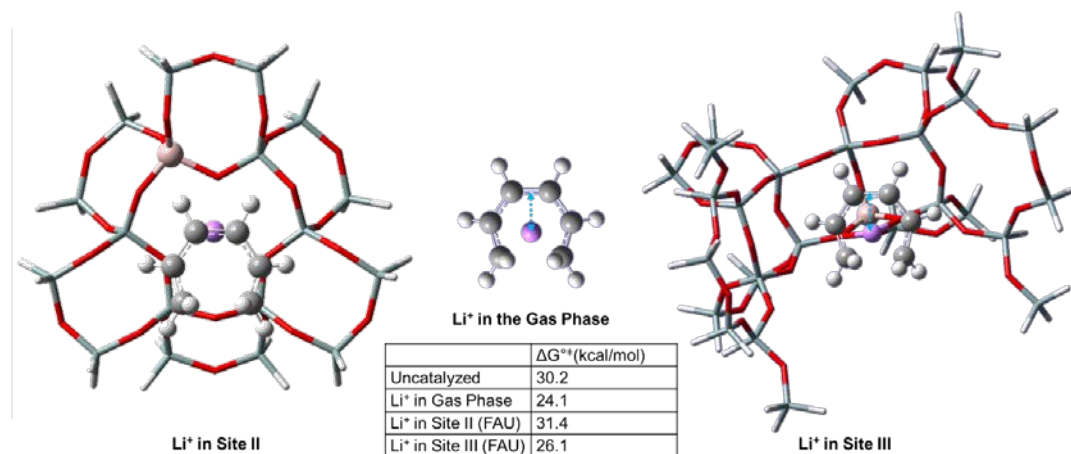


Figure 4.7: Comparison of cation-transition state orientations in the gas phase and zeolite cluster models for  $\text{Li}^+$ .  $\text{Li}^+$  cation (Magenta), aluminum (Pink), silicon (Gray), carbon (Dark Gray), oxygen (Red), and hydrogen (white). Blue arrows demonstrate how the view of the cation can be oriented such that the transition state is centered for the gas phase and Site III of Faujasite.  $\Delta G^{\ddagger}$  is listed in kcal/mol for the relevant reactions.

One explanation is that  $\text{Li}^+$  is being shielded by the surrounding framework oxygen atoms and is inaccessible to hexatriene at Site II. This seems reasonable after considering the transition state geometries. In the gas phase and at Site III, the partly formed 6-membered ring is centered over the cation such that the plane of the ring is tangent to the cation sphere at the center of the ring. This is true for all cations and cation clusters except  $\text{Li}^+$  at Site II, where the plane of the ring is tangent to the cation sphere at the central  $\pi$  bond that will be converted into a  $\sigma$  bond (Figure 4.7). In cluster

models for most other cations, the minimum interaction distance between hexatriene and cation does not change significantly from the gas phase transition state geometry. The exception is  $\text{Li}^+$ , which has about a 50% larger minimum interaction distance, as shown in Figure 4.8. One reason why this is the case is that  $\text{Li}^+$  lies in the plane of the 6-membered ring of the zeolite while all other cations are situated out of the plane. This geometry would make  $\text{Li}^+$  inaccessible to hexatriene because it would be shielded by the oxygen atoms in the 6-membered ring. In contrast, like all the other cations at Site III,  $\text{Li}^+$  does not sit in the plane of the 4-membered ring.

By this logic, the smaller  $\text{Zn}^{2+}$  cation should also lie in the plane of the 6-membered ring and experience significant shielding. Clearly from the activation energies and the transition state geometries, this is not the case. Therefore, charge density must also play some role in the interactions between cation and zeolite framework.

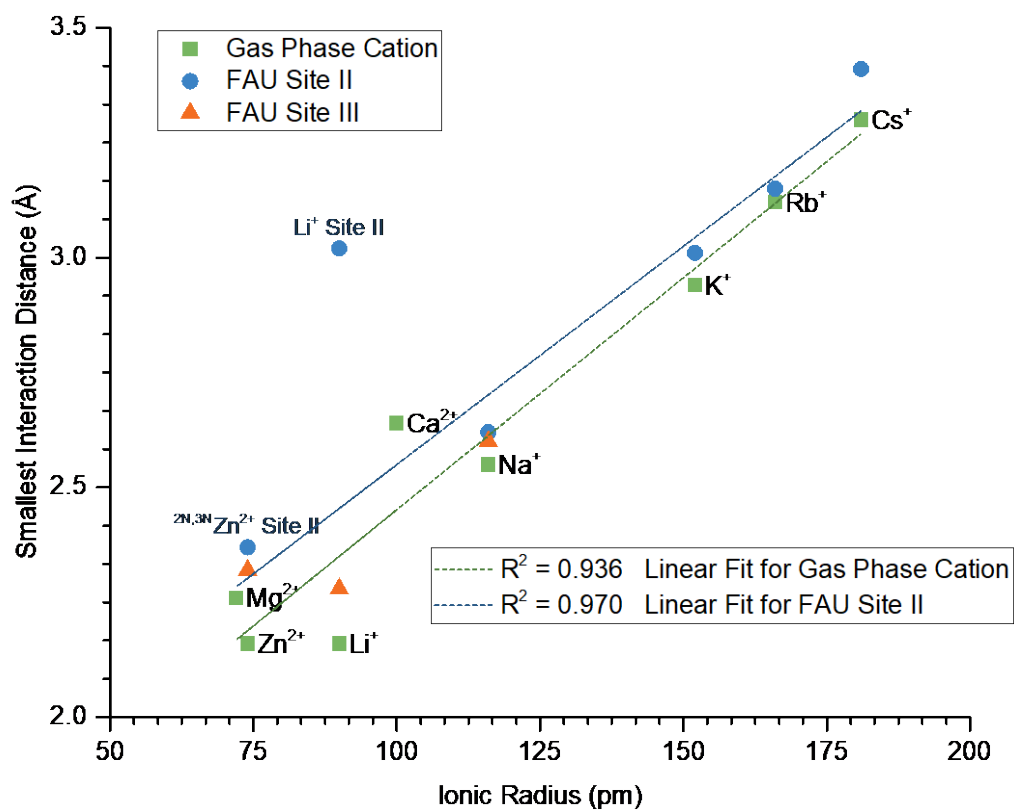


Figure 4.8: Minimum interaction distance between cation and transition state plotted against crystal ionic radius of the cation. Linear fits of the data for gas phase cations and Site II cations excluding Li<sup>+</sup> have been plotted. Li<sup>+</sup> at Site II of Faujasite was treated as an outlier.

### 4.3.3 Zeolite Clusters Lower Activation Energy without Influencing Interaction Distances

In Figure 4.8, ignoring  $\text{Li}^+$  at Site II as an outlier, there is a positive linear correlation between the smallest interaction distance between cation and hexatriene, and the crystal ionic radius. Linear fits can be made for gas-phase results and Site II cluster results independently. The interaction distances for Site II are almost the same as the gas phase except for a small systematic shift. Therefore, for all cations except  $\text{Li}^+$  at Site II, the transition state geometry is effectively identical in the optimized clusters and in the gas phase.

However,  $\Delta G^{\ddagger}$  is not linearly correlated with either cation size or interaction distance, even if gas-phase  $\text{Zn}^{2+}$  was treated as an outlier. Also, with the exception of  $\text{Li}^+$  cluster models, the activation energy for zeolite clusters is the same or lower than in the gas phase. These two observations combined with the minimal change in transition state geometry suggest that the zeolite cation exchange site is somehow contributing to the lowering of the electrocyclization activation energy. The effect of the cation site can be seen in the difference in activation energy between the 2N and 3N configurations for  $\text{Zn}^{2+}$  at Site II. Although the minimum interaction distance is 2.37 Å in both Site II clusters,  $\Delta G^{\ddagger}$  in the 2N configuration is lower than the 3N by 2.4 kcal/mol. Perhaps the arrangement of aluminum tetrahedra in the 2N configuration creates a more effective dipole that influences the effective charge of the cation. Overall, the effective cation charge density that the hexatriene sees might play a role in changing the polarizing effect of the cation on the electrocyclization transition state.

## Chapter 5

### CARBOCATION MEDIATED CYCLIZATION OF HEXATRIENE

#### 5.1 Introduction

Industrial zeolites are typically acid catalysts.[62] Hence it is reasonable to consider carbenium ion chemistry when discussing hydrocarbon rearrangements in the context of zeolite catalysis. Many of the mechanisms that would form trienes within the pores of a zeolite involve carbenium ions formed within the vicinity of Brønsted acid sites of the zeolite.[27] When the carbocation at the acid site is more favorable than the formation and release of neutral hexatriene into the gas phase, cyclization mechanisms involving carbocation intermediates will be favored over the pericyclic reactions of neutral hexatriene discussed in Chapters 3 and 4. These intermediate carbocations could form an alkoxide bond,[51] a carbenium ion-anion pair, or a radical pair near the surface of the zeolite.[63] Some of these intermediates could potentially be identified via *in situ* FTIR or UV-Vis spectroscopy.[64]

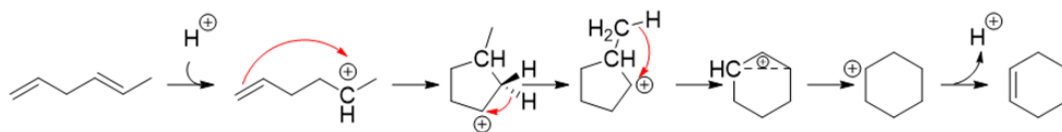


Figure 5.1: Reproduction of the cyclization mechanism for 1,4-hexadiene cyclization via carbocation intermediates established by Joshi et al. Electron arrow pushing mechanism is indicated in red.[65,66]

Many mechanisms have been put forth to describe the transformation from linear hydrocarbon to cyclic C5 to cyclic C6. The consensus is that a linear C6+ carbenium ion must first form a methyl-substituted cyclic C5 carbenium ion before expanding into a cyclic C6 carbenium ion. The cyclic C6 carbenium ion can then be deprotonated to form a neutral cyclic C6 hydrocarbon that can be further dehydrogenated to form aromatic species. The exact nature of these carbocations, especially the 5-membered rings, is still up for debate because they must be characterized *in situ* or *in operando*.<sup>[17]</sup>

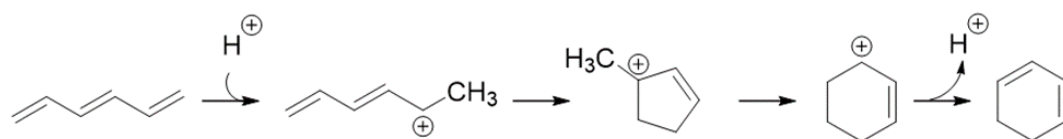


Figure 5.2: A consensus of literature mechanisms that trace their roots to the work of Poutsma that describes the conversion of hexatriene to cyclohexadiene via carbocation intermediates. Little or no mechanistic detail has been suggested connecting these stable intermediates in the zeolite catalysis literature.<sup>[17-18,65-67]</sup>

Joshi and Bhan focused on the carbocations of dienes. Using DFT, they mapped out reaction mechanisms in the gas phase that start from the protonation of a 1,4-hexadiene to form a hexenyl cation. In one mechanism, the linear hexenyl cation cyclizes into a methyl-cyclopentyl cation that then rearranges to form a cyclohexyl cation. This cation could be deprotonated to form neutral cyclohexene, which can be dehydrogenated to form aromatics.<sup>[65]</sup> They expanded their study to zeolite cluster models for H-ZSM-5 and found similar results.<sup>[66]</sup> A criticism of their mechanism is that the neutral linear hexadiene and the linear hexenyl carbocation do not have

conjugated  $\pi$  systems. This is inconsistent with computational work that suggests that conjugated olefins are favored during olefin oligomerization [25,27] and experimental work that has detected highly conjugated olefins *in situ* in various noble-metal-free acid zeolites.[28,29,68]

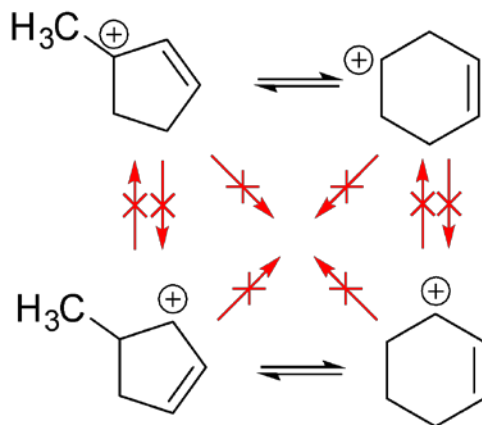


Figure 5.3: Summary of Olah's observations on cyclic carbocation rearrangements. The rearrangements marked in red were never observed in superacid systems, therefore they are disallowed.[67]

Although Joshi and Bhan did not investigate the carbocations of trienes, they acknowledged the experimental evidence of their presence in hydrocarbon aromatization and deferred to the work of Ono and colleagues from the 1980s and 1990s, which proposed an analogous mechanism. Like dienes, trienes went through a similar progression of linear cation to a methylated 5-membered cationic ring to a 6-membered cationic ring. Ono primarily analyzed product distributions of reactions of C2 to C5 alkanes over Ga-ZSM-5 and Zn-ZSM-5.[10] Ono adapted a mechanism originally proposed by Poutsma to explain his observations.[18] Figure 5.2 depicts the

latest adaptation of the mechanism that has ultimately been cited in the chain of reviews that cite older reviews. Mechanisms involving carbocations of trienes have been largely ignored, and those which have been investigated assume that the most stable carbocation intermediates are the ones that connect a 6-carbon linear molecule to a 6-membered ring.

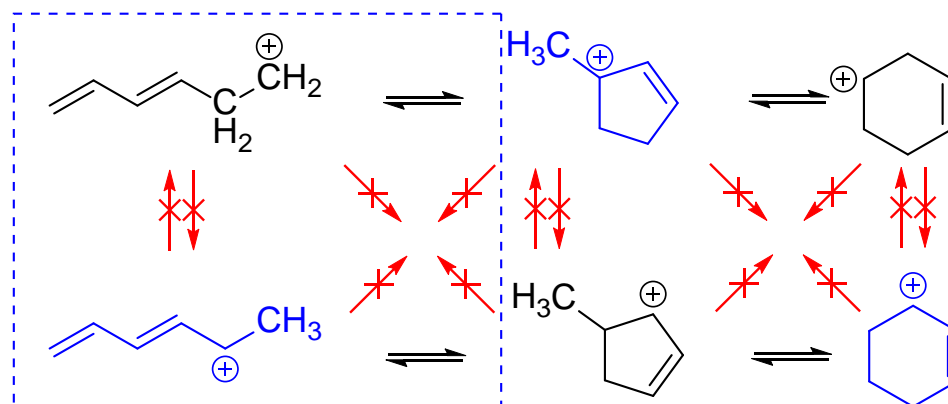


Figure 5.4: Extension of Olah's findings on carbocation rearrangements based on calculations in this work (blue box). This summarizes why existing cyclization mechanisms that connect the most stable carbocations (blue) are highly unlikely.

The problem with the consensus literature mechanism, which will be referred to as the Poutsma mechanism from here on, is that some of these carbocation rearrangements contradict observations made by Olah in his Nobel Prize winning work on carbocation chemistry.[67] Specifically, the Poutsma mechanism proposes that a tertiary methyl-cyclopentenyl carbocation will rearrange, or ring expand to form an allylic cyclohexenyl carbocation. Olah concluded that this rearrangement never happens based on his experiments in superacid systems. A tertiary methyl-

cyclopentenyl carbocation can only interconvert between a secondary cyclohexenyl cation, as shown in Figure 5.3. An allylic cyclohexenyl carbocation can only interconvert between a secondary allylic methyl-cyclopentenyl cation. Not only are certain 5-to-6 membered ring rearrangements disallowed, these cationic 5-membered and 6-membered rings must first deprotonate and re-protonate to form a different cation of the same ring size.[67] Therefore, the linear, 5-membered ring, and 6-membered intermediates that are connected to each other on the same reaction pathway can not all be the most stable carbocation in each category. Thus, it is important to further explore the carbocation mediated cyclization of hexatriene to bring consistency to the current understanding in the literature with established principles of carbocation chemistry.

## **5.2 Methods**

### **5.2.1 Reactions Considered**

A Poutsma mechanism that had a tertiary allylic methyl-cyclopentenyl carbocation intermediate was investigated. The appropriate linear and cyclohexenyl carbocation intermediates were identified. No other intermediates or alternative sequences of elementary steps were found. Intrinsic reaction coordinate calculations were used to verify that identified transition state structures connected the expected pairs of intermediates.

An alternative mechanism was proposed when the linear secondary hexadienyl carbocation in Figure 5.2 favored cyclization to form a secondary allylic methyl-cyclopentenyl carbocation. Additional elementary steps, intermediates, and transition states were identified for this reaction pathway connecting a linear secondary

hexadienyl to a secondary allylic methyl-cyclopentenyl to an allylic cyclohexenyl carbocation.

These mechanisms were first considered in the gas phase. Structures obtained in the gas phase guided analogous calculations in the zeolite clusters. In all cases, the transition states for the protonation and deprotonation steps from neutral hexatriene and cyclohexadiene were not determined.

### 5.2.2 Calculation Details

All calculations were performed using Gaussian 09, Revision A.2 at the M06-2X/6-31g(d,p) level of theory. Unless otherwise noted, all calculations are reported with thermal corrections for free energy at 298 K based on vibrational frequency analysis, which uses a harmonic oscillator approximation. As an example, the reported energy difference between a transition state structure and the preceding intermediate can be thought of as a standard state free energy change,  $\Delta G^{\ddagger}$ . For gas phase calculations, ground state structures for reactants and products were fully relaxed and vibrational frequencies were calculated. The resulting transition state was confirmed by frequency analysis and by intrinsic reaction coordinate (IRC) calculations.

A quantum cluster model was developed by excising the region within 6.0 Å of a Brønsted acid site in Faujasite as depicted in Figure 5.4. Capping hydrogens were attached to dangling bonds at the boundaries of the cluster. All other atoms were allowed to fully relax. After optimizing the cluster, structures from gas-phase calculations for the reactants, intermediates, and products, were placed close to the acidic proton as an initial guess. This provided the energetics and structures of the interactions with the acid site cluster. After optimizing the intermediate-cluster systems, transition state structures replaced the intermediate with most resemblance in

structure and energy. The separation between zeolite and cation was kept the same as the intermediate. Due to time constraints, only the rate limiting step (ring expansion) from the gas phase reactions was investigated in this manner.

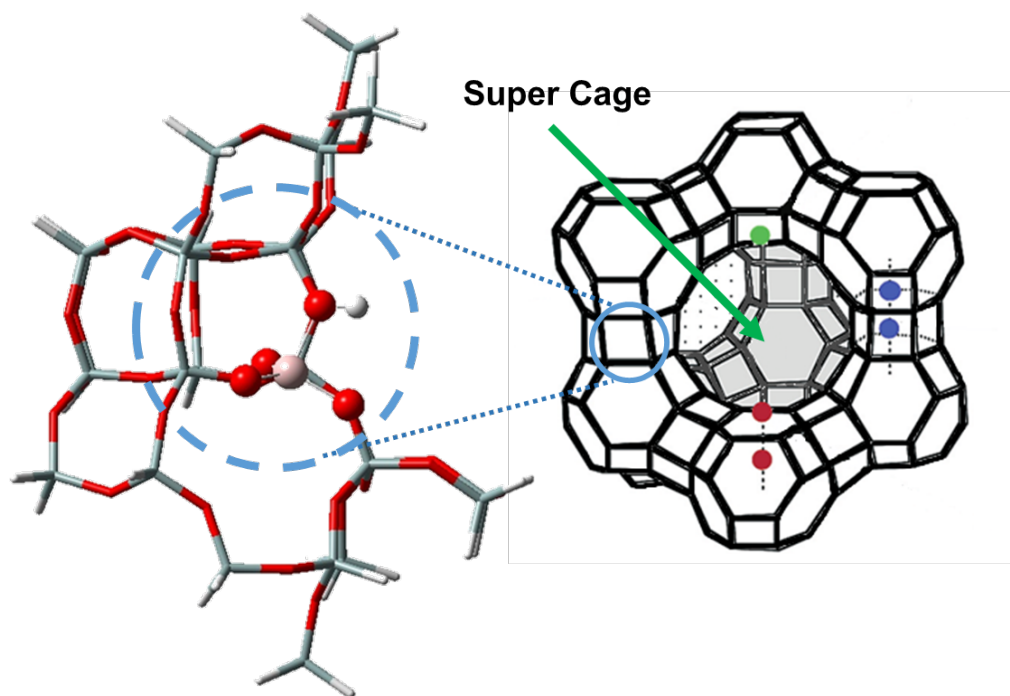


Figure 5.5: Quantum cluster built for the Brønsted acid site located as shown on the left in Faujasite. This cluster encompasses atoms within 6.0 Å of the acidic proton.[69]

## 5.3 Results

### 5.3.1 Two Independent Gas-Phase Carbocation Mediated Cyclization Mechanisms

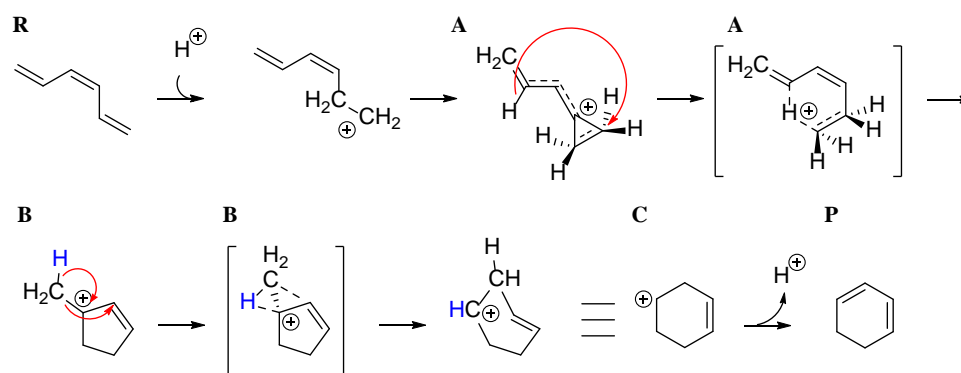


Figure 5.6: Detailed version of the Poutsma mechanism developed in this thesis. Cis-1,3,5-hexatriene is converted to 1,3-cyclohexadiene through two intermediates: a primary hexadienyl carbocation, and a tertiary methylcyclopentenyl cation.

Two independent and parallel mechanisms were developed to connect hexatriene to cyclohexadiene via carbocation intermediates. The first mechanism, depicted in Figure 5.5, will be referred to as the Poutsma mechanism. This is a more detailed version of the mechanism depicted in Figure 5.2 that has been updated based on the results of this work to be consistent with fundamental carbocation chemistry.

In the Poutsma mechanism, a primary hexadienyl carbocation is formed from neutral cis-hexatriene by protonation of C2. The lowest energy configuration for this carbocation contains a cyclopropenyl moiety. Partial double-bonds connect carbons throughout the molecule, making the difference in energy between cis- and trans- with respect to the original central double bond less than 1 kcal/mol.

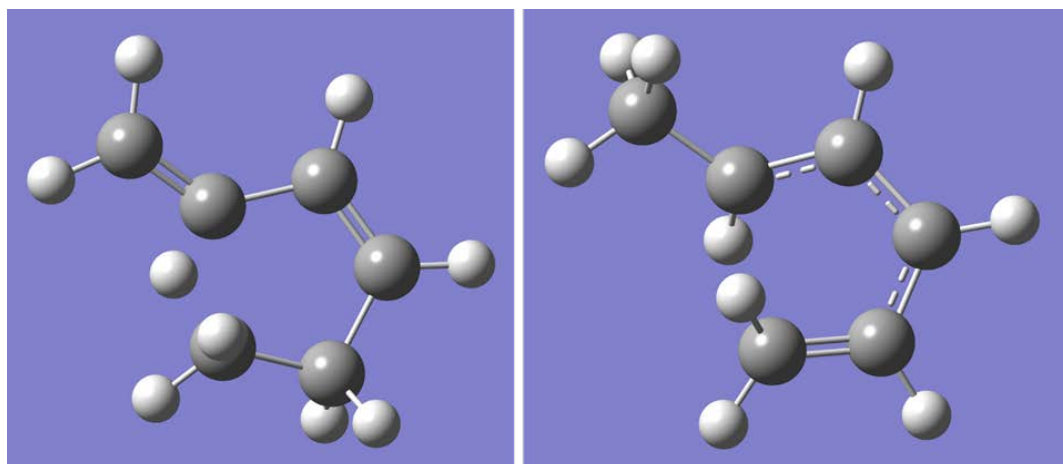


Figure 5.7: Rendering of the final cyclization transition states in the gas phase for the Poutsma (left) and Alternative (right) mechanisms. The Poutsma transition state involves a 3-center 2-electron bond.

Through a single, concerted step, the hexadienyl carbocation intermediate is converted into a tertiary methyl-cyclopentenyl carbocation. In the transition state, the cyclopropenyl ring opens and a hydrogen forms a three-center two-electron bond with the available end. The hydrogen can not be fully extracted and instead gets pushed onto the terminal carbon to form the methyl group in the resulting carbocation intermediate (Figure 5.6). Simultaneously, a 5-membered ring is formed.  $\Delta G^{\ddagger}$  is predicted to be 26.4 kcal/mol at the M06-2X/6-31g(d,p) level of theory. To the author's best knowledge, the formation of a tertiary methyl-cyclopentenyl carbocation from a linear carbocation has not been described in the literature with this mechanistic detail.

As observed experimentally by Olah in superacid systems, the tertiary methyl-cyclopentenyl carbocation can rearrange into a cyclohexadiene carbocation. In this 6-

membered ring, the charge is isolated from the remaining double-bond. This happens in a single concerted step where a 1,2-hydride shift is followed by a 1,2-methyl shift, but both complete nearly simultaneously (Figure 5.7).  $\Delta G^{\ddagger}$  is predicted to be 54.5 kcal/mol at the M06-2X/6-31g(d,p) level of theory. The mechanism for this rearrangement proposed by Olah is similar, but lacking in this insight, which was obtained from observing the structures obtained from IRC calculations.

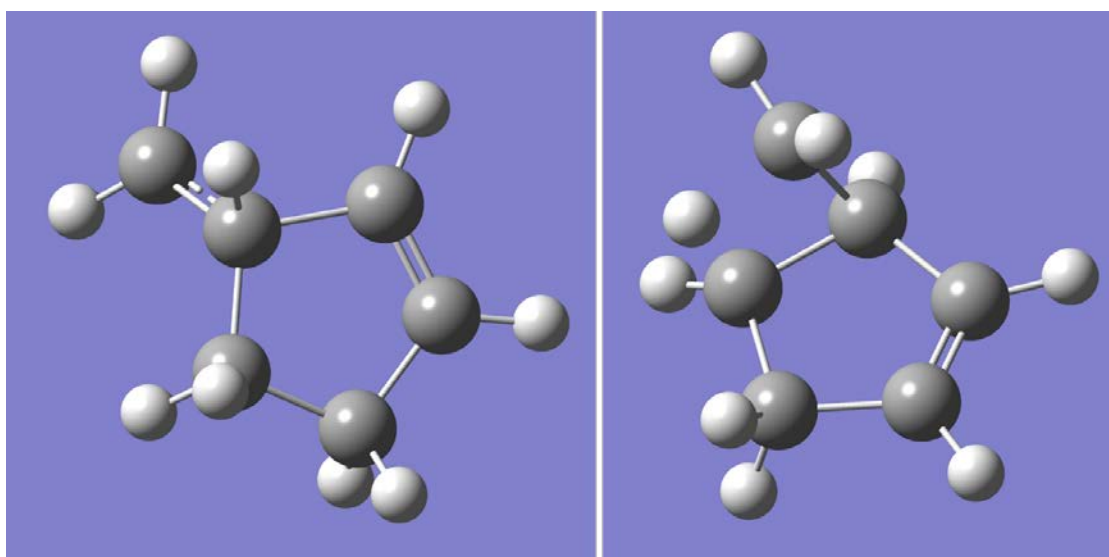


Figure 5.8: Rendering of the ring expansion transition states in the gas phase for the Poutsma (left) and Alternative (right) mechanisms. The shifting hydride is more accessible on the tertiary carbon in the Poutsma mechanism.

The second mechanism developed in this research will be referred to as the Alternative mechanism, depicted in Figure 5.8. In this mechanism, a secondary hexadienyl carbocation is formed from neutral cis-hexatriene by protonation of C1. This secondary carbocation undergoes a conformational change to form an intermediate that exhibits the beginnings of a 5-membered ring.  $\Delta G^{\ddagger}$  for this step is

predicted to be 13.1 kcal/mol at the M06-2X/6-31g(d,p) level of theory. From this intermediate, the cyclopentane ring closes and a secondary allylic methyl-cyclopentenyl carbocation is formed with  $\Delta G^{\ddagger}$  predicted to be 6.4 kcal/mol.

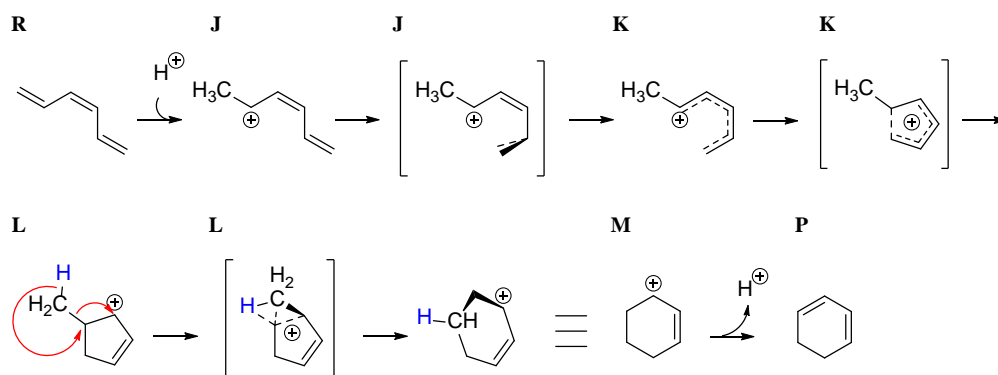


Figure 5.9: The Alternative mechanism in detail. Cis-1,3,5-hexatriene is converted to 1,3-cyclohexadiene through a secondary hexadienyl carbocation intermediate and a secondary methyl-cyclopentenyl cation intermediate. This mechanism has three transition states.

Similar to the Poutsma mechanism, the methyl-cyclopentenyl rearranges into a 6-membered ring via a single transition state. However, the resulting carbocation is an allylic cyclohexenyl carbocation. The cation is delocalized, making this carbocation more stable than its counterpart in the Poutsma mechanism. Also, the 1,2-methyl shift now precedes the 1,2-hydride shift in the concerted step.  $\Delta G^{\ddagger}$  is predicted to be 26.5 kcal/mol at the M06-2X/6-31g(d,p) level of theory. As written, this mechanism has not been proposed so far in the literature, but it does bear uncanny similarities to a Brønsted acid-mediated Nazarov cyclization mechanism for the formation of 2H-pyran from 2,4-pentadienal.[70,71]

The Poutsma and Alternative mechanisms are parallel but independent pathways that connect 1,3,5-hexatriene to 1,3-cyclohexadiene through carbocation intermediates. The pathway that a single hexatriene molecule proceeds on is determined by how it is initially protonated to form either a primary or secondary linear carbocation. After numerous DFT calculations, no transition states could be found that would connect carbocations from one mechanism to the other at any point along the pathway. This is consistent with Olah's observations in superacids that an allylic cyclohexenyl carbocation can never rearrange into either a tertiary methyl-cyclopentenyl carbocation or a charge-localized cyclohexenyl carbocation. Likewise, the charge-localized secondary cyclohexenyl carbocation can never rearrange into the secondary allylic methyl-cyclopentenyl carbocation. Conversion appears only possible through deprotonation and re-protonation to form a different cation.[67] This is likely due to constraints on orbital symmetry in these conjugated carbocations. The disallowed rearrangements generally require 1,3-hydride shifts.

### **5.3.2 Alternative Mechanism has Smaller RDS in Both Gas Phase and Cluster Calculations**

In both mechanisms, the rate determining step (RDS) is the rearrangement from a 5-membered ring to a 6-membered ring. In the gas phase,  $\Delta G^{\ddagger}$  is calculated to be 54.5 kcal/mol for the Poutsma mechanism and 26.5 kcal/mol for the Alternative mechanism. The activation energy for the rate determining step is much smaller for the Alternative mechanism, so it is most likely the dominant reaction pathway. In fact, the rate determining step for the Alternative mechanism is almost smaller than all elementary steps of the Poutsma mechanism, including the cyclization step, where  $\Delta G^{\ddagger}=26.4$  kcal/mol.

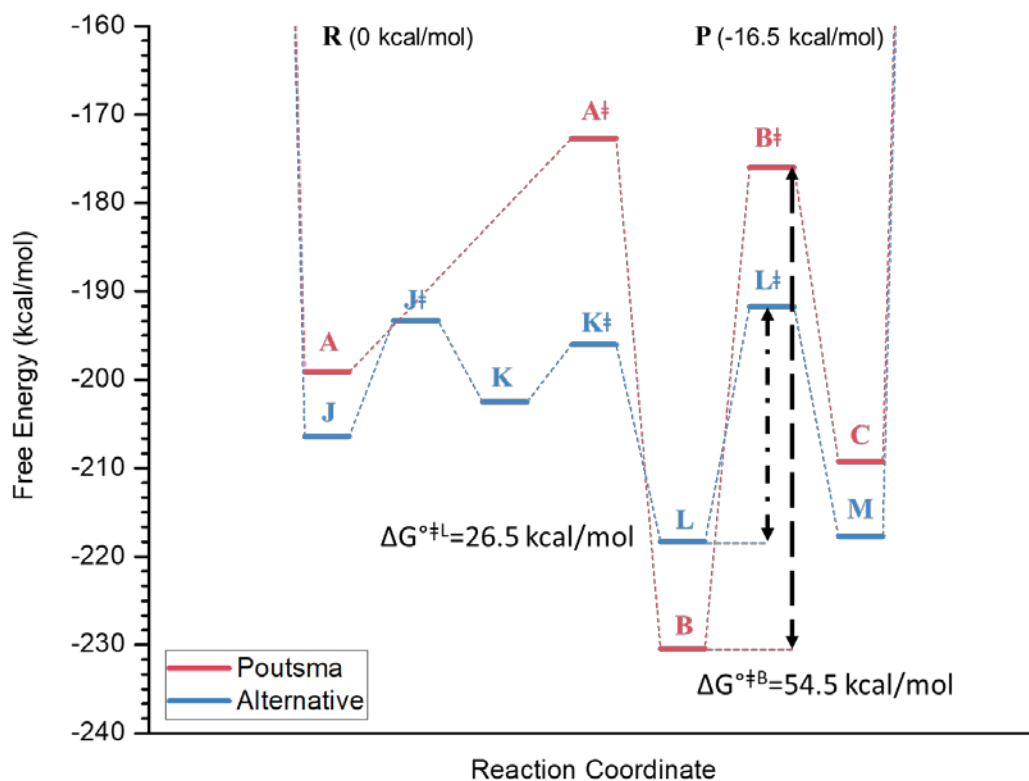


Figure 5.10: Reaction coordinate diagram comparing Poutsma (Red) and Alternative (Blue) reaction mechanism in the gas phase. Rate determining steps are shown in black.  $\Delta G^\circ=0$  corresponds to neutral cis-1,3,5-hexatriene (R) in the gas phase.  $\Delta G^\circ$  of reaction in kcal/mol is (AB) -31.3 (BC) 21.2 (JK) 3.9 (KL) -15.8 (LM) 0.6.  $\Delta G^\ddagger$  in kcal/mol is (A $^\ddagger$ ) 26.4 (B $^\ddagger$ ) 54.5 (J $^\ddagger$ ) 13.1 (K $^\ddagger$ ) 6.4 (L $^\ddagger$ ) 26.5.

Part of the reason for this massive difference is that the tertiary methylcyclopentenyl carbocation in the Poutsma mechanism is lower in energy than the analogous secondary cation in the Alternative mechanism, as shown in Figure 5.9. However, both the transition state and the cyclohexenyl carbocation are higher in

energy than their counterparts in the Alternative mechanism. The allylic cyclohexenyl carbocation in the Alternative mechanism is lower in energy because it is stabilized by resonance. Hammond's Postulate predicts that for endothermic reactions, the transition state will resemble the products, which is applicable to the ring expansion in both mechanisms. Thus, it is not surprising that the transition state for the Poutsma mechanism has higher energy than that of the Alternative mechanism because the product carbocation has higher energy for the Poutsma mechanism. Most of the intermediates and transition states in the Poutsma mechanism are much higher in energy than their counterparts in the Alternative mechanism. Hammond's Postulate appears to be also consistent with the higher activation energies for similar non-rate determining steps in the Poutsma mechanism. In short, the Poutsma mechanism transitions from a primary to allylic tertiary to secondary carbocation and the Alternative mechanism transitions from a secondary to allylic secondary to allylic secondary carbocation. It is not surprising that the activation energies for the Alternative mechanism are lower because the starting and ending points in the reaction pathway are lower in energy.

In the zeolite cluster model for a Brønsted acid site in Faujasite,  $\Delta G^{\ddagger}$  is calculated to be 48.5 kcal/mol for the Poutsma mechanism and 33.9 kcal/mol for the Alternative. The activation energy for the Alternative mechanism is still lower than the Poutsma mechanism in the Brønsted acid site cluster. However,  $\Delta\Delta G^{\ddagger}$  is negative for the Poutsma mechanism and positive for the Alternative mechanism.

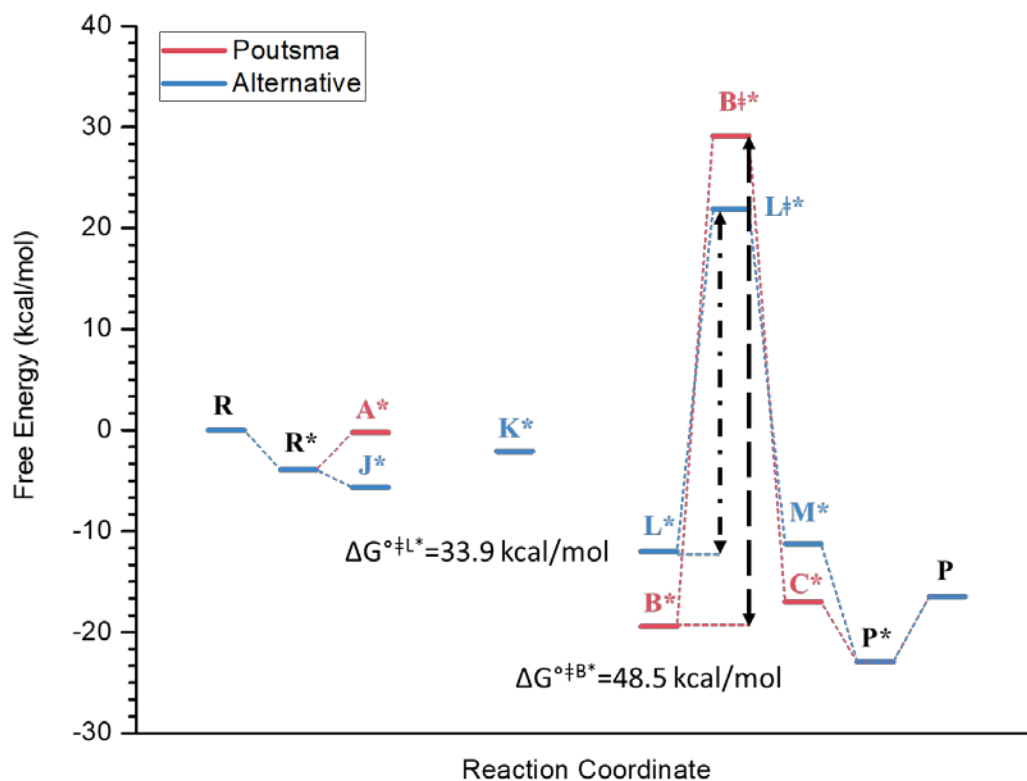


Figure 5.11: Reaction coordinate diagram comparing Poutsma (Red) and Alternative (Blue) reaction mechanism in the H-FAU cluster. Asterisks (\*) indicate species is adsorbed or bonded to the zeolite cluster. Rate determining steps are shown in black.  $\Delta G^\circ$  of adsorption in kcal/mol is (R) -3.9 (P) -6.5.  $\Delta G^\circ$  of reaction in kcal/mol is (R\*A\*) 3.7 (A\*B\*) -19.2 (B\*C\*) 2.4 (R\*J\*) -1.7 (J\*K\*) 3.6 (K\*L\*) -9.9 (L\*M\*) 0.8 (RP) -19.0 (R\*P\*) -16.5.

While there is no obvious explanation for the increase in activation energy for the Alternative mechanism, the reduction for the Poutsma ring expansion can partly be explained by possible stabilizing interactions between the Poutsma transition state and a nearby framework oxygen. As shown in Figure 5.11, the shifting hydride in the transition state is facing a framework oxygen with a separation of 1.75 Å. This oxygen is part of the aluminum tetrahedron. The shifting hydride is on the face of the 5-membered that is opposite the framework. The transition state, like the 5-membered ring and 6-membered ring intermediates for both mechanisms, has a minimum carbon to framework interaction distance between 2.5-3.0 Å. This suggests that the carbocations are not forming an alkoxide bond with the zeolite framework, but are likely adsorbed through ionic interactions. This is in contrast to the linear intermediates in both mechanisms (not shown), which do form alkoxide bonds of about 1.54 Å. Despite being alkoxides, they are higher in energy than the cyclic intermediates, which suggests that cyclization is energetically more favorable than the strength of the alkoxide bond.

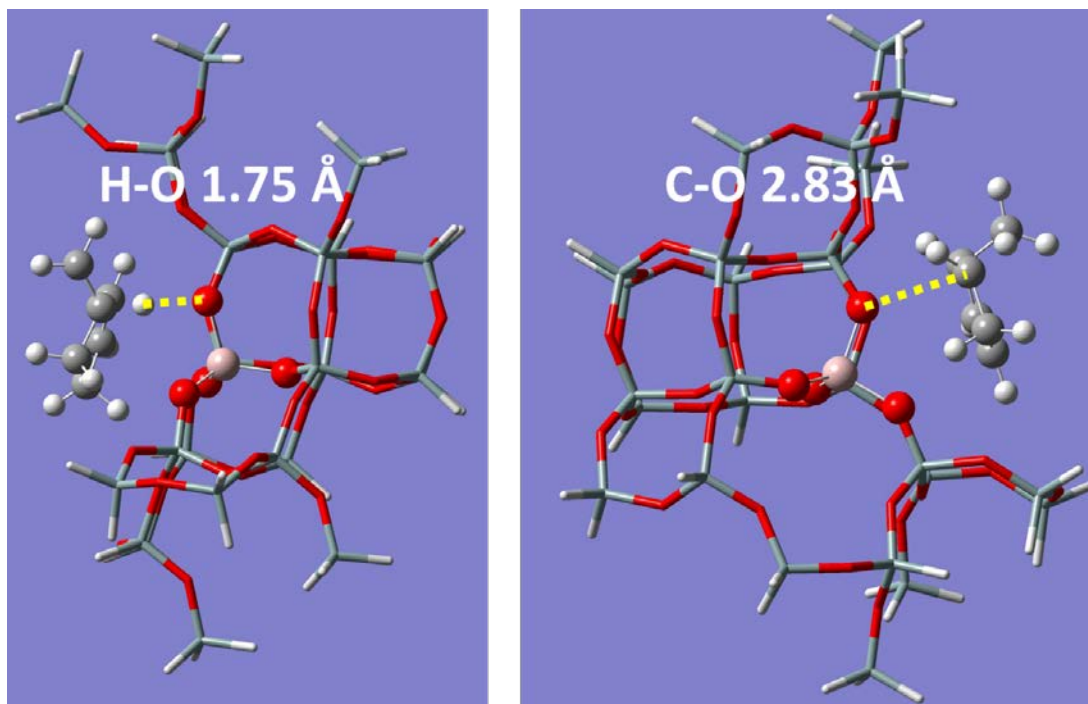


Figure 5.12: Rendering of Poutsma (Left) and Alternative (Right) ring expansion transition states interacting with the Faujasite Brønsted acid site cluster. For Poutsma, the minimum interaction distance is between and shifting hydride and a framework oxygen in the aluminum tetrahedron. For the Alternative mechanism, the shifting hydride does not interact with the framework.

## Chapter 6

### COMPARISON OF MECHANISMS AND IMPACTS ON FUTURE WORK

#### 6.1 Low Alkoxide Strength and Heats of Adsorption for Hexatriene and Cyclohexadiene

In the Alternative mechanism for cation-mediated cyclization,  $\Delta G^\circ = -1.7$  kcal/mol for the formation of a hexadienyl alkoxide on the surface of the Brønsted acid site quantum cluster from neutral hexatriene adsorbed nearby. This calculated alkoxide strength is of similar magnitude to more computationally expensive periodic DFT calculations reported by Sarazen et al. for C2-4 olefins in TON and HPW zeolite frameworks.[72] The activation energy for alkoxide formation is expected to be small because the alkoxide and the neutral adsorbed hexatriene have similar energies.

In fact,  $\Delta G^\circ$  for formation of the hexadienyl alkoxide is smaller than the  $\Delta G^\circ$  of adsorption of hexatriene near the Brønsted acid site, which is 3.9 kcal/mol. In total, the  $\Delta G^\circ$  between the secondary alkoxide in the Alternative mechanism and free hexatriene in the gas phase is predicted to be only 5.7 kcal/mol. This is still much smaller than the activation energy for the ring expansion step, which is  $\Delta G^{\circ\dagger} = 33.9$  kcal/mol over the Faujasite acid cluster. Assuming that adsorption and desorption is barrierless, a linear secondary hexadienyl alkoxide that forms at a Brønsted acid site during olefin oligomerization could potentially desorb as neutral hexatriene and cyclize through pericyclic mechanisms. This is an even greater possibility under process conditions where there might also be moisture. Water is known to be favored over hydrocarbons in competition for Brønsted acid sites in zeolites.[73] Overall, the free energy change to go from an alkoxide to neutral hexatriene is quite low.

The only other comparable free energy change is the cis/trans isomerism for the hexatriene and hexadienyl carbocation.  $\Delta G^\circ$  for the conversion of trans- to cis-hexatriene is about 2.0 kcal/mol at the M06-2X/6-31g(d,p) level of theory. However, the activation energy for this isomerism is calculated to be  $\Delta G^{\circ\dagger}=46.0$  kcal/mol under thermal conditions. For the neutral species, trans-to-cis isomerism is slow and trans-hexatriene is favored at equilibrium. That being said,  $\Delta G^\circ$  for trans-to-cis isomerism for the hexadienyl carbocations is also about 3.7 kcal/mol, but  $\Delta G^{\circ\dagger}$  is only 22.2 kcal/mol in the gas phase. This is smaller than the rate limiting steps for most of the reaction pathways discussed in this thesis. As previously stated, the free energy change from the corresponding alkoxide to neutral hexatriene is only about  $-5.7$  kcal/mol in the Faujasite acid cluster model. Although additional cluster calculations will need to be made to see if the zeolite acid site increases or decreases the barrier for trans-to-cis isomerization, it is conceivable that acid sites in the zeolite effectively catalyze trans-to-cis isomerization so that cyclization mechanisms are not rate limited by the flux of cis-hexatriene. All in all, the majority of these additional processes should be much faster than the rate determining steps in the previously discussed mechanisms.

## **6.2 Electrocyclization and Carbocation Mediated Cyclization are Predicted to be the Dominant Cyclization Pathways for Hexatriene in Cation-Exchanged Faujasite**

The rate determining step for electrocyclization in the gas phase, on some cation-exchanged Faujasite acid sites, and carbocation mediate cyclization via the Alternative mechanism over a Faujasite Brønsted acid site are similar in terms of activation energy.  $\Delta G^{\circ\dagger}$  for the rate determining step is around 30 kcal/mol for all of

these reactions. Cyclization is the rate determining step for all of these parallel reaction pathways.

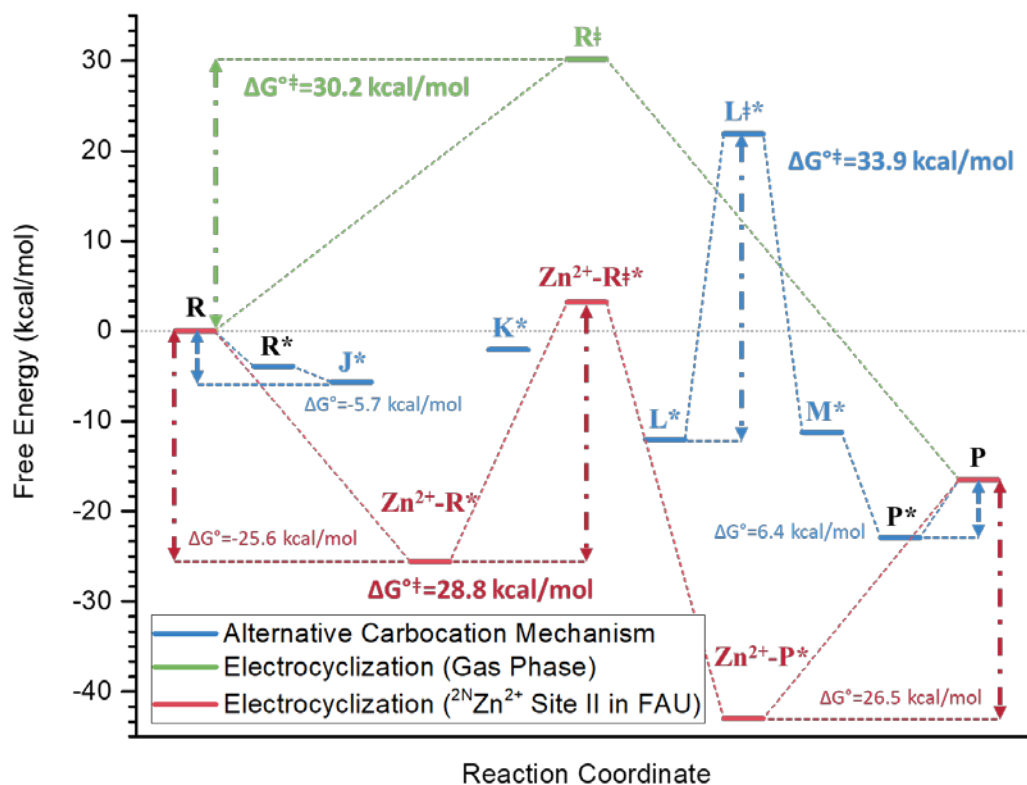


Figure 6.1: Reaction coordinate diagram comparing the Alternative carbocation mechanism in Faujasite to electrocyclization in the gas phase and on  $\text{Zn}^{2+}$  in a 2N configuration of Site II in Faujasite. Notable activation energies and adsorption/desorption energy changes have been labelled.  $\Delta G^\circ = 0$  kcal/mol corresponds to free hexatriene in the gas phase.

Even for a  $\text{Zn}^{2+}$  paired site in the 2N configuration at Site II of Faujasite, the activation energy for cyclization is larger than the calculated  $\Delta G^\circ$  of desorption of 26.5 kcal/mol for 1,3-cyclohexadiene from the  $\text{Zn}^{2+}$  cation site. The activation energy

for electrocyclization is rate limiting for the other cation clusters investigated, despite strong heats of adsorption for both neutral hexatriene and 1,3-cyclohexadiene to the cation exchange site. This assumes that adsorption and desorption are barrierless steps.

Based solely on analysis of rate determining steps, electrocyclization in the gas phase and cation exchange sites, and carbocation mediate cyclization on acid sites appear to be the dominant reaction pathways for hexatriene cyclization in Faujasite. Diels-Alder cycloaddition is bimolecular and  $\Delta G^{\ddagger}$  in the gas phase is 5.7 kcal/mol higher on average than the Alternative carbocation mechanism. The Poutsma mechanism is 14.6 kcal/mol higher than the Alternative mechanism. These two mechanisms will not contribute nearly as much as the other mechanisms discussed.

### **6.3 Future Directions with Microkinetic Modelling and *Ab Initio* Molecular Dynamics**

Without microkinetic modelling, or even an estimate of turnover frequency, it is difficult to precisely determine which mechanism will have the highest flux of 1,3-cyclohexadiene freed to the gas phase. The results presented in this thesis provide an initial prediction for computational kinetic modelling. More importantly, it has provided new mechanistic insight on some of the possible reaction pathways to convert 1,3,5-hexatriene to 1,3-cyclohexadiene. Previously, the carbocation mechanisms assumed that the most stable carbocations were the intermediates in cyclization. However, this violated established rules for carbocation rearrangements. This thesis updates chemical understanding in the field of zeolite aromatization both qualitatively and quantitatively by identifying parallel, but separate reaction networks. These results are the starting point for microkinetic models that can be used to predict

rates and products distributions for comparison to experimental data at or near process conditions.[74]

Furthermore, these pathways identify key intermediates that could be studied experimentally using *in situ* or *in operando* characterization techniques, including but not limited to infrared (IR) and UV-Vis spectroscopy.[75] While the vibrational frequencies obtained from quantum calculations can be used to predict spectra, the vibrational analysis assumes a harmonic oscillator approximation. Also, the analysis is only performed on one ground state configuration for the molecule. As a result, the predictions are only peak positions and estimates of relative amplitude.

A real molecule will sample multiple configurations at real conditions and temperatures. Vibrational modes may be asymmetric, so the harmonic oscillator model is inaccurate. The combination of all these real world factors is what produces the shape and complexity in experimental spectra. *Ab initio* molecular dynamics is one method to simulate experimental spectra for species that are normally difficult to measure due to their instability. The predicted spectra can be used to help identify intermediates within *in situ* or *in operando* measurements.[76] But first, it is important to identify which intermediates to perform these expensive calculations on first. This is another contribution of this thesis to the literature.

The combination of these two future research directions could possibly support a bold idea that has been hinted at in this work. Perhaps Zn-ZSM-5 and Ga-ZSM-5 are more selective for aromatics than cation-free acid zeolites because they bind neutral hexatriene more strongly than alkoxide formation at a Brønsted acid site. Cation sites facilitate electrocyclization of hexatriene at a faster turnover frequency than Brønsted acid sites, partly based on comparisons of the highest energy transition state with the

reference (free hexatriene in the gas phase). As a result, there are more available sites on which cyclization can occur, and carbocation-mediated cyclization does not compete with other acid catalyzed mechanisms for Brønsted acid sites to the same degree as in BAS-only zeolites.

## REFERENCES

1. DOE-OIT, U. S. "Energy and Environmental Profile of the US Chemical Industry." *Prepared by Energetics Incorporated*. Columbia, Maryland, USA (2000).
2. Hartter, D. R. "The use and importance of nitroaromatic chemicals in the chemical industry." *Toxicity of nitroaromatic compounds* (1985): 1-13.
3. Plotkin, J. S. "Benzene's Unusual Supply–Demand Dilemma." *American Chemical Society*. <https://www.acs.org/content/acs/en/pressroom/cutting-edge-chemistry/benzenes-unusual-supply-demand-dilemma.html>. Accessed May 10 (2015): 2018.
4. Mehdad, Ali, and Raul F. Lobo. "Ethane and ethylene aromatization on zinc-containing zeolites." *Catalysis Science & Technology* 7, no. 16 (2017): 3562-3572.
5. Bruijninx, Pieter CA, and Bert M. Weckhuysen. "Shale gas revolution: an opportunity for the production of biobased chemicals?." *Angewandte Chemie International Edition* 52, no. 46 (2013): 11980-11987.
6. Hamelinck, Carlo N., Geertje Van Hooijdonk, and Andre PC Faaij. "Ethanol from lignocellulosic biomass: techno-economic performance in short-, middle-and long-term." *Biomass and bioenergy* 28, no. 4 (2005): 384-410.
7. Pérez-Fortes, Mar, Jan C. Schöneberger, Aikaterini Boulamanti, and Evangelos Tzimas. "Methanol synthesis using captured CO<sub>2</sub> as raw material: Techno-economic and environmental assessment." *Applied Energy* 161 (2016): 718-732.
8. Müller, Sebastian, Yue Liu, Felix M. Kirchberger, Markus Tonigold, Maricruz Sanchez-Sanchez, and Johannes A. Lercher. "Hydrogen transfer pathways during zeolite catalyzed methanol conversion to hydrocarbons." *Journal of the American Chemical Society* 138, no. 49 (2016): 15994-16003.

9. Niziolek, Alexander M., Onur Onel, and Christodoulos A. Floudas. "Production of benzene, toluene, and xylenes from natural gas via methanol: Process synthesis and global optimization." *AIChE Journal* 62, no. 5 (2016): 1531-1556.
10. Ono, Yoshio. "Transformation of lower alkanes into aromatic hydrocarbons over ZSM-5 zeolites." *Catalysis Reviews* 34, no. 3 (1992): 179-226.
11. Corma, Avelino. "Inorganic solid acids and their use in acid-catalyzed hydrocarbon reactions." *Chemical Reviews* 95, no. 3 (1995): 559-614.
12. Davis, Mark E., and Raul F. Lobo. "Zeolite and molecular sieve synthesis." *Chemistry of Materials* 4, no. 4 (1992): 756-768.
13. Louis, Benoît, Stéphane Walspurger, and Jean Sommer. "Quantitative determination of Brønsted acid sites on zeolites: A new approach towards the chemical composition of zeolites." *Catalysis letters* 93, no. 1-2 (2004): 81-84.
14. Martínez, Cristina, and Avelino Corma. "Inorganic molecular sieves: Preparation, modification and industrial application in catalytic processes." *Coordination Chemistry Reviews* 255, no. 13-14 (2011): 1558-1580.
15. Tanabe, Kozo, and Wolfgang F. Hölderich. "Industrial application of solid acid-base catalysts." *Applied Catalysis A: General* 181, no. 2 (1999): 399-434.
16. Olson, D. H., G. T. Kokotailo, S. L. Lawton, and W. M. Meier. "Crystal structure and structure-related properties of ZSM-5." *The Journal of Physical Chemistry* 85, no. 15 (1981): 2238-2243.
17. Bhan, Aditya, and W. Nicholas Delgass. "Propane aromatization over HZSM-5 and Ga/HZSM-5 catalysts." *Catalysis Reviews* 50, no. 1 (2008): 19-151.
18. Poutsma, Marvin L, Rabo, Jule A. ed. "Unifying principles in zeolite chemistry and catalysis." *Catalysis Reviews—Science and Engineering* 23, no. 1-2 (1981): 293-313.
19. Bandiera, Jean, and Younès Ben Taarit. "Catalytic investigation of the dehydrogenation properties of pentasil type zeolites as compared with their cracking properties." *Applied Catalysis* 62, no. 1 (1990): 309-316.

20. Mole, T., J. R. Anderson, and G. Creer. "The reaction of propane over ZSM-5-H and ZSM-5-Zn zeolite catalysts." *Applied catalysis* 17, no. 1 (1985): 141-154.
21. Biscardi, Joseph A., and Enrique Iglesia. "Reaction pathways and rate-determining steps in reactions of alkanes on H-ZSM5 and Zn/H-ZSM5 catalysts." *Journal of Catalysis* 182, no. 1 (1999): 117-128.
22. Biscardi, Joseph A., George D. Meitzner, and Enrique Iglesia. "Structure and density of active Zn species in Zn/H-ZSM5 propane aromatization catalysts." *Journal of Catalysis* 179, no. 1 (1998): 192-202.
23. White, Jeffery L. "Methanol-to-hydrocarbon chemistry: The carbon pool (r)evolution." *Catalysis Science & Technology* 1, no. 9 (2011): 1630-1635.
24. Seiler, Michael, Wei Wang, Andreas Buchholz, and Michael Hunger. "Direct evidence for a catalytically active role of the hydrocarbon pool formed on zeolite H-ZSM-5 during the methanol-to-olefin conversion." *Catalysis letters* 88, no. 3-4 (2003): 187-191.
25. Ilias, Samia, and Aditya Bhan. "Tuning the selectivity of methanol-to-hydrocarbons conversion on H-ZSM-5 by co-processing olefin or aromatic compounds." *Journal of catalysis* 290 (2012): 186-192.
26. Hagen, Anke, Frank Roessner, and Wladimir Reschetilowski. "Conversion of ethane on modified zsm-5 zeolites: A study of aromatization as a function of reaction media." *Chemical Engineering & Technology: Industrial Chemistry-Plant Equipment-Process Engineering-Biotechnology* 18, no. 6 (1995): 414-419.
27. Plessow, Philipp N., and Felix Studt. "Olefin methylation and cracking reactions in H-SSZ-13 investigated with *ab initio* and DFT calculations." *Catalysis Science & Technology* 8, no. 17 (2018): 4420-4429.
28. Mordi, Raphael C., John Dwyer, and Roy Fields. "H-ZSM-5 catalysed degradation of low density polyethylene, polypropylene, polyisobutylene and squalane: Influence of polymer structure on aromatic product distribution." *Polymer degradation and stability* 46, no. 1 (1994): 57-62.
29. Pazè, Costanza, Birsel Sazak, Adriano Zecchina, and John Dwyer. "FTIR and UV-Vis Spectroscopic Study of Interaction of 1-Butene on H-Ferrierite Zeolite." *The Journal of Physical Chemistry B* 103, no. 45 (1999): 9978-9986.

30. Anslyn, Eric V., and Dennis A. Dougherty. *Modern physical organic chemistry*. University science books, 2006.
31. Springborg, Michael. *Methods of electronic-structure calculations: from molecules to solids*. 2000.
32. Young, David. *Computational chemistry: a practical guide for applying techniques to real world problems*. John Wiley & Sons, 2004.
33. Born, Max, and Robert Oppenheimer. "Zur quantentheorie der molekeln." *Annalen der physik* 389, no. 20 (1927): 457-484.
34. Moller, C., and M. S. Plesset. "Phys Rev 46: 618." In Pople JA, Seeger R, Krishnan R (1977) *Int J Quantum Chem Symp*, vol. 11, p. 149. 1934.
35. Čížek, Jiří. "On the correlation problem in atomic and molecular systems. Calculation of wavefunction components in Ursell-type expansion using quantum-field theoretical methods." *The Journal of Chemical Physics* 45, no. 11 (1966): 4256-4266.
36. Levine, Ira N. *Quantum Chemistry* Prentice-Hall, Inc., 2000.
37. Kohn, Walter, and Lu Jeu Sham. "Self-consistent equations including exchange and correlation effects." *Physical review* 140, no. 4A (1965): A1133.
38. Sousa, Sérgio Filipe, Pedro Alexandrino Fernandes, and Maria Joao Ramos. "General performance of density functionals." *The Journal of Physical Chemistry A* 111, no. 42 (2007): 10439-10452.
39. Hohenberg, Pierre, and Walter Kohn. "Inhomogeneous electron gas." *Physical review* 136, no. 3B (1964): B864.
40. Becke, Axel D. "A new mixing of Hartree–Fock and local density-functional theories." *The Journal of chemical physics* 98, no. 2 (1993): 1372-1377.
41. Brion, Francis. "On the lewis acid catalyzed diels-alder reaction of furan. regio-and stereospecific synthesis of substituted cyclohexenols and cyclohexadienols." *Tetrahedron Letters* 23, no. 50 (1982): 5299-5302.
42. Sholl, David, and Janice A. Steckel. *Density functional theory: a practical introduction*. John Wiley & Sons, 2011.

43. Mansoor, Erum, Jeroen Van der Mynsbrugge, Martin Head-Gordon, and Alexis T. Bell. "Impact of long-range electrostatic and dispersive interactions on theoretical predictions of adsorption and catalysis in zeolites." *Catalysis Today* 312 (2018): 51-65.
44. Foresman, James B., and A. Frisch. "Exploring chemistry with electronic structure methods: a guide to using Gaussian." (1996).
45. Chung, Lung Wa, W. M. C. Sameera, Romain Ramozzi, Alister J. Page, Miho Hatanaka, Galina P. Petrova, Travis V. Harris et al. "The ONIOM method and its applications." *Chemical reviews* 115, no. 12 (2015): 5678-5796.
46. Remediakis, Ioannis N., Nuria Lopez, and Jens K. Nørskov. "CO oxidation on gold nanoparticles: Theoretical studies." *Applied Catalysis A: General* 291, no. 1-2 (2005): 13-20.
47. Sauer, Joachim, Uwe Eichler, Ulrich Meier, Ansgar Schäfer, Malte von Arnim, and Reinhart Ahlrichs. "Absolute acidities and site specific properties of zeolite catalysts modelled by advanced computational chemistry technology." *Chemical physics letters* 308, no. 1-2 (1999): 147-154.
48. Brändle, Martin, Joachim Sauer, Roberto Dovesi, and Nicholas M. Harrison. "Comparison of a combined quantum mechanics/interatomic potential function approach with its periodic quantum-mechanical limit: Proton siting and ammonia adsorption in zeolite chabazite." *The Journal of chemical physics* 109, no. 23 (1998): 10379-10389.
49. Yang, Yunxia, Nick Burke, Junfang Zhang, Stanley Huang, Seng Lim, and Yonggang Zhu. "Influence of charge compensating cations on propane adsorption in X zeolites: experimental measurement and mathematical modeling." *RSC Advances* 4, no. 14 (2014): 7279-7287.
50. Feuerstein, M., and R. F. Lobo. "Characterization of Li cations in zeolite LiX by solid-state NMR spectroscopy and neutron diffraction." *Chemistry of materials* 10, no. 8 (1998): 2197-2204.
51. Jones, Andrew J., and Enrique Iglesia. "The strength of Brønsted acid sites in microporous aluminosilicates." *Acs Catalysis* 5, no. 10 (2015): 5741-5755.
52. Maskill, Howard. *The physical basis of organic chemistry*. No. 547 M38. 1985.

53. Jiao, Haijun, and Paul von Rague Schleyer. "Electrostatic acceleration of electrolytic reactions by metal cation complexation: the cyclization of 1, 3-cis-5-hexatriene into 1, 3-cyclohexadiene and the 1, 5-hydrogen shift in cyclopentadiene. The aromaticity of the transition structures." *Journal of the American Chemical Society* 117, no. 46 (1995): 11529-11535.
54. Casaschi, Adele, Giovanni Desimoni, Giuseppe Faita, Anna Gamba Invernizzi, Simonetta Lanati, and PierPaolo Righetti. "Catalysis with inorganic cations. 2. The effect of some perchlorates on Diels-Alder reaction rates." *Journal of the American Chemical Society* 115, no. 18 (1993): 8002-8007.
55. Nystrom, Steven, Alexander Hoffman, and David Hibbitts. "Tuning Brønsted acid strength by altering site proximity in CHA framework zeolites." *ACS Catalysis* 8, no. 9 (2018): 7842-7860.
56. Hoffman, Alexander, Mykela DeLuca, and David Hibbitts. "Restructuring of MFI Framework Zeolite Models and Their Associated Artifacts in Density Functional Theory Calculations." *The Journal of Physical Chemistry C* 123, no. 11 (2019): 6572-6585.
57. Grimme, Stefan, Jan Gerit Brandenburg, Christoph Bannwarth, and Andreas Hansen. "Consistent structures and interactions by density functional theory with small atomic orbital basis sets." *The Journal of chemical physics* 143, no. 5 (2015): 054107.
58. Xu, Xuefei, and Donald G. Truhlar. "Accuracy of effective core potentials and basis sets for density functional calculations, including relativistic effects, as illustrated by calculations on arsenic compounds." *Journal of chemical theory and computation* 7, no. 9 (2011): 2766-2779.
59. Weigend, Florian, and Reinhart Ahlrichs. "Balanced basis sets of split valence, triple zeta valence and quadruple zeta valence quality for H to Rn: Design and assessment of accuracy." *Physical Chemistry Chemical Physics* 7, no. 18 (2005): 3297-3305.
60. Shannon, Robert D. "Revised effective ionic radii and systematic studies of interatomic distances in halides and chalcogenides." *Acta crystallographica section A: crystal physics, diffraction, theoretical and general crystallography* 32, no. 5 (1976): 751-767.
61. Rappoport, Zvi, and Ilan Marek, eds. *The Chemistry of Organozinc Compounds: R-Zn*. Vol. 170. John Wiley & Sons, 2007.

62. Kulprathipanja, Santi, ed. *Zeolites in industrial separation and catalysis*. John Wiley & Sons, 2010.
63. Jentoft, Friederike C., and Bruce C. Gates. "Solid-acid-catalyzed alkane cracking mechanisms: evidence from reactions of small probe molecules." *Topics in catalysis* 4, no. 1-2 (1997): 1-13.
64. Jentoft, Friederike C. "Ultraviolet–visible–near infrared spectroscopy in catalysis: theory, experiment, analysis, and application under reaction conditions." *Advances in catalysis* 52 (2009): 129-211.
65. Joshi, Yogesh V., Aditya Bhan, and Kendall T. Thomson. "DFT-based reaction pathway analysis of hexadiene cyclization via carbenium ion intermediates: Mechanistic study of light alkane aromatization catalysis." *The Journal of Physical Chemistry B* 108, no. 3 (2004): 971-980.
66. Joshi, Yogesh V., and Kendall T. Thomson. "Embedded cluster (QM/MM) investigation of C<sub>6</sub> diene cyclization in HZSM-5." *Journal of Catalysis* 230, no. 2 (2005): 440-463.
67. Olah, George A., Gao Liang, and Y. K. Mo. "Stable carbocations. CXXVII. Cyclohexenyl and cyclopentenyl cations and their methylated derivatives." *Journal of the American Chemical Society* 94, no. 10 (1972): 3544-3551.
68. Mehdad, Ali, Nicholas S. Gould, Bingjun Xu, and Raul F. Lobo. "Effect of steam and CO<sub>2</sub> on ethane activation over Zn-ZSM-5." *Catalysis Science & Technology* 8, no. 1 (2018): 358-366.
69. Rhodes, Christopher J. "Properties and applications of zeolites." *Science progress* 93, no. 3 (2010): 223-284.
70. Jacob, Steven D., Joshua L. Brooks, and Alison J. Frontier. "No Acid Required: 4 $\pi$  and 6 $\pi$  Electrocyclization Reactions of Dienyl Diketones for the Synthesis of Cyclopentenones and 2 H-Pyrans." *The Journal of organic chemistry* 79, no. 21 (2014): 10296-10302.
71. Riveira, Martín J., Lucía A. Marsili, and Mirta P. Mischne. "The iso-Nazarov reaction." *Organic & biomolecular chemistry* 15, no. 44 (2017): 9255-9274.
72. Sarazen, Michele L., and Enrique Iglesia. "Stability of bound species during alkene reactions on solid acids." *Proceedings of the National Academy of Sciences* 114, no. 20 (2017): E3900-E3908.

73. Marchi, A. J., and G. F. Froment. "Catalytic conversion of methanol into light alkenes on mordenite-like zeolites." *Applied Catalysis A: General* 94, no. 1 (1993): 91-106.
74. Broadbelt, Linda J., and Randall Q. Snurr. "Applications of molecular modeling in heterogeneous catalysis research." *Applied Catalysis A: General* 200, no. 1-2 (2000): 23-46.
75. Bañares, Miguel A. "Operando methodology: combination of *in situ* spectroscopy and simultaneous activity measurements under catalytic reaction conditions." *Catalysis Today* 100, no. 1-2 (2005): 71-77.
76. Thomas, Martin, Martin Brehm, Reinhold Fligg, Peter Vöhringer, and Barbara Kirchner. "Computing vibrational spectra from *ab initio* molecular dynamics." *Physical Chemistry Chemical Physics* 15, no. 18 (2013): 6608-6622.

## Appendix A

### SUPPORTING DATA FOR DIELS-ALDER STUDIES

Table A.1: DFT-calculated  $\Delta E^{\circ\dagger}$  (Single Point Electronic energy),  $\Delta H^{\circ\dagger}$ ,  $\Delta G^{\circ\dagger}$  of the 12 Diels-Alder Cycloadditions using an energy span approach at the M06-2X/6-31g(d,p) level of theory. This data was used for Figure 3.4.

Reaction #	$\Delta E^{\circ\dagger}$ (kcal/mol)	$\Delta H^{\circ\dagger}$ (kcal/mol)	$\Delta G^{\circ\dagger}$ (kcal/mol)
1	19.70685	20.48189	35.36515
2	21.87738	22.53259	36.9289
3	21.15403	22.12471	36.87243
4	19.50459	20.35953	35.4072
5	23.68872	24.79288	38.74115
6	21.50087	22.39893	36.76073
7	27.74368	28.89993	42.61727
8	26.07076	27.30292	41.88811
9	26.216	27.29915	41.39677
10	24.95792	26.0115	40.40593
11	29.49888	30.67327	44.80163
12	28.62598	29.82676	44.02917

The energy span approach is defined in this case as:

$$\Delta X^{\circ\dagger}_{Energy\ Span} = X^{\circ}_{Transition\ State} - (X^{\circ}_{Triene\ A} + X^{\circ}_{Triene\ B}) \quad A.1$$

where  $X$  can be any DFT-calculated electronic energy with zero-point or thermal corrections. Triene A and B are the energy of cis- or trans-hexatriene at the same level of theory. Effectively, the initial state from which this activation energy is calculated is the two hexatriene molecules separated infinitely apart. This activation energy does

not account for any stabilization that may occur from bringing the two molecules close together.

Table A.2: DFT-calculated  $\Delta E^{\ddagger}$  (Single Point Electronic energy),  $\Delta H^{\ddagger}$ ,  $\Delta G^{\ddagger}$  of the 12 Diels-Alder Cycloadditions using a preceding intermediate approach at the M06-2X/6-31g(d,p) level of theory.

Reaction #	$\Delta E^{\ddagger}$ (kcal/mol)	$\Delta H^{\ddagger}$ (kcal/mol)	$\Delta G^{\ddagger}$ (kcal/mol)
1	22.07285	21.38174	26.69674
2	24.09629	23.46068	28.74932
3	23.72342	22.92039	28.39227
4	22.37878	21.72499	26.58442
5	24.94113	24.41324	28.32576
6	22.21348	21.79213	25.58982
7	25.4716	25.60174	28.49267
8	24.33978	24.12082	28.45753
9	27.46253	27.05756	30.71092
10	25.3151	25.00435	29.67176
11	27.12699	26.75196	30.87219
12	26.76566	26.16336	29.21117

The preceding intermediate approach is defined in this case as:

$$\Delta X^{\ddagger}_{IA} = X^{\circ}_{Transition\ State} - X^{\circ}_{Triene\ A+B\ Complex} \quad A.2$$

where  $X$  can be any DFT-calculated electronic energy with zero-point or thermal corrections. Unlike Equation A.1, the initial state from which the activation energy is calculated is the complex that forms between the two trienes prior to cycloaddition. There are various orientations of two hexatriene molecules that are stationary points, or stable intermediate states. For the 12 reactions, the preceding intermediate to the transition state is lower in energy than the two hexatriene molecules held apart an infinite distance. As a result, the activation energies in Table A.2 are higher than their counterparts in Table A.1.

Table A.3: DFT-calculated  $\Delta E^\circ$  (Single Point Electronic energy),  $\Delta H^\circ$ ,  $\Delta G^\circ$  of reaction for the 12 Diels-Alder Cycloadditions the M06-2X/6-31g(d,p) level of theory.

Reaction #	$\Delta E^\circ(\text{kcal/mol})$	$\Delta H^\circ(\text{kcal/mol})$	$\Delta G^\circ(\text{kcal/mol})$
1	-34.79466	-31.35349	-16.59761
2	-34.94551	-31.47585	-16.60138
3	-27.37195	-23.85726	-9.71572
4	-27.25764	-23.68093	-9.40887
5	-40.02094	-36.1966	-21.14517
6	-38.97233	-35.08089	-20.35263
7	-35.99042	-31.99794	-17.21194
8	-36.34323	-32.28785	-17.47989
9	-39.26137	-35.40092	-21.2531
10	-33.01818	-29.15156	-14.89957
11	-36.28183	-32.09709	-17.41588
12	-30.16268	-26.1301	-12.11908

Here, the energy change of reaction is defined as:

$$\Delta X^\circ = X^\circ_{DA\ cyclic\ product} - (X^\circ_{Triene\ A} + X^\circ_{Triene\ B}) \quad \text{A.3}$$

where  $X$  can be any DFT-calculated electronic energy with zero-point or thermal corrections. The initial state is the two hexatriene molecules held apart an infinite distance. In other words, the initial state is the sum of the DFT-calculated energies for the individual molecules.

Table A.4A: Summary (Part A) of log files for specific DFT calculations (Diels Alder). All energies are reported in units of Hartrees. Abbreviations: R (Reactant), RC (Reactant Complex), TS (Transition State), P (Product). "Reactant Complex" refers to a calculation for two hexatriene molecules starting in close proximity to each other.

Species or Reaction #	Type	Electronic Energy	Zero-point Corrected	Short Filename
Cis-Hexatriene	R	-233.279344815	-233.159240	CisHexatriene
Trans-Hexatriene	R	-233.281831563	-233.162326	TransHexatriene

Table A.4A continued.

1	RC	-466.5649468	-466.323754	Tail3Bo
1	TS	-466.5297715	-466.287247	Tail3BTS
1	P	-466.6166252	-466.369502	Tail3B
2	RC	-466.5647125	-466.323985	Tail3Ao
2	TS	-466.5263125	-466.284154	Tail3ATS
2	P	-466.6168656	-466.369654	Tail3A
3	RC	-466.5677577	-466.326653	Tail3Co
3	TS	-466.529952	-466.287725	Tail3CTS
3	P	-466.6072831	-466.360624	Tail3C
4	RC	-466.5682435	-466.327409	Tail3Do
4	TS	-466.5325806	-466.290433	Tail3DTS
4	P	-466.607101	-466.360295	Tail3D
5	RC	-466.5631722	-466.321480	Tail2DDo
5	TS	-466.523426	-466.280566	Tail2DDTS
5	P	-466.6249538	-466.376995	Tail2DD
6	RC	-466.562312	-466.321137	Tail2CCo
6	TS	-466.5269125	-466.284413	Tail2CCTS
6	P	-466.6232828	-466.375274	Tail2CC
7	RC	-466.5600423	-466.319285	Tail2Do
7	TS	-466.5194507	-466.277152	Tail2DTS
7	P	-466.6210176	-466.373383	Tail2D
8	RC	-466.5609046	-466.320166	Tail2Co
8	TS	-466.5221167	-466.279442	Tail2CTSb
8	P	-466.6215798	-466.373852	Tail2C
9	RC	-466.5631629	-466.321619	Tail2BBo
9	TS	-466.5193985	-466.276439	Tail2BBTS
9	P	-466.6237434	-466.375795	Tail2BB
10	RC	-466.5617456	-466.320766	Tail2AAo
10	TS	-466.5214034	-466.278467	Tail2AATS
10	P	-466.6137942	-466.365927	Tail2AA
11	RC	-466.5598833	-466.319029	Tail2Bo
11	TS	-466.5166536	-466.274149	Tail2BTS
11	P	-466.6214819	-466.373569	Tail2B
12	RC	-466.5606985	-466.319082	Tail2Ao
12	TS	-466.5180447	-466.275497	Tail2ATS
12	P	-466.6117305	-466.364149	Tail2A

Table A.4B: Summary (Part B) of log files for specific DFT calculations (Diels Alder). All energies are reported in units of Hartrees. Abbreviations: R (Reactant), RC (Reactant Complex), TS (Transition State), P (Product). “Reactant Complex” refers to a calculation for two hexatriene molecules starting in close proximity to each other. U, H, G are thermally corrected electronic energies based on vibrational frequency analysis.

Species or Reaction #	Type	U (Energy)	H (Enthalpy)	G (Free Energy)
Cis-Hexatriene	R	-233.152570	-233.151626	-233.189481
Trans-Hexatriene	R	-233.155533	-233.154589	-233.192595
1	RC	-466.308593	-466.307649	-466.368262
1	TS	-466.274519	-466.273575	-466.325718
1	P	-466.357125	-466.356180	-466.408526
2	RC	-466.308638	-466.307694	-466.369041
2	TS	-466.271251	-466.270307	-466.323226
2	P	-466.357319	-466.356375	-466.408532
3	RC	-466.311390	-466.310446	-466.371676
3	TS	-466.274864	-466.273920	-466.326430
3	P	-466.348142	-466.347197	-466.400673
4	RC	-466.312298	-466.311354	-466.371130
4	TS	-466.277677	-466.276733	-466.328765
4	P	-466.347860	-466.346916	-466.400184
5	RC	-466.306554	-466.305610	-466.365478
5	TS	-466.267649	-466.266705	-466.320338
5	P	-466.364842	-466.363898	-466.415773
6	RC	-466.306193	-466.305248	-466.364274
6	TS	-466.271464	-466.270520	-466.323494
6	P	-466.363064	-466.362120	-466.414510
7	RC	-466.304866	-466.303922	-466.362681
7	TS	-466.264068	-466.263123	-466.317275
7	P	-466.361114	-466.360170	-466.412619
8	RC	-466.305051	-466.304107	-466.363787
8	TS	-466.266612	-466.265668	-466.318437
8	P	-466.361576	-466.360632	-466.413046
9	RC	-466.306775	-466.305830	-466.365047
9	TS	-466.263655	-466.262711	-466.316106
9	P	-466.363574	-466.362630	-466.415945

Table A.4B continued.

10	RC	-466.305555	-466.304610	-466.364970
10	TS	-466.265707	-466.264763	-466.317685
10	P	-466.353615	-466.352671	-466.405820
11	RC	-466.303873	-466.302929	-466.362992
11	TS	-466.261241	-466.260297	-466.313794
11	P	-466.361272	-466.360328	-466.412944
12	RC	-466.304284	-466.303340	-466.361576
12	TS	-466.262590	-466.261646	-466.315025
12	P	-466.351763	-466.350819	-466.404503

## Appendix B

### SUPPORTING DATA FOR ELECTROCYCLIZATION STUDIES

Table B.1: DFT-calculated  $\Delta E^{\ddagger}$  (Single Point Electronic energy),  $\Delta H^{\ddagger}$ ,  $\Delta G^{\ddagger}$  for monovalent cation-mediate electrocyclization in the gas phase using various basis sets at the M06-2X level of theory. These activation energies were calculated using a preceding intermediate approach.

Basis Set	Cation	$\Delta E^{\ddagger}(\text{kcal/mol})$	$\Delta H^{\ddagger}(\text{kcal/mol})$	$\Delta G^{\ddagger}(\text{kcal/mol})$
6-31g(d,p)	Uncatalyzed	28.76564	30.17252	29.50246
	Li	21.62459	24.09509	21.78591
	Na	26.1552	27.26527	26.80809
	K	27.85575	29.33228	28.51503
6-311g (3df,3pd)	Uncatalyzed	29.61089	30.90356	30.39479
	Li	21.62835	24.01414	21.93014
	Na	27.25272	29.09069	27.95195
	K	28.38725	29.97924	29.04657
def2svp	Uncatalyzed	28.79764	30.20766	29.5245
	Li	21.43884	23.80706	21.69225
	Na	26.37671	28.08668	26.88386
	K	27.67315	29.68808	28.17681
	Rb	28.24167	30.23213	28.77216
	Cs	28.29877	30.0878	28.8822
def2tzvpp	Uncatalyzed	29.81484	31.12947	30.58294
	Li	21.89379	24.11643	22.22126
	Na	27.43407	29.01288	28.12362
	K	28.74305	30.46431	29.3642
	Rb	28.67277	32.17929	29.88541
	Cs	28.67653	32.1203	29.89929

To clarify, these activation energies were calculated as follows:

$$\Delta X^{\ddagger}_{PI} = X^{\circ}_{\text{Transition State Complex}} - X^{\circ}_{\text{Triene-Cation Complex}} \quad \text{B.1}$$

It is important to note that in all cases, the Triene-Cation complex is lower in energy than the sum of individual energies for the cation and hexatriene.

Table B.2A: Summary (Part A) of log files for monovalent cation-mediated electrocyclization at the M06-2X/6-31g(d,p) level of theory. All energies are reported in units of Hartrees. Abbreviations: T (trans-hexatriene), Cat(ion), C (cis-hexatriene), TS (transition state), Cy(cyclohexadiene). All results are for cation-molecule complexes.

<b>Cation</b>	<b>Molecule</b>	<b>Electronic Energy</b>	<b>Zero-Point Corrected</b>	<b>Short Filename (Squid 631gdp)</b>
None	T	-233.28183	-233.16233	TransHexatriene.log
	C	-233.27934	-233.15924	CisHexatriene.log
	TS	-233.23233	-233.11222	TransitionStateG.log
	Cy	-233.31101	-233.18749	Cyclohexadiene.log
Li	T	-240.62049	-240.49897	LiTransHexatriene.log
	Cat	-7.28102	-7.28102	Li.log
	C	-240.62118	-240.49952	LiCisHexatriene.log
	TS	-240.58646	-240.46339	LiTS.log
	Cy	-240.65376	-240.52822	LiCyclohexadiene.log
Na	T	-395.36757	-395.24684	NaTransHexatriene.log
	Cat	-162.0445	-162.0445	Na.log
	C	-395.36784	-395.24663	NaCisHexatriene.log
	TS	-395.32512	-395.20374	NaTS.log
	Cy	-395.39907	-395.27435	NaCyclohexadiene.log
K	T	-833.01079	-832.89036	KTransHexatriene.log
	Cat	-599.70114	-599.70114	K.log
	C	-833.01131	-832.89038	KCisHexatriene.log
	TS	-832.96586	-832.84474	KTS.log
	Cy	-833.04152	-832.91697	KCyclohexadiene.log

Table B.2B: Summary (Part B) of log files for monovalent cation-mediated electrocyclization at the M06-2X/6-31g(d,p) level of theory. All energies are reported in units of Hartrees. Abbreviations: T (trans-hexatriene), Cat(ion), C (cis-hexatriene), TS (transition state), Cy(cyclohexadiene). All results are for cation-molecule complexes. U, H, G are thermally corrected electronic energies based on vibrational frequency analysis.

<b>Cation</b>	<b>Molecule</b>	<b>U (Energy)</b>	<b>H (Enthalpy)</b>	<b>G (Free Energy)</b>
None	T	-233.15553	-233.15459	-233.1926
	C	-233.15257	-233.15163	-233.18948
	TS	-233.10673	-233.10578	-233.1414
	Cy	-233.18233	-233.18138	-233.21572
Li	T	-240.49074	-240.4898	-240.53112
	Cat	-7.2796	-7.27866	-7.29377
	C	-240.49127	-240.49032	-240.53216
	TS	-240.45681	-240.45586	-240.49377
	Cy	-240.52172	-240.52077	-240.55784
Na	T	-395.23814	-395.2372	-395.28084
	Cat	-162.04308	-162.04214	-162.05893
	C	-395.23803	-395.23708	-395.28035
	TS	-395.19635	-395.1954	-395.2369
	Cy	-395.26733	-395.26638	-395.30566
K	T	-832.88146	-832.88051	-832.92571
	Cat	-599.69973	-599.69878	-599.71632
	C	-832.8816	-832.88065	-832.9251
	TS	-832.83721	-832.83626	-832.87835
	Cy	-832.90979	-832.90884	-832.94934

Table B.3A: Summary (Part A) of log files for monovalent cation-mediated electrocyclization at the M06-2X/6-311g(3df,2pd) level of theory. All energies are reported in units of Hartrees. Abbreviations: T (trans-hexatriene), Cat(ion), C (cis-hexatriene), TS (transition state), Cy(cyclohexadiene). All results are for cation-molecule complexes.

<b>Cation</b>	<b>Molecule</b>	<b>Electronic Energy</b>	<b>Zero-Point Corrected</b>	<b>Short Filename (Squid 6311g3df2pd)</b>
None	T	-233.35547	-233.23637	TransHexatriene.log
	C	-233.35293	-233.23328	CisHexatriene.log
	TS	-233.3045	-233.18495	TransitionStateG.log
	Cy	-233.38074	-233.25778	Cyclohexadiene.log
Li	T	-240.69169	-240.57064	LiTransHexatriene.log
	Cat	-7.28119	-7.28119	Li.log
	C	-240.69172	-240.57027	LiCisHexatriene.log
	TS	-240.65677	-240.53409	LiTS.log
	Cy	-240.72225	-240.59705	LiCyclohexadiene.log
Na	T	-395.44402	-395.32375	NaTransHexatriene.log
	Cat	-162.05014	-162.05014	Na.log
	C	-395.44391	-395.32315	NaCisHexatriene.log
	TS	-395.39936	-395.27844	NaTS.log
	Cy	-395.47167	-395.34747	NaCyclohexadiene.log
K	T	-833.12626	-833.00622	KTransHexatriene.log
	Cat	-599.74316	-599.74316	K.log
	C	-833.12658	-833.0062	KCisHexatriene.log
	TS	-833.08029	-832.95968	KTS.log
	Cy	-833.15322	-833.02915	KCyclohexadiene.log

Table B.3B: Summary (Part B) of log files for monovalent cation-mediated electrocyclization at the M06-2X/6-311g(3df,2pd) level of theory. All energies are reported in units of Hartrees. Abbreviations: T (trans-hexatriene), Cat(ion), C (cis-hexatriene), TS (transition state), Cy(cyclohexadiene). All results are for cation-molecule complexes. U, H, G are thermally corrected electronic energies based on vibrational frequency analysis.

<b>Cation</b>	<b>Molecule</b>	<b>U (Energy)</b>	<b>H (Enthalpy)</b>	<b>G (Free Energy)</b>
None	T	-233.22963	-233.22869	-233.26657
	C	-233.22665	-233.22571	-233.26347
	TS	-233.17946	-233.17852	-233.21423
	Cy	-233.25264	-233.25169	-233.28598
Li	T	-240.56243	-240.56149	-240.60281
	Cat	-7.27978	-7.27883	-7.29394
	C	-240.56204	-240.5611	-240.60287
	TS	-240.52758	-240.52663	-240.5646
	Cy	-240.59063	-240.58969	-240.62651
Na	T	-395.31506	-395.31412	-395.3578
	Cat	-162.04872	-162.04778	-162.06456
	C	-395.31453	-395.31358	-395.35707
	TS	-395.2711	-395.27015	-395.31071
	Cy	-395.34043	-395.33948	-395.37889
K	T	-832.99738	-832.99644	-833.04146
	Cat	-599.74174	-599.7408	-599.75833
	C	-832.99741	-832.99647	-833.04098
	TS	-832.95217	-832.95123	-832.9932
	Cy	-833.02199	-833.02105	-833.06147

Table B.4A: Summary (Part A) of log files for monovalent cation-mediated electrocyclization at the M06-2X/def2svp level of theory. All energies are reported in units of Hartrees. Abbreviations: T (trans-hexatriene), Cat(ion), C (cis-hexatriene), TS (transition state), Cy(cyclohexadiene). All results are for cation-molecule complexes.

<b>Cation</b>	<b>Molecule</b>	<b>Electronic Energy</b>	<b>Zero-Point Corrected</b>	<b>Short Filename (Squid 631gdp)</b>
None	T	-233.05209	-232.9325	DEF_TransHexatriene.log
	C	-233.13106	-233.00808	DEF_CisHexatriene.log
	TS	-240.43092	-240.31004	DEF_TransitionStateG.log
	Cy	-7.27768	-7.27768	DEF_Cyclohexadiene.log
Li	T	-240.43078	-240.30953	DEF_LiTransHexatriene.log
	Cat	-240.39621	-240.27371	DEF_Li.log
	C	-240.46539	-240.34043	DEF_LiCisHexatriene.log
	TS	-395.14419	-395.02404	DEF_LiTS.log
	Cy	-162.00614	-162.00614	DEF_LiCyclohexadiene.log
Na	T	-395.14427	-395.0238	DEF_NaTransHexatriene.log
	Cat	-395.10143	-394.98047	DEF_Na.log
	C	-395.17631	-395.05217	DEF_NaCisHexatriene.log
	TS	-832.79384	-832.67399	DEF_NaTS.log
	Cy	-599.66653	-599.66653	DEF_NaCyclohexadiene.log
K	T	-832.79434	-832.67424	DEF_KTransHexatriene.log
	Cat	-832.74944	-832.62877	DEF_K.log
	C	-832.82542	-832.7015	DEF_KCisHexatriene.log
	TS	-256.99624	-256.87662	DEF_KTS.log
	Cy	-23.87209	-23.87209	DEF_KCyclohexadiene.log
Rb	T	-256.99647	-256.87656	RbTransHexatriene.log
	Cat	-256.95062	-256.8302	Rb.log
	C	-257.02745	-256.9037	RbCisHexatriene.log
	TS	-253.05575	-252.93621	RbTS.log
	Cy	-19.93347	-19.93347	RbCyclohexadiene.log
Cs	T	-253.05614	-252.93615	CsTransHexatriene.log
	Cat	-253.01012	-252.88979	Cs.log
	C	-253.08687	-252.9631	CsCisHexatriene.log
	TS	-233.05209	-232.9325	CsTS.log
	Cy	-233.13106	-233.00808	CsCyclohexadiene.log

Table B.4B: Summary (Part B) of log files for monovalent cation-mediated electrocyclization at the M06-2X/def2svp level of theory. All energies are reported in units of Hartrees. Abbreviations: T (trans-hexatriene), Cat(ion), C (cis-hexatriene), TS (transition state), Cy(cyclohexadiene). All results are for cation-molecule complexes. U, H, G are thermally corrected electronic energies based on vibrational frequency analysis.

<b>Cation</b>	<b>Molecule</b>	<b>U (Energy)</b>	<b>H (Enthalpy)</b>	<b>G (Free Energy)</b>
None	T	-232.97557	-232.97463	-233.01261
	C	-232.97288	-232.97194	-233.00981
	TS	-232.92699	-232.92604	-232.96167
	Cy	-233.00291	-233.00197	-233.03631
Li	T	-240.30174	-240.3008	-240.34229
	Cat	-7.27626	-7.27532	-7.29043
	C	-240.30125	-240.30031	-240.34201
	TS	-240.26708	-240.26614	-240.30407
	Cy	-240.33392	-240.33297	-240.37003
Na	T	-395.0153	-395.01436	-395.0582
	Cat	-162.00472	-162.00378	-162.02057
	C	-395.0151	-395.01415	-395.05785
	TS	-394.97306	-394.97212	-395.01309
	Cy	-395.04511	-395.04417	-395.0836
K	T	-832.66505	-832.66411	-832.70943
	Cat	-599.66511	-599.66417	-599.68171
	C	-832.66534	-832.66439	-832.70932
	TS	-832.62123	-832.62029	-832.66201
	Cy	-832.69427	-832.69332	-832.73397
Rb	T	-256.86753	-256.86658	-256.91347
	Cat	-23.87067	-23.86973	-23.88837
	C	-256.8675	-256.86656	-256.91316
	TS	-256.82249	-256.82155	-256.86498
	Cy	-256.89634	-256.8954	-256.93746
Cs	T	-252.92707	-252.92612	-252.97398
	Cat	-19.93205	-19.93111	-19.95038
	C	-252.92714	-252.9262	-252.97315
	TS	-252.88205	-252.8811	-252.9252
	Cy	-252.95574	-252.95479	-252.99748

Table B.5A: Summary (Part A) of log files for monovalent cation-mediated electrocyclization at the M06-2X/def2tzvpp level of theory. All energies are reported in units of Hartrees. Abbreviations: T (trans-hexatriene), Cat(ion), C (cis-hexatriene), TS (transition state), Cy(cyclohexadiene). All results are for cation-molecule complexes.

<b>Cation</b>	<b>Molecule</b>	<b>Electronic Energy</b>	<b>Zero-Point Corrected</b>	<b>Short Filename (Squid 631gdp)</b>
None	T	-233.36885	-233.24973	DEF_TransHexatriene.log
	C	-233.36643	-233.24665	DEF_CisHexatriene.log
	TS	-233.31769	-233.19799	DEF_TransitionStateG.log
	Cy	-233.39382	-233.27073	DEF_Cyclohexadiene.log
Li	T	-240.70411	-240.58296	DEF_LiTransHexatriene.log
	Cat	-7.28288	-7.28288	DEF_Li.log
	C	-240.70395	-240.58227	DEF_LiCisHexatriene.log
	TS	-240.66853	-240.54572	DEF_LiTS.log
	Cy	-240.73431	-240.60905	DEF_LiCyclohexadiene.log
Na	T	-395.46114	-395.34077	DEF_NaTransHexatriene.log
	Cat	-162.05679	-162.05679	DEF_Na.log
	C	-395.46076	-395.33993	DEF_NaCisHexatriene.log
	TS	-395.41594	-395.29494	DEF_NaTS.log
	Cy	-395.4886	-395.3642	DEF_NaCyclohexadiene.log
K	T	-833.13518	-833.01512	DEF_KTransHexatriene.log
	Cat	-599.7413	-599.7413	DEF_K.log
	C	-833.13523	-833.01491	DEF_KCisHexatriene.log
	TS	-833.08843	-832.96777	DEF_KTS.log
	Cy	-833.16193	-833.0377	DEF_KCyclohexadiene.log
Rb	T	-257.26317	-257.14334	RbTransHexatriene.log
	Cat	-23.87237	-23.87237	Rb.log
	C	-257.26319	-257.14303	RbCisHexatriene.log
	TS	-257.21556	-257.09516	RbTSb.log
	Cy	-257.28956	-257.16552	RbCyclohexadiene.log
Cs	T	-253.3227	-253.20292	CsTransHexatriene.log
	Cat	-19.93347	-19.93347	Cs.log
	C	-253.32286	-253.20268	CsCisHexatriene.log
	TS	-253.27522	-253.15481	CsTS.log
	Cy	-253.34906	-253.22505	CsCyclohexadiene.log

Table B.5B: Summary (Part B) of log files for monovalent cation-mediated electrocyclization at the M06-2X/def2tzvpp level of theory. All energies are reported in units of Hartrees. Abbreviations: T (trans-hexatriene), Cat(ion), C (cis-hexatriene), TS (transition state), Cy(cyclohexadiene). All results are for cation-molecule complexes. U, H, G are thermally corrected electronic energies based on vibrational frequency analysis.

<b>Cation</b>	<b>Molecule</b>	<b>U (Energy)</b>	<b>H (Enthalpy)</b>	<b>G (Free Energy)</b>
None	T	-233.24298	-233.24203	-233.27994
	C	-233.24002	-233.23908	-233.27683
	TS	-233.19251	-233.19157	-233.22722
	Cy	-233.26558	-233.26464	-233.29894
Li	T	-240.57473	-240.57378	-240.61516
	Cat	-7.28147	-7.28052	-7.29563
	C	-240.57407	-240.57313	-240.6147
	TS	-240.53918	-240.53824	-240.57627
	Cy	-240.60261	-240.60167	-240.63854
Na	T	-395.33206	-395.33111	-395.37494
	Cat	-162.05537	-162.05443	-162.07122
	C	-395.33126	-395.33032	-395.37396
	TS	-395.28755	-395.2866	-395.32772
	Cy	-395.35716	-395.35621	-395.39561
K	T	-833.00622	-833.00528	-833.05053
	Cat	-599.73988	-599.73894	-599.75648
	C	-833.00602	-833.00507	-833.05006
	TS	-832.96021	-832.95927	-833.00151
	Cy	-833.03053	-833.02958	-833.07006
Rb	T	-257.13429	-257.13335	-257.18016
	Cat	-23.87096	-23.87001	-23.88865
	C	-257.13403	-257.13309	-257.17954
	TS	-257.08834	-257.08739	-257.12826
	Cy	-257.1582	-257.15726	-257.19917
Cs	T	-253.19385	-253.1929	-253.24052
	Cat	-19.93205	-19.93111	-19.95038
	C	-253.19369	-253.19275	-253.23969
	TS	-253.14799	-253.14705	-253.1885
	Cy	-253.21772	-253.21677	-253.25934

Table B.6: Crystal ionic radii of relevant cations as reported in Reference 60.

<b>Cation</b>	<b>Ionic Radius (pm)</b>	<b>Ionic Radius (Å)</b>
Li <sup>+</sup>	90	0.90
Na <sup>+</sup>	116	1.16
K <sup>+</sup>	152	1.52
Rb <sup>+</sup>	166	1.66
Cs <sup>+</sup>	181	1.81
Mg <sup>2+</sup>	72	0.72
Ca <sup>2+</sup>	100	1.00
Zn <sup>2+</sup>	74	0.74

Table B.7: DFT-calculated  $\Delta E^{\ddagger}$  (Single Point Electronic energy),  $\Delta H^{\ddagger}$ ,  $\Delta G^{\ddagger}$  for divalent cation-mediate electrocyclization in the gas phase at the M06-2X/6-31g(d,p) level of theory. These activation energies were calculated using a preceding intermediate approach. See Equation B.1

<b>Cation</b>	<b><math>\Delta E^{\ddagger}</math>(kcal/mol)</b>	<b><math>\Delta H^{\ddagger}</math>(kcal/mol)</b>	<b><math>\Delta G^{\ddagger}</math>(kcal/mol)</b>
Mg	26.44013	26.36667	27.80367
Ca	27.68044	27.16361	28.81082
Zn	37.025	36.48212	37.50496

Table B.8: Summary of log files for divalent cation-mediated electrocyclization at the M06-2X/6-31g(d,p) level of theory. All energies are reported in units of Hartrees. Abbreviations: T (trans-hexatriene), Cat(ion), C (cis-hexatriene), TS (transition state), Cy(cyclohexadiene). All results are for cation-molecule complexes.

<b>Cation</b>	<b>Molecule</b>	<b>Electronic Energy</b>	<b>Zero-Point Corrected</b>	<b>Short Filename</b>
Mg	Cat	-199.19524	-199.19524	Mgonly.log
	C	-432.68788	-432.56687	cis_Mg_optC.log
	TS	-432.64574	-432.52353	TS_Mg_opt.log
	Cy	-432.70493	-432.58058	cyc_Mg_optC.log
Ca	Cat	-676.85202	-676.85202	Caonly.log
	C	-910.25609	-910.13488	cis_Ca_opt2.log
	TS	-910.21198	-910.09029	TS_Ca_opt.log
	Cy	-910.28023	-910.1557	cyc_Ca_opt2.log
Zn	Cat	-2011.65698	-2011.53522	ZnCis.log
	C	-2011.61965	-2011.49894	cis_Zn_optC.log
	TS	-2011.59798	-2011.47621	TS_zn_opt.log
	Cy	-2011.65514	-2011.5317	cyc_Zn_optC.log
<b>Cation</b>	<b>Molecule</b>	<b>U (Energy)</b>	<b>H (Enthalpy)</b>	<b>G (Free Energy)</b>
Mg	Cat	-199.19383	-199.19288	-199.20973
	C	-432.55878	-432.55784	-432.5993
	TS	-432.51676	-432.51582	-432.555
	Cy	-432.57418	-432.57323	-432.61066
Ca	Cat	-676.85061	-676.84966	-676.86723
	C	-910.12649	-910.12555	-910.16849
	TS	-910.0832	-910.08226	-910.12258
	Cy	-910.14898	-910.14804	-910.1869
Zn	Cat	-2011.52747	-2011.52652	-2011.56789
	C	-2011.49034	-2011.4894	-2011.53365
	TS	-2011.46933	-2011.46839	-2011.50813
	Cy	-2011.52514	-2011.5242	-2011.56272

Table B.9: DFT-calculated  $\Delta E^{\ddagger}$  (Single Point Electronic energy),  $\Delta H^{\ddagger}$ ,  $\Delta G^{\ddagger}$  for cation-mediate electrocyclization in the FAU cluster (Site II) at the M06-2X/6-31g(d,p) or M06-2X/def2svp (\*) level of theory. These activation energies were calculated using a preceding intermediate approach. See Equation B.1.

Cation	$\Delta E^{\ddagger}$ (kcal/mol)	$\Delta H^{\ddagger}$ (kcal/mol)	$\Delta G^{\ddagger}$ (kcal/mol)
Li	30.86788	30.20389	31.41059
Na	25.49464	24.81359	26.23615
K	28.06582	27.64993	29.60776
Rb*	27.16696	26.75134	28.1237
Cs*	28.43326	27.90784	27.87897
Zn (Adjacent)	28.75982	28.11366	28.79702
Zn (Opposite)	30.66006	30.04764	31.2192

Table B.10: Summary of log files for electrocyclization at FAU Site II at the M06-2X/6-31g(d,p) or M06-2X/def2svp (Rb, Cs) level of theory. All energies are reported in units of Hartrees. Abbreviations: T (trans-hexatriene), Clu(ster), C (cis-hexatriene), TS (transition state), Cy(cyclohexadiene). All results are for cluster-molecule complexes.

Cation	Molecule	Electronic Energy	Zero-Point Corrected	Short Filename
Li	Clu	-6992.39231	-6992.22796	LiXSII.log
	C	-7225.70533	-7225.41974	LiXSIIcishexatriene.log
	TS	-7225.65614	-7225.37051	TSLiXSIIhexatrieneto cyclohexadiene.log
	Cy	-7225.73436	-7225.44522	LiXSIIcyclo13 hexadiene.log
Na	Clu	-7147.11854	-7146.95512	NaS2.log
	C	-7380.42949	-7380.14407	NaS2Cis.log
	TS	-7380.38886	-7380.10336	NaS2TSg.log
	Cy	-7380.46054	-7380.17219	NaS2Cyc.log
K	Clu	-7584.74102	-7584.57798	KS2.log
	C	-7818.04827	-7817.76407	KS2Cis.log
	TS	-7818.00354	-7817.71862	KS2TSgb.log
	Cy	-7818.07735	-7817.78936	KS2Cyc.log

Table B.10 continued.

Rb	Clu	-7006.29898	-7006.1357	RbS2.log
	C	-7239.42054	-7239.13675	RbS2Cis.log
	TS	-7239.37725	-7239.09282	RbS2TSgb.log
	Cy	-7239.45155	-7239.16398	RbS2Cyc.log
Cs	Clu	-7002.352	-7002.18893	CsS2.log
	C	-7235.42746	-7235.14327	CsS2TSg.log
	TS	-7235.50415	-7235.21724	CsS2Cyc.log
	Cy	-7235.47277	-7235.1886	CsS2Cis.log
Zn (Adjacent)	Clu	-8716.8491	-8716.68682	ZnS2A.log
	C	-8950.19281	-8949.90899	ZnS2ACis.log
	TS	-8950.14698	-8949.86323	ZnS2ACisTS.log
	Cy	-8950.22648	-8949.93845	ZnS2ACyc.log
Zn (Opposite)	Clu	-8716.85858	-8716.69633	ZnS2B.log
	C	-8950.2019	-8949.9179	ZnS2BCis.log
	TS	-8950.15304	-8949.86887	ZnS2BCycTS.log
	Cy	-8950.23361	-8949.94608	ZnS2BCyc.log
<b>Cation</b>	<b>Molecule</b>	<b>U (Energy)</b>	<b>H (Enthalpy)</b>	<b>G (Free Energy)</b>
Li	Clu	-6992.18918	-6992.18823	-6992.29086
	C	-7225.37272	-7225.37177	-7225.49243
	TS	-7225.32459	-7225.32364	-7225.44237
	Cy	-7225.39948	-7225.39853	-7225.51752
Na	Clu	-7146.91545	-7146.9145	-7147.02045
	C	-7380.09645	-7380.0955	-7380.2185
	TS	-7380.0569	-7380.05596	-7380.17669
	Cy	-7380.12566	-7380.12472	-7380.24708
K	Clu	-7584.53805	-7584.53711	-7584.64364
	C	-7817.71582	-7817.71487	-7817.83992
	TS	-7817.67175	-7817.67081	-7817.79274
	Cy	-7817.74253	-7817.74158	-7817.86429
Rb	Clu	-7006.09562	-7006.09467	-7006.20257
	C	-7239.08829	-7239.08735	-7239.21349
	TS	-7239.04566	-7239.04472	-7239.16868
	Cy	-7239.11688	-7239.11594	-7239.24054
Cs	Clu	-7002.14877	-7002.14782	-7002.25607
	C	-7235.09587	-7235.09493	-7235.22041
	TS	-7235.16986	-7235.16892	-7235.29555
	Cy	-7235.14035	-7235.1394	-7235.26483
Zn (Adjacent)	Clu	-8716.64702	-8716.64607	-8716.75199
	C	-8949.86136	-8949.86041	-8949.98224
	TS	-8949.81656	-8949.81561	-8949.93635
	Cy	-8949.89235	-8949.89141	-8950.01001

Table B.10 continued.

Zn (Opposite)	Clu	-8716.6564	-8716.65545	-8716.76321
	C	-8949.87021	-8949.86927	-8949.99174
	TS	-8949.82233	-8949.82138	-8949.94199
	Cy	-8949.89965	-8949.89871	-8950.01906

Table B.11: Interaction distances between cation and hexatriene in the various transition states. Asterisk indicates asymmetric orientation of the hexatriene over the cation (lack of  $C_v$ ).

Cation	Gas Phase	Cluster Site II	Cluster Site III
Li	2.16	3.02*	2.28*
Na	2.55	2.62	2.6
K	2.94	3.01	N/A
Rb	3.12	3.15*	N/A
Cs	3.3	3.41*	N/A
Mg	2.26	N/A	N/A
Ca	2.64	N/A	N/A
Zn (adjacent)	2.16	2.37*	2.32*
Zn (opposite)	N/A	2.37*	N/A

Table B.12: DFT-calculated  $\Delta E^{\ddagger}$  (Single Point Electronic energy),  $\Delta H^{\ddagger}$ ,  $\Delta G^{\ddagger}$  for cation-mediate electrocyclization in the FAU cluster (Site III) at the M06-2X/6-31g(d,p) level of theory. These activation energies were calculated using a preceding intermediate approach. See Equation B.1.

Cation	$\Delta E^{\ddagger}$ (kcal/mol)	$\Delta H^{\ddagger}$ (kcal/mol)	$\Delta G^{\ddagger}$ (kcal/mol)
Li	22.89755	22.46921	26.08806
Na	24.66901	24.11705	26.53987
Zn	27.96073	27.5489	28.39102

Table B.13: Summary of log files for electrocyclozation at FAU Site III at the M06-2X/6-31g(d,p) level of theory. All energies are reported in units of Hartrees. Abbreviations: T (trans-hexatriene), Clu(ster), C (cis-hexatriene), TS (transition state), Cy(cyclohexadiene). All results are for cluster-molecule complexes.

<b>Cation</b>	<b>Molecule</b>	<b>Electronic Energy</b>	<b>Zero-Point Corrected</b>	<b>Short Filename</b>
Li	Clu	-6992.39231	-6992.22796	LiS2Opt.log
	C	-11033.40889	-11033.03694	LiClusBv2Cis.log
	TS	-11033.37241	-11032.99941	LiS3CyCTS.log
	Cy	-11033.44229	-11033.06645	LiClusBv2Cyc.log
Na	Clu	-10954.82021	-10954.571	NaS3.log
	C	-11188.13523	-11187.7641	NaS3Cis.log
	TS	-11188.09592	-11187.72425	NaS3TSg.log
	Cy	-11188.16693	-11187.79243	NaS3Cyc.log
Zn	Clu	-12524.51181	-12524.26431	ZnClusS3A.log
	C	-12757.87892	-12757.50947	ZnClusS3Cis.log
	TS	-12757.83436	-12757.46458	ZnClusS3TS.log
	Cy	-12757.91304	-12757.54011	ZnClusS3Cyc.log
<b>Cation</b>	<b>Molecule</b>	<b>U (Energy)</b>	<b>H (Enthalpy)</b>	<b>G (Free Energy)</b>
Li	Clu	-6992.18918	-6992.18823	-6992.29086
	C	-11032.97173	-11032.97079	-11033.12608
	TS	-11032.93593	-11032.93498	-11033.08451
	Cy	-11033.00303	-11033.00208	-11033.15225
Na	Clu	-10954.51349	-10954.51255	-10954.65108
	C	-11187.69843	-11187.69749	-11187.85378
	TS	-11187.66	-11187.65905	-11187.81149
	Cy	-11187.72817	-11187.72723	-11187.88026
Zn	Clu	-12524.20711	-12524.20616	-12524.34206
	C	-12757.44433	-12757.44338	-12757.59589
	TS	-12757.40042	-12757.39948	-12757.55065
	Cy	-12757.47632	-12757.47537	-12757.62556

## Appendix C

### SUPPORTING INFORMATION FOR CARBOCATION STUDIES

Table C.1A: Gas phase calculation results for the Poutsma mechanism (electronic and zero point corrected energies). Refer to Figure 5.10 for molecule labels.

<b>Molecule</b>	<b>Electronic Energy (Hartrees)</b>	<b>Zero-Point Corrected (Hartrees)</b>	<b>Short Filename</b>
R	-233.27934	-233.15924	CisHexatriene.log
A	-233.6102	-233.47699	StatABIRCgLEFT.log
A <sup>‡</sup>	-233.56601	-233.43581	MLTSg1.log
B	-233.65993	-233.52705	MCpenta1allylIRCleft.log
B <sup>‡</sup>	-233.57161	-233.44061	MCpenta1allylITSg.log
C	-233.62923	-233.49445	MCpenta1allylIRCright.log
P	-233.31101	-233.18749	cyclo13hexadiene.log

Table C.1B: Gas phase calculation results for the Poutsma mechanism (thermal corrections for internal energy, enthalpy, and free energy). Refer to Figure 5.10 for molecule labels. All results are in Hartrees.

<b>Molecule</b>	<b>U (Energy)</b>	<b>H (Enthalpy)</b>	<b>G (Free Energy)</b>
R	-233.15257	-233.15163	-233.18948
A	-233.47055	-233.4696	-233.50684
A <sup>‡</sup>	-233.43006	-233.42911	-233.4647
B	-233.52087	-233.51993	-233.55672
B <sup>‡</sup>	-233.43494	-233.43399	-233.46994
C	-233.48897	-233.48802	-233.52292
P	-233.18233	-233.18138	-233.21572

Table C.2A: Gas phase calculation results for the Alternative mechanism (electronic and zero point corrected energies). Refer to Figure 5.10 for molecule labels.

<b>Molecule</b>	<b>Electronic Energy (Hartrees)</b>	<b>Zero-Point Corrected (Hartrees)</b>	<b>Short Filename</b>
J	-233.6193	-233.4875	RcA.log
J <sup>‡</sup>	-233.59705	-233.46703	C1PhexadienylcataTSg.log
K	-233.61361	-233.48182	C1PhexadienylcataIRCleft.log
K <sup>‡</sup>	-233.60414	-233.47272	PARAts1.log
L	-233.6417	-233.50801	PA.log
L <sup>‡</sup>	-233.59994	-233.46712	methyl1ABTSg.log
M	-233.64256	-233.50779	methyl1ABIRCright.log

Table C2.B: Gas phase calculation results for the Alternative mechanism (thermal corrections for internal energy, enthalpy, and free energy). Refer to Figure 5.10 for molecule labels. All results are in Hartrees.

<b>Molecule</b>	<b>U (Energy)</b>	<b>H (Enthalpy)</b>	<b>G (Free Energy)</b>
J	-233.48024	-233.4793	-233.51846
J <sup>‡</sup>	-233.46024	-233.45929	-233.49756
K	-233.47491	-233.47396	-233.51219
K <sup>‡</sup>	-233.46678	-233.46584	-233.50192
L	-233.50206	-233.50111	-233.53737
L <sup>‡</sup>	-233.46222	-233.46127	-233.49508
M	-233.50224	-233.5013	-233.5364

Table C.3A: FAU zeolite cluster calculation results for the Poutsma mechanism (electronic and zero point corrected energies). Refer to Figure 5.11 for molecule labels.

<b>Molecule</b>	<b>Electronic Energy (Hartrees)</b>	<b>Zero-Point Corrected (Hartrees)</b>	<b>Short Filename</b>
Zeolite Cluster	-10649.53728	-10649.27425	FAUHguess3.log
R*	-10882.84717	-10882.46227	F_CisTriene.log
A*	-10882.84475	-10882.45527	F_CisDienylC2.log
A*‡	-10882.78029	-10882.39629	F_PouRCTSo1.log
B*	-10882.87472	-10882.48795	F_M1C5enylO2.log
B*‡	-10882.79579	-10882.41145	F_M1C5enylO2TSo1.log
C*	-10882.8781	-10882.48627	F_C6ene4nylO2.log
P*	-10882.88093	-10882.49239	F_C6Diene.log

Table C.3B: FAU zeolite cluster calculation results for the Poutsma mechanism (thermal corrections for internal energy, enthalpy, and free energy). Refer to Figure 5.10 for molecule labels. All results are in Hartrees.

<b>Molecule</b>	<b>U (Energy)</b>	<b>H (Enthalpy)</b>	<b>G (Free Energy)</b>
Zeolite Cluster	-10649.21599	-10649.21504	-10649.35556
R*	-10882.39646	-10882.39551	-10882.55129
A*	-10882.39037	-10882.38942	-10882.54539
A*‡	-10882.33175	-10882.33081	-10882.48454
B*	-10882.42322	-10882.42227	-10882.57601
B*‡	-10882.34735	-10882.3464	-10882.49863
C*	-10882.42326	-10882.42231	-10882.57212
P*	-10882.42787	-10882.42693	-10882.58157

Table C.4A: FAU zeolite cluster calculation results for the Alternative mechanism (electronic and zero point corrected energies). Refer to Figure 5.11 for molecule labels.

<b>Molecule</b>	<b>Electronic Energy (Hartrees)</b>	<b>Zero-Point Corrected (Hartrees)</b>	<b>Short Filename</b>
J*	-10882.85339	-10882.46558	F_CisDienyl.log
J*‡	-10882.83226	-10882.44743	F_CisReOTSo4.log
K*	-10882.84909	-10882.46131	F_CCDienylO1.log
K*‡	-10882.82238	-10882.438	F_MCpentenylTSo3.log
L*	-10882.8636	-10882.47632	F_MC5enyl.log
L*‡	-10882.80967	-10882.42329	F_CruTSg2.log
M*	-10882.86258	-10882.47454	F_C6enyl.log

Table C.4B: FAU zeolite cluster calculation results for the Alternative mechanism (thermal corrections for internal energy, enthalpy, and free energy). Refer to Figure 5.10 for molecule labels. All results are in Hartrees.

<b>Molecule</b>	<b>U (Energy)</b>	<b>H (Enthalpy)</b>	<b>G (Free Energy)</b>
J*	-10882.40052	-10882.39958	-10882.55407
J*‡	-10882.38202	-10882.38108	-10882.53679
K*	-10882.39648	-10882.39553	-10882.54837
K*‡	-10882.37317	-10882.37222	-10882.5261
L*	-10882.41176	-10882.41081	-10882.56418
L*‡	-10882.35954	-10882.3586	-10882.51014
M*	-10882.41002	-10882.40908	-10882.56296

## Appendix D

### STRUCTURE INFORMATION FOR OPTIMIZED ZEOLITE CLUSTERS

The following tables contain atomic coordinates and structure information for the cluster models of Faujasite zeolite. Unless otherwise noted, these are optimized “bare” frameworks.

Table D.1: Structure information for bare FAUH Brønsted acid site cluster. Taken from FAUHguess3.log.

Atom Type	Frozen?	X	Y	Z
O	NO	36.526314	21.737729	14.749882
O	NO	32.999015	12.131245	15.618234
O	NO	33.035693	15.632229	12.187154
O	NO	30.239078	21.0381	14.677957
O	NO	33.008753	14.809043	18.366744
O	NO	27.951805	20.890463	12.269641
O	NO	30.383905	15.733447	9.597399
O	NO	31.145485	16.627933	13.739129
O	NO	28.625208	19.01701	14.029824
O	NO	28.593378	16.405754	11.451414
O	NO	34.820384	22.60811	12.886758
O	NO	26.144345	18.972547	16.462655
O	NO	31.241039	13.840889	16.624925
O	NO	28.603909	14.031254	18.992348
O	NO	29.612219	20.058016	10.362706
O	NO	32.267203	17.456526	10.36179
O	NO	32.085988	19.898431	13.145556
O	NO	30.545161	14.665024	12.058889
O	NO	30.574496	18.625756	15.794264
O	NO	26.951245	18.404817	12.057029
O	NO	36.592758	20.763861	12.242956
O	NO	27.893336	18.340472	18.329208
O	NO	30.505018	15.731915	18.324051
O	NO	30.491559	12.144919	14.717025

Table D.1 continued.

O	NO	30.501336	21.789301	12.133413
O	NO	33.939714	18.17139	12.246612
O	NO	34.751579	16.450306	10.41522
O	NO	32.136038	14.129589	14.11446
O	NO	28.528992	20.175338	16.438299
O	NO	32.254365	16.323346	16.402137
O	NO	32.353344	22.438922	13.9167
O	NO	28.652882	16.472743	20.088073
O	NO	34.662326	20.133051	13.906024
Si	NO	31.685723	15.274152	13.053501
Si	NO	29.510433	19.67799	15.247306
Si	NO	33.487793	13.471593	19.17435
Si	NO	27.421549	19.576986	13.084477
Al	NO	31.570178	17.365395	15.233877
Si	NO	29.537017	15.185919	10.893098
Si	NO	33.531848	23.479013	13.44129
Si	NO	31.746789	15.195156	17.414182
Si	NO	29.1751	21.334591	11.281801
Si	NO	31.327401	16.972239	9.107428
Si	NO	33.48294	19.149393	13.433199
Si	NO	35.66904	21.327903	13.439064
Si	NO	31.709932	13.065553	15.259678
Si	NO	29.564569	15.226262	19.554394
Si	NO	27.361859	19.559845	17.391025
Si	NO	33.482339	16.90735	11.298099
Si	NO	31.283219	21.306112	13.474633
Si	NO	37.410724	23.054225	15.228905
Si	NO	33.48004	11.273685	16.938525
Si	NO	27.386103	17.355108	10.884508
Si	NO	25.212746	19.539969	15.232908
Si	NO	27.389303	13.059076	19.542033
Si	NO	29.147165	19.134988	9.095386
Si	NO	37.821836	21.294057	11.271803
Si	NO	27.38844	17.371646	19.558914
Si	NO	29.540039	10.886705	15.20858
Si	NO	35.641996	16.963768	9.123889
H	YES	32.390059	13.020709	20.029564
O	NO	33.94056	12.271322	18.155077
H	YES	34.629654	13.878393	19.957662
O	NO	26.151639	20.045351	13.978717
H	YES	28.7321	14.060289	10.466622
H	YES	33.936538	24.268002	14.601158
H	YES	33.076154	24.343777	12.360143

Table D.1 continued.

H	YES	28.725359	22.457197	10.47337
O	NO	30.424031	18.23962	8.621321
H	YES	32.130432	16.552842	7.97406
H	YES	30.354259	14.753426	20.687377
H	YES	26.925993	20.687387	18.181719
H	YES	38.288161	23.496748	14.131307
H	YES	36.518713	24.157344	15.613838
H	YES	38.216698	22.639096	16.370973
H	YES	32.390066	10.40172	17.410525
H	YES	34.629667	10.473552	16.55288
O	NO	27.909635	18.1721	9.560605
H	YES	26.232813	16.559558	10.466608
H	YES	24.346242	18.446395	14.817441
H	YES	24.422028	20.687411	15.677749
H	YES	27.850291	12.2495	20.687404
H	YES	26.989896	12.173705	18.446398
H	YES	26.232777	13.8717	19.964646
H	YES	28.725345	19.957927	7.974047
H	YES	38.946161	21.76404	12.09551
H	YES	37.365726	22.38619	10.401839
H	YES	38.223404	20.146518	10.4733
H	YES	26.92598	18.181746	20.687381
H	YES	26.303806	16.488077	19.107007
H	YES	30.354249	9.743864	15.67781
H	YES	28.66054	11.324259	16.299939
H	YES	28.732099	10.466615	14.060296
H	YES	36.440509	15.83009	8.667202
H	YES	34.746834	17.410516	8.045074
H	YES	36.516285	18.071104	9.527589
H	NO	33.947716	17.93569	15.375634
O	NO	33.206938	18.21551	14.818404
O	NO	36.526314	21.737729	14.749882

Table D.2: Structure information for bare FAU cation exchange site II cluster. Taken from SilaXS2.log

Atom Type	Frozen?	X	Y	Z
O	NO	14.746652	12.186921	21.75354
O	NO	14.742579	8.676727	18.240155
O	NO	8.676463	12.190779	15.687118
O	NO	12.187086	14.746594	21.753587
O	NO	8.67642	14.742023	18.240188
O	NO	12.190419	8.676175	15.686935
O	NO	12.911475	7.886138	20.019585
O	NO	10.408572	7.88912	17.517784
O	NO	7.886973	12.911556	20.020758
O	NO	7.888888	10.408602	17.517409
O	NO	12.911992	10.411257	22.544319
O	NO	10.410726	12.912231	22.543782
O	NO	12.251006	9.663645	18.178607
O	NO	9.663251	12.250357	18.179241
O	NO	13.963178	10.348721	20.081292
O	NO	10.35121	10.35125	16.463918
O	NO	10.349776	13.963366	20.080335
Si	NO	13.460563	9.138696	19.127393
Si	NO	9.160171	6.960705	16.976322
Si	NO	6.960725	13.453747	21.270516
Si	NO	9.139756	11.30281	16.968086
Si	NO	9.138932	13.460456	19.127669
Si	NO	6.960592	9.160041	16.976289
Si	NO	13.453613	6.960789	21.270101
Si	NO	11.302806	9.139834	16.968016
Si	NO	13.454181	9.161364	23.470436
Si	NO	11.302877	13.462487	21.291695
Si	NO	9.161173	13.454374	23.470506
Si	NO	15.233778	13.056029	23.06036
Si	NO	15.233584	7.369538	17.373696
Si	NO	7.369444	13.057594	15.196177
Si	NO	13.056095	15.233831	23.060429
Si	NO	7.369471	15.233365	17.373672
Si	NO	13.057595	7.369418	15.196043
H	YES	9.591911	6.162901	15.829544
H	YES	8.73157	6.087932	18.070619
O	NO	7.918958	7.918937	16.484244
H	YES	6.163217	14.601167	20.839741

Table D.2 continued.

H	YES	6.087463	12.360147	21.700123
O	NO	7.92096	13.945297	22.510411
H	YES	6.162885	9.591939	15.829563
H	YES	6.087823	8.731519	18.070662
H	YES	14.601157	6.163277	20.839735
H	YES	12.360199	6.08749	21.699966
O	NO	13.944764	7.921309	22.509913
H	YES	14.601686	9.591892	24.26834
H	YES	12.360594	8.731538	24.34342
H	YES	9.591893	14.601761	24.268481
H	YES	8.731512	12.36061	24.343417
O	NO	13.997713	13.997705	23.598399
H	YES	15.613387	12.174329	24.157028
H	YES	16.369173	13.870591	22.639358
O	NO	14.000795	6.828093	16.429609
H	YES	15.613577	6.274452	18.257365
H	YES	16.369565	7.79154	16.560474
O	NO	6.827807	14.000549	16.429773
H	YES	6.273854	12.173807	14.817373
H	YES	7.792231	13.871647	14.060438
H	YES	12.174328	15.613418	24.157018
H	YES	13.870565	16.369281	22.639423
H	YES	6.274351	15.613489	18.257092
H	YES	7.791769	16.369292	16.560619
H	YES	12.173565	6.273958	14.817312
H	YES	13.871747	7.792043	14.060241
O	NO	12.254128	12.254122	20.768337
Si	NO	13.462305	11.302856	21.291851

Table D.3 Structure information for bare FAU cation exchange site III cluster.  
Taken from SilaXS3.log

Atom Type	Frozen?	X	Y	Z
O	NO	14.69817	12.212287	21.769455
O	NO	6.034074	14.692327	20.87129
O	NO	8.660165	12.212565	15.733461
O	NO	15.669971	18.260832	21.783
O	NO	12.225499	14.691133	21.731961
O	NO	8.697126	14.69063	18.206446
O	NO	2.588747	18.261039	20.820742
O	NO	8.647081	18.262418	14.762026
O	NO	13.998869	14.026413	23.622415
O	NO	7.80898	12.921932	19.983051
O	NO	10.448928	12.922891	22.620889
O	NO	6.808214	14.028488	16.429853
O	NO	4.258966	14.025889	18.983018
O	NO	12.036607	15.692585	24.209198
O	NO	6.071725	12.19329	21.827267
O	NO	9.652918	12.191702	18.24678
O	NO	6.136439	18.307602	15.690201
O	NO	14.743555	18.307433	24.294377
O	NO	12.184759	12.192012	20.776407
O	NO	3.515135	18.307545	18.309421
O	NO	6.21978	15.692562	18.393086
O	NO	7.977246	13.936047	22.45403
O	NO	13.943144	16.470033	22.54423
O	NO	10.280645	13.936458	20.149821
O	NO	7.887751	16.471316	16.489718
O	NO	4.31522	16.470127	20.059925
Si	NO	6.967727	13.432763	21.292235
Si	NO	9.148128	11.26655	16.984376
Si	NO	15.206871	17.359536	23.051836
Si	NO	13.047016	15.218019	23.033762
Si	NO	1.29286	19.149984	21.313707
Si	NO	7.379219	17.360403	15.226104
Si	NO	11.290227	13.43264	21.311414
Si	NO	3.051744	17.359661	19.551938
Si	NO	7.396469	15.218448	17.383907
Si	NO	9.139665	13.432393	23.462656
Si	NO	13.447133	11.266667	21.281072
Si	NO	7.362443	13.070213	15.208342

Table D.3 continued.

Si	NO	5.211086	15.218064	19.570009
O	NO	9.559837	14.690938	24.397909
O	NO	9.611951	18.262652	27.841728
O	NO	11.449647	14.027257	26.172603
O	NO	8.605761	12.1917	24.357473
O	NO	12.122327	18.307522	26.913188
O	NO	10.370758	16.470541	26.114891
Si	NO	10.86122	15.218178	25.219703
Si	NO	10.879659	17.360406	27.377776
Si	NO	15.221385	13.069384	23.068284
Si	NO	16.96583	19.149916	21.290053
Si	NO	9.139341	19.150303	13.465182
Si	NO	3.03554	13.069221	19.535833
Si	NO	4.810358	11.266597	21.322477
Si	NO	5.198265	19.564541	15.212594
Si	NO	15.220478	19.564469	25.232866
Si	NO	3.038249	19.564507	17.370839
Si	NO	9.119415	19.150334	29.138577
Si	NO	10.896215	13.069942	27.395316
Si	NO	9.110624	11.266452	25.619729
Si	NO	13.060455	19.564486	27.391103
H	YES	8.043555	10.400704	17.410994
H	YES	10.28306	10.474482	16.553533
H	YES	16.301147	16.487057	23.497142
H	YES	0.848286	20.029376	20.217586
H	YES	0.187725	18.259998	21.700067
H	YES	6.934633	16.48808	14.131565
H	YES	13.020784	10.401755	22.386211
H	YES	13.878322	10.473593	20.146723
H	YES	6.274019	12.173825	14.817556
H	YES	7.792187	13.871689	14.060319
H	YES	11.324196	16.488069	28.472228
H	YES	15.613414	12.174171	24.156903
H	YES	16.369226	13.870605	22.639471
H	YES	17.410436	20.02936	22.386169
H	YES	18.071042	18.259993	20.903678
H	YES	16.552841	19.957916	20.146565
H	YES	8.04366	20.030357	13.020298
H	YES	9.527193	18.26035	12.360665
H	YES	10.283102	19.956956	13.877921
O	NO	3.558242	12.210947	20.834206
H	YES	2.644993	12.173785	18.446431
H	YES	5.238017	10.401871	20.217524

Table D.3 continued.

H	YES	4.380444	10.473294	22.45719
H	YES	6.009236	20.687353	14.753496
H	YES	4.315639	19.10699	14.131366
O	NO	4.303058	20.092727	16.476621
H	YES	15.678165	20.687878	24.421598
H	YES	16.301296	19.106467	26.116588
O	NO	13.955606	20.092628	26.127027
H	YES	2.580571	20.687906	18.182123
H	YES	1.957416	19.106493	16.48713
H	YES	10.21509	20.030344	29.583436
H	YES	8.731561	18.260349	30.243061
H	YES	7.975658	19.956947	28.725821
O	NO	9.5984	12.21165	26.871349
H	YES	11.984841	12.173772	27.786277
H	YES	10.46656	13.87165	28.543341
H	YES	10.215156	10.400783	25.192712
H	YES	7.975686	10.474436	26.050336
H	YES	12.249501	20.687351	27.850228
H	YES	13.943117	19.10698	28.472385
H	YES	1.705906	19.95792	22.457177
H	YES	1.957546	16.487117	19.106569
H	YES	1.887826	13.871657	19.964653
Si	NO	9.118163	13.432164	19.1415